

EXPERIMENTALLY ALTERING THE COMPLIANCE
OF TITIN'S SPRING REGION

by

Mathew Michael Bull

A Dissertation Submitted to the Faculty of the

GRADUATE INTERDISCIPLINARY PROGRAM
IN PHYSIOLOGICAL SCIENCES

In Partial Fulfillment of the Requirements

For the Degree of

DOCTOR OF PHILOSOPHY

In the Graduate College

THE UNIVERSITY OF ARIZONA

2016

THE UNIVERSITY OF ARIZONA
GRADUATE COLLEGE

As members of the Dissertation Committee, we certify that we have read the dissertation prepared by Mathew Michael Bull, titled Experimentally Altering the Compliance of Titin's Spring Region and recommend that it be accepted as fulfilling the dissertation requirement for the Degree of Doctor of Philosophy.

_____ Date: 4/25/2016
Henk Granzier

_____ Date: 4/25/2016
Jil Tardiff

_____ Date: 4/25/2016
John Konhilas

_____ Date: 4/25/2016
Samantha Harris

_____ Date: 4/25/2016
Tom Doetschman

Final approval and acceptance of this dissertation is contingent upon the candidate's submission of the final copies of the dissertation to the Graduate College.

I hereby certify that I have read this dissertation prepared under my direction and recommend that it be accepted as fulfilling the dissertation requirement.

_____ Date: 5/2/2016
Dissertation Director: Henk Granzier

STATEMENT BY AUTHOR

This dissertation has been submitted in partial fulfillment of the requirements for an advanced degree at the University of Arizona and is deposited in the University Library to be made available to borrowers under rules of the Library.

Brief quotations from this dissertation are allowable without special permission, provided that an accurate acknowledgement of the source is made. Requests for permission for extended quotation from or reproduction of this manuscript in whole or in part may be granted by the head of the major department or the Dean of the Graduate College when in his or her judgment the proposed use of the material is in the interests of scholarship. In all other instances, however, permission must be obtained from the author.

SIGNED: Mathew Bull

ACKNOWLEDGEMENT

First and foremost, I give all praise and thanks to my Lord and savior Jesus Christ. I want to thank my loving wife Kara, who has supported me throughout my graduate work. I thank all my friends and family for their encouragement. I sincerely thank my mentor Henk Granzier for his support and guidance during my time spent in his lab. I am grateful for my committee members, Jil Tardiff, John Konhilas, Samantha Harris and Tom Doetschman for their input and valuable discussions. I am very thankful for the past and present members of the Granzier lab, without them my work would not be possible. I also want to acknowledge Dr. Jeffrey Pyun and the Pyun lab for giving me a start in research and an opportunity to be creative. I truly appreciate all of the financial support from the department of Physiology and the NIH training grant by which my work was funded. I thank Mrs. Van Denburgh and the ARCS association for their support. Lastly, I thank the MD/PhD program at the University of Arizona for accepting me into their program and giving me an opportunity.

Sincerely,

Mathew Bull

ACKNOWLEDGEMENT OF WORK PERFORMED

I collaborated with various colleagues on this work. The ACF surgeries and pressure-volume analysis was performed by Dr. Josh Strom at the University of Arizona Phenotyping core. Pooja Nair and Chanda Saripalli contributed to protein analysis. Dr. Mei Methajit performed skinned cardiomyocyte mechanics. Dr. Kirk Hutchinson taught me the TAC surgery and transcript analysis was performed by Dr. John Smith III and members of the lab of Dr. Michael Gotthardt. I also want to acknowledge Luann Wiley for her support with the mice and Dr. Liu Xiangdang for PCR support. Finally, I want to acknowledge, Javier Saldana-Perez, Erin Hartnett and Vanessa Fernandez for their various experimental support.

TABLE OF CONTENTS

List of Figures and Tables	9
Abstract	16
References of Abstract.....	18
Introduction	19
References of Introduction.....	25
CHAPTER 1: Alternative Splicing of Titin Restores Diastolic Function and Improves HFpEF Associated Symptoms in a Genetic Murine Model (<i>Ttn</i>^{ΔIAjxn})	32
1.1 Abstract	33
1.2 Introduction	34
1.3 Materials and Methods	36
1.4 Results	
1.4.1 Inhibition of Rbm20 upregulates super compliant titin isoforms (N2BAsc) and normalizes passive stiffness in cardiomyocytes of <i>Ttn</i> ^{ΔIAjxn} mice.....	39
1.4.2 Reduction of RBM20 expression restores diastolic function to <i>Ttn</i> ^{ΔIAjxn} mice	40
1.4.3 Assessment of associated HFpEF symptoms.....	42
1.4.4 Table 1 and Figures 1-6	45
1.5 Discussion and Summary	53
1.6 References of Chapter 1	58
1.7 Supplemental	
1.7.1 Supplemental Methods of Chapter 1	

1.7.1.1	Generation of Mice	64
1.7.1.2	Skinned Cell Mechanics	64
1.7.1.3	Echocardiography	66
1.7.1.4	Pressure-Volume Analysis	67
1.7.1.5	Exercise Testing	69
1.7.1.6	Quantification of Protein Expression	69
1.7.1.7	Transverse Aortic Constriction	70
1.7.2	Supplemental Figures S1-2	72
1.7.3	Supplemental Tables S1-3	74
1.7.4	References of Chapter 1 Supplemental Methods	77
CHAPTER 2: The Cardiac Specific N2B Element in Titin is Necessary for Volume Overload Induced Hypertrophy		78
2.1	Abstract	79
2.2	Introduction	81
2.3	Materials and Methods	84
2.4	Results	
2.4.1	Basic characterization.....	87
2.4.2	Intermittent versus continuous exercise	88
2.4.3	Normal pressure response abnormal volume response	89
2.4.4	Abnormal hypertrophy response to isoproterenol injections	90
2.4.5	Alterations in Signal Transduction	91
2.4.6	Table 1 and Figures 1-7	93

2.5 Discussion and Summary	103
2.6 References of Chapter 2	108
2.7 Supplemental	
2.7.1 Supplemental Methods of Chapter 1	
2.7.1.1 Generation of Mice	116
2.7.1.2 Echocardiography	116
2.7.1.3 Pressure-Volume Analysis	117
2.7.1.4 Voluntary Running.....	118
2.7.1.5 Continuous Swimming	118
2.7.1.6 Quantification of Protein Expression	118
2.7.1.7 Transverse Aortic Constriction	120
2.7.1.8 Aortocaval Fistula	121
2.7.1.9 Isoproterenol Injections	122
2.7.1.10 Gene expression analysis	122
2.7.2 Supplemental Figures 1-3.....	123
2.7.3 References of Chapter 2 Supplemental Methods	126
Discussion and Summary	127
References of Discussion and Summary	138

LIST OF FIGURES AND TABLES

INTRODUCTION: Figure 1. Schematic of cardiac titin isoforms in the half-sarcomere. Upper inset: the N2B isoform; Right inset: FHL2 localization to the N2B element in titin. Murine models used in dissertation work in (A-D): A) WT titin; B) $Ttn^{\Delta IAjxn}$; C) $Ttn^{\Delta IAjxn}$ crossed to $Rbm20^{\Delta RRM}$; D) N2B KO.....25

CHAPTER 1: Alternative Splicing of Titin Restores Diastolic Function and Improves HFpEF Associated Symptoms in a Genetic Murine Model ($Ttn^{\Delta IAjxn}$)

Chapter1 Table 1: Data shown as mean \pm SEM. Abbreviations: $\Delta IAjxn$: ($Ttn^{\Delta IAjxn}$); ΔRRM ($Rbm20^{\Delta RRM+/-}$); HR: heart rate; BPM: beats per minute; FS: fractional shortening; LVIDd: left ventricular internal diastolic diameter; LVIDs; left ventricular internal systolic diameter; LVPWd: left ventricular posterior wall thickness in diastole; LVPWs: left ventricular posterior wall thickness in systole. Eccentricity: LVDD/WT; MV DT: mitral valve deceleration time; E/A: LV pulse wave Doppler ratio; LA: left atrium PV: All measurements were obtained during a pause in ventilation. Inferior venal caval occlusions were performed to assess load - independent parameters. ESP: end - systolic pressure; EDP: end - diastolic pressure; ESV: end systolic volume; EDV: end - diastolic volume; EF: ejection fraction; Ea: effective arterial elastance; ESPVR: end - systolic PV relationship; EDPVR: end - diastolic PV relationship. Statistical significance calculated with one-way ANOVA with Bonferroni correction: * $p < 0.05$; ** $p < 0.01$; *** $p < 0.001$; **** $p < 0.0001$; (versus WT ****, versus $\Delta IAjxn^{-/-}$ ****).....45

Chapter 1 Figure 1: A) Half sarcomere models of 3 genotypes used in this work: WT, $\Delta IAjxn$ and $\Delta IAjxn/\Delta RRM$. The domain composition of titin's spring region (N2B isoform) is shown at the top. B) Representative image of 1% agarose gel for titin analysis of LV

myocardium. WT myocardium expresses N2BA and N2B titin (T2 is a minor degradation product). The $\Delta IAjxn$ mouse expresses titin with a slightly higher mobility consistent with the deletion of the IA junction. Crossing the $\Delta IAjxn$ with the ΔRRM mouse results in expression of two very large N2BA isoforms that we refer to as super compliant (N2BA_{sc}). C) Ratio of N2BA isoforms over total titin. D) Representative skinned cardiomyocyte with passive stress in cardiomyocytes. E). Passive stiffness in cardiomyocytes. Abbreviations: $\Delta IAjxn$: $Ttn^{\Delta IAjxn}$; ΔRRM : $Rbm20^{\Delta RRM}$ x α MHC); N2BA_{sc}: super compliant N2BA titin. Data shown as mean \pm SEM. Statistical significance calculated by one-way ANOVA with Bonferroni correction: p<0.05; versus WT ****, versus $\Delta IAjxn$ †††).....47

Chapter 1 Figure 2: Diastolic function of $Ttn^{\Delta IAjxn}$ mice and $Ttn^{\Delta IAjxn}$ mice constitutively expressing N2BA_{sc}. A) Representative pulse-wave Doppler E and A waves; B-C) cardiac catheterization PV loops; D) E/A ratio; E) MVDT: mitral valve deceleration time; F) Stiffness coefficient β of EDPVR (end-diastolic pressure volume relationship). Data shown as mean \pm SEM. Statistical significance calculated by one-way ANOVA with Bonferroni correction: p<0.05; versus WT ****, versus $\Delta IAjxn$ †††).....48

Chapter 1 Figure 3: Diastolic function $Ttn^{\Delta IAjxn}$ mice and $Ttn^{\Delta IAjxn}$ mice with inducible expression of N2BA_{sc}. A) Representative image of 1% agarose gel for titin analysis of LV myocardium. WT myocardium expresses N2BA and N2B titin (T2 is a minor degradation product). Crossing the $\Delta IAjxn$ with the ΔRRM mouse results in expression of two very large N2BA isoforms (scN2BA1 and 2). Right gel image: MCM-inducible $\Delta IAjxn/\Delta RRM$; Vehicle: DMSO and saline (50/50 mixture); Treatment: raloxifene dissolved in DMSO and saline (50/50 mixture). B) E/A ratio; C) MVDT: mitral valve deceleration time; D) EDPVR (β): end diastolic pressure volume relationship. Data shown as mean \pm SEM. Statistical significance calculated with two-way ANOVA and Bonferroni correction (B and C) or t-test (D), (* p<0.05; ** p<0.01; *** p<0.001; **** p<0.0001 as indicated).....49

Chapter 1 Figure 4: Mice with upregulated compliant titin display enhanced exercise performance. A) Voluntary running wheel max speed of *Ttn^{ΔIAjxn}* mice and *Ttn^{ΔIAjxn}* mice constitutively expressing N2BAsc; B) Voluntary running wheel average speed C-D) Time and distance ran on treadmill of *Ttn^{ΔIAjxn}* mice and *Ttn^{ΔIAjxn}* mice constitutively expressing N2BAsc; E-F) Time and distance of *Ttn^{ΔIAjxn}* mice and *Ttn^{ΔIAjxn}* mice with inducible expression of N2BAsc. Data shown as mean ± SEM. Statistical significance calculated with either t-test (C-F), linear (A) and non-linear (B) regression analysis testing whether lines are significantly different from one another : * p<0.05 considered significant.....50

Chapter 1 Figure 5: Increased strain on the N2B element of *Ttn^{ΔIAjxn}* mice results in an exaggerated response to TAC. A) Hypertrophy; B) Concentricity: WT: wall thickness in diastole; LVDD: left ventricular diameter in diastole. C) E/A ratio. D) MVDT: mitral valve deceleration time. Data shown as mean ± SEM. Statistical significance calculated by one or two-way ANOVA with Bonferroni correction: * p<0.05; ** p<0.01; *** p<0.001; **** p<0.0001; (versus WT ****, versus *Ttn^{ΔIAjxn}* †††).....51

Chapter 1 Figure 6: N2B element localized binding proteins and response to TAC. A and D) αB-crystallin; B and E) FHL1; C and F) FHL2. Data shown as mean ± SEM. Statistical significance calculated by two-way ANOVA with Bonferroni correction: * p<0.05; ** p<0.01; *** p<0.001; **** p<0.0001; (versus WT ****, versus *ΔIAjxn* †††)..52

Chapter 1 Supplemental Figure 1: Schematic explaining breeding of *Ttn^{ΔIAjxn}* to *Rbm20^{ARRM}* mice^{1,2}. Generation of constitutive and inducible homozygous *Ttn^{ΔIAjxn}* mice with heterozygous reduction of functional Rbm20.....72

Chapter 1 Supplemental Figure 2: LVW:BW increases with age in *Ttn^{ΔIAjxn}* compared with WT mice. A) Left ventricular weight (LVW) normalized to body weight (BW). B) Percent left ventricle (LV) mass increase in WT and *Ttn^{ΔIAjxn}* mice. Data shown as mean

± SEM. Statistical significance calculated with two-way ANOVA and Bonferroni correction (A) and t-test (B), (* p<0.05; ** p<0.01; *** p<0.001; **** p<0.0001 as indicated).....73

Chapter 1 Supplemental Table 1: Data shown as mean ± SEM.; Abbreviations: ΔIA_{jxn} : ($Ttn^{\Delta IA_{jxn}}$); ΔRRM ($Rbm20^{\Delta RRM+/-}$); TT: total titin; MHC: myosin heavy chain; T1: sum of titin isoforms N2BA and N2B; T2: titin degradation product. Statistical significance calculated with one-way ANOVA with Bonferroni correction: * p<0.05; ** p<0.01; *** p<0.001; **** p<0.0001; (versus WT ****, versus $Ttn^{\Delta IA_{jxn}}$ ††††).....74

Chapter 1 Supplemental Table 2: Dissection of male mice age ~4 months old. Abbreviations: ΔIA_{jxn} : ($Ttn^{\Delta IA_{jxn}}$); ΔRRM ($Rbm20^{\Delta RRM+/-}$); BW: body weight; HW: heart weight; LV: left ventricle; RV: right ventricle; ATR: atrium. Data shown as mean ± SEM; statistical significance calculated with one-way ANOVA with Bonferroni correction: * p<0.05; ** p<0.01; *** p<0.001; **** p<0.0001; (versus WT ****, versus $Ttn^{\Delta IA_{jxn}}$ ††††).....75

Chapter 1 Supplemental Table 3: Vehicle: DMSO and saline. Treatment: (40 mg/kg) raloxifene injections (x8 days). Abbreviations: HR: heart rate; BPM: beats per minute; FS: fractional shortening; LVIDd: left ventricular internal diastolic diameter; LVIDs: left ventricular internal systolic diameter; LVPWd: left ventricular posterior wall thickness in diastole; LVPWs: left ventricular posterior wall thickness in systole. Eccentricity: LVDD/WT. Data shown as mean ± SEM; statistical significance calculated with Student's t-test: * p<0.05 considered significant.....76

CHAPTER 2: The Cardiac Specific N2B Element in Titin is Necessary for Volume Overload Induced Hypertrophy

Chapter 2 Table 1: Extensive studies were performed to determine the cardiac specific N2B element's role in hypertrophy and remodeling responses to stress in the heart.

Abbreviations: HR: heart rate; BPM: beats per minute; FS: fractional shortening; Eccentricity: LVDD/WT; LV/BW: left ventricular weight normalized to body weight; Calculated LV mass for 1 week TAC was obtained by M-Mode echocardiography in the short axis view because tissue weights were not available. Data shown as mean \pm SEM; statistical significance calculated with A. Student's T-test: * $p < 0.05$ considered significant.....93

Chapter 2 Figure 1: Basic Characterization of N2B KO mice. A-B) Representative cardiac catheterization PV loops; C) Slope (Ees) of ESPVR (end-systolic pressure volume relationship); D) Stiffness coefficient β of EDPVR (end-diastolic pressure volume relationship); E) Left atrial weight (LA) normalized to body weight (BW); F-G) representative M-Mode, (LVIDd): left ventricular internal diastolic diameter; (LVIDs): left ventricular internal systolic diameter; H) cardiac titin I-band binding proteins. Data shown as mean \pm SEM; statistical significance calculated with t-test (C-E) or one-way ANOVA and Bonferroni correction (H), (* $p < 0.05$; ** $p < 0.01$; *** $p < 0.001$; **** $p < 0.0001$ as indicated).....95

Chapter 2 Figure 2: Voluntary and controlled exercise. A) Voluntary running left ventricular weight (LV) normalized to body weight (BW); B) Percent left ventricle (LV) mass increase in running study; C) Chronic swimming left ventricular weight (LV) normalized to body weight (BW); B) Percent left ventricle (LV) mass increase in swimming study; data shown as mean \pm SEM. Statistical significance calculated with two-way ANOVA and Bonferroni correction (A and C) and t-test (B and D), (* $p < 0.05$; ** $p < 0.01$; *** $p < 0.001$; **** $p < 0.0001$ as indicated).....96

Chapter 2 Figure 3: Chronic pressure and volume overload. A) TAC left ventricular weight (LV) normalized to body weight (BW); B) Percent left ventricle (LV) mass increase in afterload study; C) 1 week ACF left ventricular weight (LV) normalized to body weight (BW); D) 4 week ACF left ventricular weight (LV) normalized to body weight (BW); E) Percent left ventricle (LV) mass increase in ACF studies; F) ACF survival curve. Data

shown as mean \pm SEM. Statistical significance calculated with two-way ANOVA and Bonferroni correction (A and C-E), t-test (B) and Log-Rank Mantel-Cox test (F); (* p<0.05; ** p<0.01; *** p<0.001; **** p<0.0001 as indicated).....97

Chapter 2 Figure 4: Isoproterenol injection study. A) 2 and 20 mg/kg dose injection studies, (LV) normalized to body weight (BW); B-C) Percent left ventricle (LV) mass increase in low dose (B) and high dose (C); D) dPmax; E) Slope (Ees) of ESPVR (end-systolic pressure volume relationship); F) Stiffness coefficient β of EDPVR (end-diastolic pressure volume relationship). Data shown as mean \pm SEM. Statistical significance calculated with two-way ANOVA and Bonferroni correction (A and D-F) and t-test (B-C), (* p<0.05; ** p<0.01; *** p<0.001; **** p<0.0001 as indicated).....98

Chapter 2 Figure 5: Transcriptional targets differentially regulated in isoproterenol study. A) Heat-plot; B) Venn diagram.....99

Chapter 2 Figure 6: Western blot analysis of signal transduction. A) pAkt/Akt; B) PKC α / β -tubulin; C) pGSK3 β /GSK3 β ; D) pAkt/Akt in 1 week ACF study; E) pAkt/Akt in 4 week ACF study; F) pMTOR/MTOR in 1 week ACF study; G) pMTOR/MTOR in 4 week ACF study; H-I) FHL2 western blot images and corresponding images to (D-G). Data shown as mean \pm SEM. Statistical significance calculated with t-test (A-C) and two-way ANOVA and Bonferroni correction (D-G), (* p<0.05; ** p<0.01; *** p<0.001; **** p<0.0001 as indicated).....100

Chapter 2 Figure 7: Eccentricity of WT mice in response to cardiac stress. Abbreviations: SED: sedentary analysis; SWIM: controlled swim training; RUN: voluntary wheel running; ISO: daily isoproterenol injections (2 mg/kg); TAC 1WK: 1 week chronic pressure overload induced by transverse aortic constriction; TAC 4WK: 4 week chronic pressure overload induced by transverse aortic constriction; ACF 1WK: 1 week chronic volume

overload induced by aortocaval fistula; ACF 4WK: 4 week chronic volume overload induced by aortocaval fistula. Data shown as mean \pm SEM. Statistical significance calculated with one-way ANOVA and Bonferroni correction (D-G), (* $p < 0.05$; ** $p < 0.01$; *** $p < 0.001$; **** $p < 0.0001$ compared to SED).....102

Chapter 2 Supplemental Figure 1: Representative Doppler characterization of WT and N2B KO mice. Upper left: WT tissue Doppler; Lower left: WT pulse-wave Doppler; Upper right: N2B tissue Doppler; Lower right N2B pulse-wave Doppler.....123

Chapter 2 Supplemental Figure 2: Voluntary wheel running in WT and KO mice. A) Average speed; B) time; C) distance.....124

Chapter 2 Supplemental Figure 3: Low dose (2 mg/kg) isoproterenol injection study in WT, N2B KO and FHL2 KO mice. A) Normalized left ventricular weight to body weight; B) percent LV mass increase. Data shown as mean \pm SEM. Statistical significance calculated with one or two-way ANOVA and Bonferroni correction (* $p < 0.05$; ** $p < 0.01$; *** $p < 0.001$; **** $p < 0.0001$).....125

ABSTRACT

Chapter 1 of this work focuses on alternative splicing of titin as a proof of concept therapy for treating diastolic dysfunction and restrictive filling in a genetic murine model (*Ttn* ^{Δ I A_{jxn}})¹. The *Ttn* ^{Δ I A_{jxn}} mouse has increased strain on the spring region of titin and acts as a mechanical analogue of the titin-based increase in passive myocardial stiffness found in patients with heart failure and preserved ejection fraction (HFpEF). HFpEF is a complex disease characterized by diastolic dysfunction, exercise intolerance, and concentric hypertrophic remodeling. Approximately half all of heart failure patients suffer from diastolic dysfunction, however, no effective therapy exists for treating this pervasive syndrome². Titin, the largest known protein and molecular spring in the heart, has emerged as a prime candidate for therapeutic targets aimed at restoring compliance to the sarcomere in order to improve diastolic function. Titin has two main cardiac isoforms that are regulated by alternative splicing; the smaller N2B isoform (~3.0 MDa) and the larger more compliant N2BA isoform (~3.3 MDa)³. Diastolic stiffness of the left ventricle is dependent upon the N2BA:N2B isoform ratio. In the first half of this work, we modified these two primary isoforms by inhibiting the known titin splicing factor Rbm20. We demonstrate that Rbm20 reduction restores diastolic function, improves exercise tolerance and attenuates afterload induced pathologic remodeling of the left ventricle in *Ttn* ^{Δ I A_{jxn}} mice.

The work in chapter 2 is focused on studies using the previously published N2B knock out (KO) murine model⁴. The N2B spring element found in cardiac titin's I-band region has been proposed as a sensor and signaling "hot spot" in the sarcomere. This study investigates the role of titin's cardiac specific N2B element as a mechano-sensor for stress and strain induced remodeling of the heart. The N2B KO mouse was subjected to a variety

of stressors including transverse aortic constriction (TAC), aortocaval fistula (ACF), chronic swimming, voluntary running and isoproterenol stimulation. Our data revealed that the N2B element is essential in preload stimulated cardiac hypertrophy as well as remodeling due to *beta*-adrenergic stress. Cardiac hypertrophy is a common maladaptive feature of heart failure patients and the mechanical triggers that determine pathologic growth are not well understood. My work in the N2B KO mouse reveal titin's important role in cardiac remodeling.

References of Abstract

1. Granzier HL, Hutchinson KR, Tonino P, Methawasin M, Li FW, Slater RE, Bull MM, Saripalli C, Pappas CT, Gregorio CC and Smith JE, 3rd. Deleting titin's I-band/A-band junction reveals critical roles for titin in biomechanical sensing and cardiac function. *Proc Natl Acad Sci U S A*. 2014;111:14589-94.
2. Writing Committee M, Yancy CW, Jessup M, Bozkurt B, Butler J, Casey DE, Jr., Drazner MH, Fonarow GC, Geraci SA, Horwich T, Januzzi JL, Johnson MR, Kasper EK, Levy WC, Masoudi FA, McBride PE, McMurray JJ, Mitchell JE, Peterson PN, Riegel B, Sam F, Stevenson LW, Tang WH, Tsai EJ, Wilkoff BL and American College of Cardiology Foundation/American Heart Association Task Force on Practice G. 2013 ACCF/AHA guideline for the management of heart failure: a report of the American College of Cardiology Foundation/American Heart Association Task Force on practice guidelines. *Circulation*. 2013;128:e240-327.
3. Granzier H and Labeit S. Cardiac titin: an adjustable multi-functional spring. *J Physiol*. 2002;541:335-42.
4. Radke MH, Peng J, Wu Y, McNabb M, Nelson OL, Granzier H and Gotthardt M. Targeted deletion of titin N2B region leads to diastolic dysfunction and cardiac atrophy. *Proc Natl Acad Sci U S A*. 2007;104:3444-9.

INTRODUCTION

Titin is third myofilament in striated muscle and spans the half sarcomere from Z-disk to M-band (see Figure 1 A below). The N-terminus of titin embeds in the Z-disk followed by the elastic I-band region, ridged A-band segment and finally C-terminal binding in the M-band. In contrast to the thick and thin filaments which are primarily involved in active muscle contraction, titin contains a 1.0 MDa elastic spring region that governs the passive tension in the myocyte¹. In cardiac titin, there are two principal isoforms; N2B (~3.0 MDa) and N2BA (~3.3 MDa) that are co-expressed at the level of the half sarcomere². Variation in titin isoforms occur through alternative splicing by RBM20 in a dose dependent manner, and dominates the spring region of the molecule (the rest of titin is largely identical)³. The human left ventricle has approximately 60:40 N2B:N2BA titin and shifting of this ratio occurs during heart disease⁴. In this work I focus on the spring (I-band) region of titin, its regulation and its role as a mechanotransducer of cardiac remodeling. To investigate these topics, I have integrated work in previously published murine models (*Ttn*^{ΔIAjxn}⁵, *Rbm20*^{ARRM}⁶, and N2B KO⁷) which I will introduce in detail below.

The *Ttn*^{ΔIAjxn} murine model so named because titin's I-band – A-band junction is removed, was originally created for the purpose of determining titin's role as a molecular ruler that determines the length of the thick filament regulation. The IA junction is encoded by exons 251 – 269 in the TTN gene and comprises a ~153 kDa Ig/FnIII modular domain in titin. Using super resolution (SIM) and transmission electron microscopy (TEM) it was

found that the IA junction in titin is not responsible for thick filament length regulation⁵. There was, however, an interesting cardiac phenotype observed that has many similarities to heart failure patients with preserved ejection fraction (HFpEF); notably, diastolic dysfunction, reduced exercise tolerance and mild hypertrophic concentric remodeling of the left ventricle. Deleting the IA junction in titin extends the anchoring point of the distal Ig spring element in titin further from the Z-disk. By increasing the strain on the spring in titin, greater tension is generated at a given sarcomere length. Greater tension in titin is also generated in HFpEF patients that have increased oxidative stress and display deranged phosphorylation in titin⁸. Oxidative stress and reduced PKG phosphorylation of titin reduces the contour length of the spring and enhances passive stiffness in cardiomyocytes⁹.¹⁰. Thus, the *Ttn* ^{Δ IAjxn} model acts as a mechanical analogue that imitates increased titin strain in HFpEF patients.

In contrast to the *Ttn* ^{Δ IAjxn} model, the *Rbm20* ^{Δ RRM} mouse has super compliant titin isoforms⁶ referred to as N2BAsc. This genetic murine model was created in the Granzier lab by deleting exons 6 and 7 of the RNA recognition motif in the Rbm20 gene. Heterozygous reduction of RBM20 protein in *Rbm20* ^{Δ RRM} mice produces a beneficial effect in diastole. Studies in intact myocytes revealed that passive stiffness (slope of stress-SL relation for the first 10% SL increases) was 87% less in -/- mice (relative to +/+) and 61% less in +/- mice, while the steady-state systolic stress at base length was the same in +/+ and +/- *Rbm20* ^{Δ RRM} cells: 5.1 ± 0.3 mN/ mm² and 4.9 ± 0.3 mN/ mm² respectively⁶. Cardiac function was also evaluated at the chamber level and revealed that +/- mice have similar systolic function as +/+ controls, while diastolic function was improved⁶. We

hypothesized that reducing RBM20 levels in *Ttn^{ΔIAjxn}* mice would recover the observed HFpEF-like symptoms. As demonstrated in chapter 1, RBM20 reduction restores diastolic function, improves exercise tolerance and attenuates afterload induced pathologic remodeling of the left ventricle in *Ttn^{ΔIAjxn}* mice (see Chapter 1).

Heart Failure with Preserved Ejection Fraction

HFpEF is a clinical syndrome in which patients have normal left ventricular ejection fraction (LVEF > 50 percent), yet display signs and symptoms of heart failure¹¹. Women are more frequently diagnosed with HFpEF, while heart failure with reduced ejection fraction (HFrEF) is more common in men^{12, 13}. The prevalence of HFpEF increases with age, and at a rate of 1% increase per year, by 2020 HFpEF will make up nearly 70% of all heart failure patients¹⁴. Current therapies are aimed at managing the associated comorbidities (hypertension, lung disease, coronary artery disease, atrial fibrillation, obesity, anemia, diabetes mellitus, kidney disease, and sleep disordered breathing)¹⁵ often present in HFpEF patients that impact the clinical course. In contrast to HFrEF, HFpEF lacks effective pharmacotherapy, primarily due to the poorly understood pathophysiology surrounding this clinical syndrome¹⁶. Pharmacological approaches using renin-angiotensin-aldosterone system (RAAS) inhibitors have been unsuccessful in the treatment of HFpEF¹⁷ suggesting RAAS is less prominent in HFpEF compared to HFrEF.

A hallmark of HFpEF patients is diastolic dysfunction, characterized by slowed relaxation and elevated filling pressures¹⁸. Studies on myocardial biopsies taken from HFpEF patients have revealed that increased myocardial stiffness contributes to diastolic

dysfunction at the organ level^{8, 19, 20}. Furthermore, altered signal transduction in myocytes of HFpEF patients contributes to increased passive stiffness due to downregulation of cyclic guanosine monophosphate (cGMP)-protein kinase G (PKG) signaling^{21, 22}. Titin, the molecular spring in the heart, is the chief protein responsible for passive stiffness in cardiomyocytes²³. Titin is a substrate of PKG signaling in the myocyte and reduced PKG phosphorylation of titin's N2B element leads to reduced elasticity²⁴. Moreover, titin's PEVK region is phosphorylated by protein kinase C alpha (PKC α) increasing the passive stiffness of the myocyte. Reducing PKC signaling in HFpEF patients may benefit cardiac function in diastole as titin based passive tension is reduced²⁵. Inhibition of phosphodiesterase(PDE)5^{26, 27} and 9²⁸, also has the potential to increase titin spring compliance through upregulating active PKG levels in the cell. A combinatorial approach may be necessary, however, since the recent RELAX trial results were not successful using PDE5 inhibitor, sildenafil, alone. While tuning titin's passive stiffness through phosphorylation is a valid therapeutic target, increasing compliance of this molecular giant can be achieved post-transcriptionally as well.

The recently discovered titin splicing factor RBM20³ regulates titin splicing in a dose dependent manner⁶. By reducing RBM20 levels in the myocyte, additional titin spring exons are incorporated causing reduced passive tension in the cell. Our work in chapter 1 of this dissertation is the first evidence that reducing RBM20 levels is an effective therapy in a rodent model exhibiting symptoms of HFpEF. More work is necessary in larger animal models to confirm the beneficial results from our studies. Furthermore, selective antagonists of RBM20s interaction with titin may result in less off target side effects that may occur with full inhibition of RBM20. As awareness of post-transcriptional

modification of titin builds, development of small molecule inhibitors of RBM20 are likely to follow.

The N2B Knockout (KO) mouse

To address the role of titin as a mechanosensor for cardiac hypertrophy, studies were performed using the **N2B** KO murine model. Genetic deletion of exon 49 in the Ttn gene removed the cardiac specific N2B element in titin. This model is characterized by altered cardiac function, (enhanced systolic function and restrictive diastolic dysfunction) as revealed previously⁷ and in chapter 2. Furthermore, the N2B element is the chief localizer of four and a half LIM domains protein 2 (FHL2). FHL2 is a scaffolding protein that is expressed predominantly in the heart and has greater than 80 verified protein-protein interactions at the sarcolemma, cytoplasm and nucleus²⁹. Removing the N2B element in titin severely affects protein levels of FHL2 in the heart while transcript levels remain unaltered. Furthermore, N2B KO mice are characterized by cardiac atrophy while other spring element deletion models (Ig³⁰, PEVK³¹, IA that enhance FHL2 protein expression) have increased LV size compared to WT littermates. My work in chapter 2 establishes that the N2B element is necessary for hypertrophy in the heart in response to volume overload and *beta*-adrenergic stimulation.

In summary, the work in this thesis addresses whether titin might be a plausible therapeutic target for HFpEF and in particular whether increasing compliance of titin's spring region is beneficial in a HFpEF-like state in the mouse. Additionally, it tests

whether the mechanotransduction that occurs through titin's cardiac specific N2B spring element is important for stretch-activated cardiac remodeling.

Figure 1 of Introduction

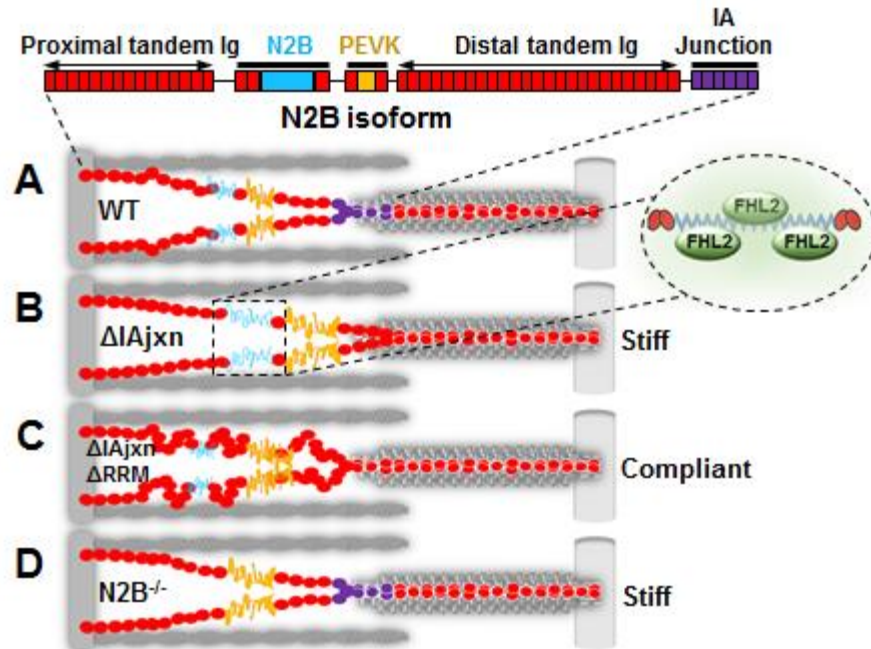


Figure 1. Schematic of cardiac titin isoforms in the half-sarcomere. Upper inset: the N2B isoform; Right inset: FHL2 localization to the N2B element in titin. Murine models used in dissertation work in (A-D): A) WT titin; B) $Ttn^{\Delta IAjxn}$; C) $Ttn^{\Delta IAjxn}$ crossed to $Rbm20^{ARRM}$; D) N2B KO.

References of Introduction

1. Trombitas K, Freiburg A, Centner T, Labeit S and Granzier H. Molecular dissection of N2B cardiac titin's extensibility. *Biophysical journal*. 1999;77:3189-96.
2. Trombitas K, Wu Y, Labeit D, Labeit S and Granzier H. Cardiac titin isoforms are coexpressed in the half-sarcomere and extend independently. *Am J Physiol Heart Circ Physiol*. 2001;281:H1793-9.
3. Guo W, Schafer S, Greaser ML, Radke MH, Liss M, Govindarajan T, Maatz H, Schulz H, Li S, Parrish AM, Dauksaite V, Vakeel P, Klaassen S, Gerull B, Thierfelder L, Regitz-Zagrosek V, Hacker TA, Saupe KW, Dec GW, Ellinor PT, MacRae CA, Spallek B, Fischer R, Perrot A, Ozcelik C, Saar K, Hubner N and Gotthardt M. RBM20, a gene for hereditary cardiomyopathy, regulates titin splicing. *Nature medicine*. 2012;18:766-73.
4. Neagoe C, Kulke M, del Monte F, Gwathmey JK, de Tombe PP, Hajjar RJ and Linke WA. Titin isoform switch in ischemic human heart disease. *Circulation*. 2002;106:1333-41.
5. Granzier HL, Hutchinson KR, Tonino P, Methawasin M, Li FW, Slater RE, Bull MM, Saripalli C, Pappas CT, Gregorio CC and Smith JE, 3rd. Deleting titin's I-band/A-band junction reveals critical roles for titin in biomechanical sensing and cardiac function. *Proc Natl Acad Sci U S A*. 2014;111:14589-94.
6. Methawasin M, Hutchinson KR, Lee EJ, Smith JE, 3rd, Saripalli C, Hidalgo CG, Ottenheijm CA and Granzier H. Experimentally increasing titin compliance in a

novel mouse model attenuates the frank-starling mechanism but has a beneficial effect on diastole. *Circulation*. 2014;129:1924-36.

7. Radke MH, Peng J, Wu Y, McNabb M, Nelson OL, Granzier H and Gotthardt M. Targeted deletion of titin N2B region leads to diastolic dysfunction and cardiac atrophy. *Proc Natl Acad Sci U S A*. 2007;104:3444-9.
8. Zile MR, Baicu CF, Ikonomidis JS, Stroud RE, Nietert PJ, Bradshaw AD, Slater R, Palmer BM, Van Buren P, Meyer M, Redfield MM, Bull DA, Granzier HL and LeWinter MM. Myocardial stiffness in patients with heart failure and a preserved ejection fraction: contributions of collagen and titin. *Circulation*. 2015;131:1247-59.
9. Nedrud J, Labeit S, Gotthardt M and Granzier H. Mechanics on myocardium deficient in the N2B region of titin: the cardiac-unique spring element improves efficiency of the cardiac cycle. *Biophysical journal*. 2011;101:1385-92.
10. Kruger M, Kotter S, Grutzner A, Lang P, Andresen C, Redfield MM, Butt E, dos Remedios CG and Linke WA. Protein kinase G modulates human myocardial passive stiffness by phosphorylation of the titin springs. *Circulation research*. 2009;104:87-94.
11. Borlaug BA and Paulus WJ. Heart failure with preserved ejection fraction: pathophysiology, diagnosis, and treatment. *European heart journal*. 2011;32:670-9.
12. Yusuf S, Pfeffer MA, Swedberg K, Granger CB, Held P, McMurray JJ, Michelson EL, Olofsson B and Ostergren J. Effects of candesartan in patients with chronic

- heart failure and preserved left-ventricular ejection fraction: the CHARM-Preserved Trial. *Lancet* (London, England). 2003;362:777-81.
13. Masoudi FA, Havranek EP, Smith G, Fish RH, Steiner JF, Ordin DL and Krumholz HM. Gender, age, and heart failure with preserved left ventricular systolic function. *Journal of the American College of Cardiology*. 2003;41:217-23.
 14. Steinberg BA, Zhao X, Heidenreich PA, Peterson ED, Bhatt DL, Cannon CP, Hernandez AF and Fonarow GC. Trends in patients hospitalized with heart failure and preserved left ventricular ejection fraction: prevalence, therapies, and outcomes. *Circulation*. 2012;126:65-75.
 15. Mentz RJ, Kelly JP, von Lueder TG, Voors AA, Lam CS, Cowie MR, Kjeldsen K, Jankowska EA, Atar D, Butler J, Fiuzat M, Zannad F, Pitt B and O'Connor CM. Noncardiac comorbidities in heart failure with reduced versus preserved ejection fraction. *Journal of the American College of Cardiology*. 2014;64:2281-93.
 16. van Heerebeek L and Paulus WJ. Understanding heart failure with preserved ejection fraction: where are we today? *Netherlands heart journal : monthly journal of the Netherlands Society of Cardiology and the Netherlands Heart Foundation*. 2016;24:227-36.
 17. Pitt B, Pfeffer MA, Assmann SF, Boineau R, Anand IS, Claggett B, Clausell N, Desai AS, Diaz R, Fleg JL, Gordeev I, Harty B, Heitner JF, Kenwood CT, Lewis EF, O'Meara E, Probstfield JL, Shaburishvili T, Shah SJ, Solomon SD, Sweitzer NK, Yang S and McKinlay SM. Spironolactone for heart failure with preserved ejection fraction. *The New England journal of medicine*. 2014;370:1383-92.

18. Zile MR, Baicu CF and Gaasch WH. Diastolic heart failure--abnormalities in active relaxation and passive stiffness of the left ventricle. *The New England journal of medicine*. 2004;350:1953-9.
19. van Heerebeek L, Borbely A, Niessen HW, Bronzwaer JG, van der Velden J, Stienen GJ, Linke WA, Laarman GJ and Paulus WJ. Myocardial structure and function differ in systolic and diastolic heart failure. *Circulation*. 2006;113:1966-73.
20. Borbely A, van der Velden J, Papp Z, Bronzwaer JG, Edes I, Stienen GJ and Paulus WJ. Cardiomyocyte stiffness in diastolic heart failure. *Circulation*. 2005;111:774-81.
21. van Heerebeek L, Hamdani N, Falcao-Pires I, Leite-Moreira AF, Begieneman MP, Bronzwaer JG, van der Velden J, Stienen GJ, Laarman GJ, Somsen A, Verheugt FW, Niessen HW and Paulus WJ. Low myocardial protein kinase G activity in heart failure with preserved ejection fraction. *Circulation*. 2012;126:830-9.
22. Kruger M, Kotter S, Grutzner A, Lang P, Andresen C, Redfield MM, Butt E, dos Remedios CG and Linke WA. Protein kinase G modulates human myocardial passive stiffness by phosphorylation of the titin springs. *Circulation research*. 2009;104:87-94.
23. Anderson BR and Granzier HL. Titin-based tension in the cardiac sarcomere: molecular origin and physiological adaptations. *Prog Biophys Mol Biol*. 2012;110:204-17.

24. Hudson B, Hidalgo C, Saripalli C and Granzier H. Hyperphosphorylation of mouse cardiac titin contributes to transverse aortic constriction-induced diastolic dysfunction. *Circulation research*. 2011;109:858-66.
25. LeWinter MM and Granzier HL. Cardiac titin and heart disease. *J Cardiovasc Pharmacol*. 2014;63:207-12.
26. Degen CV, Bishu K, Zakeri R, Ogut O, Redfield MM and Brozovich FV. The emperor's new clothes: PDE5 and the heart. *PLoS One*. 2015;10:e0118664.
27. Bishu K, Hamdani N, Mohammed SF, Kruger M, Ohtani T, Ogut O, Brozovich FV, Burnett JC, Jr., Linke WA and Redfield MM. Sildenafil and B-type natriuretic peptide acutely phosphorylate titin and improve diastolic distensibility in vivo. *Circulation*. 2011;124:2882-91.
28. Lee DI, Zhu G, Sasaki T, Cho GS, Hamdani N, Holewinski R, Jo SH, Danner T, Zhang M, Rainer PP, Bedja D, Kirk JA, Ranek MJ, Dostmann WR, Kwon C, Margulies KB, Van Eyk JE, Paulus WJ, Takimoto E and Kass DA. Phosphodiesterase 9A controls nitric-oxide-independent cGMP and hypertrophic heart disease. *Nature*. 2015;519:472-6.
29. Tran MK, Kurakula K, Koenis DS and de Vries CJM. Protein–protein interactions of the LIM-only protein FHL2 and functional implication of the interactions relevant in cardiovascular disease. *Biochimica et Biophysica Acta (BBA) - Molecular Cell Research*. 2016;1863:219-228.
30. Chung CS, Hutchinson KR, Methawasin M, Saripalli C, Smith JE, 3rd, Hidalgo CG, Luo X, Labeit S, Guo C and Granzier HL. Shortening of the elastic tandem

immunoglobulin segment of titin leads to diastolic dysfunction. *Circulation*. 2013;128:19-28.

31. Granzier HL, Radke MH, Peng J, Westermann D, Nelson OL, Rost K, King NM, Yu Q, Tschope C, McNabb M, Larson DF, Labeit S and Gotthardt M. Truncation of titin's elastic PEVK region leads to cardiomyopathy with diastolic dysfunction. *Circulation research*. 2009;105:557-64.

CHAPTER 1

**Alternative Splicing of Titin Restores Diastolic Function
and Improves HFpEF Associated Symptoms in a Genetic
Murine Model (*Ttn* ^{$\Delta IAxn$})**

Abstract

Rationale – HFpEF patients experience elevated filling pressures and reduced ventricular compliance. The splicing factor RBM20 regulates the contour length of titin's spring region and thereby determines the passive stiffness of cardiomyocytes. Inhibition of RBM20 leads to super compliant titin isoforms (N2BAsc) that reduce passive stiffness.

Objective – To determine the therapeutic potential of upregulating compliant titin isoforms in a HFpEF-like state in the mouse.

Methods and Results – Constitutive and inducible cardiomyocyte specific RBM20 inhibited mice were produced on a *Ttn*^{Δ*Ajxn*} background to assess the effect of upregulating compliant titin at the cellular and organ levels. Genetic deletion of the I-band – A-band junction (*IAjxn*) in titin increases strain on the spring region and causes a HFpEF-like syndrome in the mouse without pharmacological or surgical intervention. The increased strain represents a mechanical analogue of deranged post-translational modification of titin that results in increased passive myocardial stiffness in HFpEF patients. Upon inhibition of RBM20 in *Ttn*^{Δ*Ajxn*} mice, compliant titin isoforms were expressed and diastolic function was normalized, exercise performance was improved and pathologic hypertrophy was attenuated.

Conclusions – We report for the first time a benefit from upregulating compliant titin isoforms in a murine model with HFpEF-like symptoms. Constitutive and inducible RBM20 inhibition improves diastolic function resulting in greater tolerance to exercise. No effective therapies exist for treating this pervasive syndrome, therefore our data on RBM20 inhibition are clinically significant.

Introduction

Greater than half of all heart failure (HF) patients suffer from increased diastolic stiffness and impaired relaxation of the left ventricle while their ejection fraction (EF) is preserved (HFpEF)¹. HFpEF is a complex syndrome that includes diastolic dysfunction, exercise intolerance, and concentric hypertrophic remodeling^{2, 3}. No effective therapies exist for treating this pervasive syndrome due in part to the limited understanding of the underlying pathophysiology. Titin, the largest known protein and molecular spring in the heart, has emerged as a prime therapeutic target aimed at restoring compliance to the sarcomere and thereby improving diastolic function⁴. The titin gene (TTN) contains 364 exons that encode the third myofilament of the sarcomere that spans from Z-disk to M-band⁵. Titin's I-band region acts as a molecular spring that is responsible for maintaining the structural integrity of the sarcomere⁶. Additionally, titin's molecular spring is the chief contributor of passive stiffness in the heart, and functions as a mechano-sensor for stress and strain in the myocyte⁷. Alternative splicing produces two main cardiac isoforms; the smaller N2B isoform (~3.0 MDa) and the larger more compliant N2BA isoform (~3.3 MDa). Diastolic stiffness of the left ventricle is in large part dependent upon the N2BA:N2B isoform ratio⁸. Stiffness can also be tuned through post-translational modification (PTM) of these primary isoforms, particularly through phosphorylation of titin's spring region⁹⁻¹¹.

PTM of titin's spring region is deranged in HFpEF patients^{4, 12}, which contributes to increased diastolic stiffness. Since protein kinase G (PKG) phosphorylation of titin's N2B element enhances spring compliance, targeted treatment of HFpEF by enhancing PKG activity with the phosphodiesterase(PDE)5 inhibitor sildenafil was performed

(summarized in the recent RELAX trial)¹³, however, exercise capacity was unimproved and clinical outcomes were similar to placebo¹³. Another potential therapeutic approach is upregulation of compliant titin isoforms. Alternative splicing of messenger RNA occurs primarily in transcripts encoding the spring region of titin and therefore regulates the elastic properties of titin through changes in contour length of the spring. Since the discovery of RBM20 as a titin splicing factor^{10, 14}, modification of titin size through RBM20 inhibition has become possible.

The current study evaluates whether manipulating post-transcriptional modification of titin isoforms through reduction of the titin splicing factor RBM20 has a beneficial effect on the diastolic function of mice with restrictive cardiomyopathy. A previously published mouse model¹⁵ deficient in titin's IA junction (*Ttn*^{ΔIAjxn}) places increased strain on the spring region of titin. The *Ttn*^{ΔIAjxn} mouse is a choice tool for studying diastolic dysfunction as this model displays similar phenotypic characteristics found in the HFpEF patients, notably diastolic dysfunction, reduced exercise tolerance and concentric remodeling of the left ventricular chamber in response to stress. Furthermore, all known signaling elements in titin remain intact and therefore the pathology can be attributed solely to increases in titin-based strain. We aimed to determine if inhibition of RBM20 could recover function in this model back to a wild-type (WT) state. Our data establish that inhibiting titin splicing factor RBM20 in the *Ttn*^{ΔIAjxn} mouse improves diastolic function, restores exercise tolerance, and attenuates afterload induced pathologic concentric remodeling.

Materials and Methods

Generation of mice homozygous for $Ttn^{\Delta I Ajxn}$ and heterozygous for cardiac specific $Rbm20^{\Delta RRM}$

We bred two previously published murine models the $Ttn^{\Delta I Ajxn}$ ² and the cardiac specific $Rbm20^{\Delta RRM}$ ¹ in order to compare effects of increased or decreased strain in titin, respectively. To study the effect of RBM20 inhibition in $Ttn^{\Delta I Ajxn}$ mice we crossed these two models to create hybrid $Ttn^{\Delta I Ajxn}$ mice with intermediate expression levels of WT RBM20, abbreviated $\Delta I Ajxn/\Delta RRM$; details in supplemental Figure 1. Additionally, we used a Tg(Myh6-cre/Esr1) mouse strain (Jackson Laboratory) that has the mouse Myh6 promoter (myosin, heavy polypeptide 6, cardiac muscle, alpha; alpha-MHC) directing expression of a selective estrogen receptor modulator (SERM) inducible Cre recombinase (Mer-Cre-Mer) to cardiac myocytes. Mer-Cre-Mer engineered $\Delta I Ajxn/\Delta RRM$ mice were injected intraperitoneal with raloxifene (40 mg/kg) or vehicle for 8 days to induce reduction of WT RBM20. After day 28, mice were examined by echo and catheterization and then euthanized. Hearts were dissected, weighed and flash frozen at -80°C for further titin isoform analysis using standard procedures (Supplemental Methods).

Protein Expression Analysis

Protein expression analysis was performed by using standard gel electrophoresis methods³.

Cell Mechanics

Skinned cardiac myocyte mechanics were performed as previously reported⁴. (See Supplemental Methods for details.)

Hemodynamics

Anesthetized and conscious echocardiography was performed on mice and pressure volume relations were evaluated using admittance-based cardiac catheterization. Cardiac function in diastole was assessed in mice using continuous flow two percent isoflurane inhaled anesthetic with a target heart rate of 450 ± 25 bpm. (See Supplemental Methods for details.)

Exercise Performance

Exercise tolerance was evaluated by measuring time and distance ran using a treadmill running test. Exercise capacity was studied by measuring average and max speed in *Ttn*^{ΔIAjxn} and *Ttn*^{ΔIAjxn} mice expressing compliant N2BAsc titin given access to a voluntary running wheel for 3 weeks (see Supplemental Methods for details).

TAC Surgery

Male mice 3-4 months old were subjected to minimally invasive transverse aortic constriction (TAC)⁵ performed under Ketamine/Xylazine (120/12 mg/kg) anesthesia; details are explained in the Supplemental methods. Briefly, 27-gauge needle was used for banding and mice were studied by echocardiography at 28 days and then euthanized. Hearts were immediately dissected, weighed and frozen for further analysis. Experiments were approved by the University of Arizona Institutional Animal Care and Use Committee

and followed the U.S. National Institutes of Health *Using Animals in Intramural Research guidelines for animal use*.

Statistics

Statistical analysis was performed in Graphpad Prism (GraphPad Software, Inc). Group significance was defined using one or two-way ANOVA followed by multiple testing correction. Student t-test was used in figures 3A and 4A-D. Linear and non-linear regression analysis testing whether slopes are significantly different from one another in figure 4 E-F. Results are shown as mean \pm standard error of the mean. $P < 0.05$ was considered significant.

Results

Inhibition of Rbm20 upregulates super compliant titin isoforms (N2BA_{sc}) and normalizes passive stiffness in cardiomyocytes of $Ttn^{ΔIAjxn}$ mice

$Rbm20^{ARRM}$ mice are deficient in titin splicing factor RBM20 and as previously described¹, they upregulate large N2BA titin isoforms that we refer to as super compliant titin (N2BA_{sc}) (see Figure 1 A for model description). Mice deficient of the IA junction in titin ($Ttn^{ΔIAjxn}$) have normal expression of the adult N2B and N2BA isoforms, however, both are reduced in size as revealed by their slight increase in mobility in gel electrophoresis (compare Fig. 1 B left and middle lanes). The larger and more compliant N2BA isoform (~3.3 MDa in WT and ~3.15 MDa in $Ttn^{ΔIAjxn}$) comprises ~ 20 percent of total titin in both genotypes (Fig. 1B, left and middle bar). It was recently shown that moving the attachment point of titin's spring region away from the Z-disk results in greater titin strain in $Ttn^{ΔIAjxn}$ mice².

To determine the therapeutic potential of RBM20 inhibition, we bred $Ttn^{ΔIAjxn}$ mice with cardiac specific $Rbm20^{ARRM}$ mice in order to produce $Ttn^{ΔIAjxn}$ mice that are heterozygous deficient in splicing factor RBM20 (see Fig. S1 for more detail). $Ttn^{ΔIAjxn}$ mice constitutively inhibiting RBM20 express super compliant N2BA titin isoforms estimated ~3.35 and ~3.45 MDa (Fig. 1 B, right lane; Table S1) encompassing 80% of total titin in the murine left ventricle (Fig. 1 C, right bar). Altering the size of titin had no significant effect on normalized cardiac tissue weights (Table S2). Thus, heterozygous

inhibition of the titin splicing factor RBM20 is highly effective in upregulating compliant titin (see Table S1).

Previously we have shown that altering titin size and therefore strain on titin's spring region directly affects passive stress in skinned left ventricular (LV) cardiomyocytes². We tested whether inhibiting RBM20 in *Ttn*^{ΔA₁Δ₂} mice reduces the elevated diastolic stress in skinned myocytes to WT levels. Cardiomyocytes were skinned and isolated in relaxing solution and cells were attached at one end to a force transducer and at the other end to a servomotor and subjected to a stretch–hold–release protocol using standard procedures (see Supplemental Methods for details). Passive stress was significantly increased in *Ttn*^{ΔA₁Δ₂} mice but was normalized in *Ttn*^{ΔA₁Δ₂} mice expressing super compliant titin (Fig. 1 D). Passive stiffness (slope of stress–sarcomere length (SL) relation within physiologic SL range) was similarly reduced to WT levels (Fig. 1 E).

*Reduction of RBM20 expression restores diastolic function to *Ttn*^{ΔA₁Δ₂} mice*

Results on the cellular level were further evaluated at the organ level to assess cardiac function in diastole. Pulse wave Doppler in the 4-chamber apical view revealed significant differences in mitral valve deceleration time (MVDT) and E/A ratios of *Ttn*^{ΔA₁Δ₂} mice compared to WT control, indicating diastolic dysfunction (Fig. 2 A, D-E and Table 1). A greater E/A ratio in *Ttn*^{ΔA₁Δ₂} mice (1.5 ± 0.1 vs. 1.3 ± 0.03 in WT) indicates higher LV filling pressures, and this was improved to WT levels in *Ttn*^{ΔA₁Δ₂} mice expressing super compliant titin (1.2 ± 0.03). Additionally, the MVDT is significantly reduced in *Ttn*^{ΔA₁Δ₂} mice (21.9 ± 1.0 vs. 25.9 ± 0.7 ms in WT), a parameter inversely related to diastolic

stiffness⁶. The MVDT was found to be at WT levels (26.5 ± 1.5 ms) in *Ttn^{ΔIAjxn}* mice expressing N2BAsc titin, indicating restored LV chamber compliance.

Concurring with echocardiography, diastolic dysfunction was also demonstrated in *Ttn^{ΔIAjxn}* mice using high fidelity pressure-volume admittance catheters. Occlusion of the inferior vena cava allowed us to determine the slope of the end-diastolic pressure-volume relationship (EDPVR), β , which is a load-independent parameter (Fig. 2 B-C and Table 1). The EDPVR (β) is the coefficient of stiffness in the LV and was found to be in 0.03 ± 0.004 mmHg/ μ L in WT mice. *Ttn^{ΔIAjxn}* mice had an elevated EDPVR (β) of 0.08 ± 0.01 mmHg/ μ L that was normalized to WT levels in *Ttn^{ΔIAjxn}* mice expressing N2BAsc titin (0.02 ± 0.002 mmHg/ μ L), (Fig. 2 F and Table 1). Therefore, consistent with our skinned cell experiments, compliance in the LV chamber was recovered in *Ttn^{ΔIAjxn}* mice deficient in splicing factor RBM20.

We further examined diastolic recovery of *Ttn^{ΔIAjxn}* mice with inducible (α -MHC-MCM *Rbm20^{ΔRRM}*) N2BAsc titin expression (see breeding scheme in Fig. S1 for further details). This evaluation is important because it allows us to test whether diastolic dysfunction, once it has occurred, is recoverable therapeutically by upregulating compliant titin. Inducible MCM-*Ttn^{ΔIAjxn}* mice were echoed at day 0 and then injected intraperitoneal for 8 days with either vehicle or selective estrogen receptor modulator (SERM) raloxifene (see Methods for additional details). Pilot studies determined that 8 days of raloxifene injections resulted in greater than 60% N2BAsc titin expression at 28 days (Fig. 3 A, Table S1). At day 28, mice were echoed to assess diastolic function and then evaluated with a terminal cardiac catheterization procedure for studying the effect of expressing N2BAsc titin. Similar to our constitutive model, diastolic function was improved in the inducible

mice as shown by pulse-wave Doppler revealing significant reductions in the E/A ratio and a greater duration of the mitral valve deceleration time (Fig. 3 B and C). Moreover, pressure volume loop analysis showed a significant improvement of the EDPVR (β) upon induction of N2BAsc expression (Fig. 3 D). Systolic function was unaltered between vehicle and treatment groups (Table S3). Thus, reducing strain in titin, has a beneficial effect on the diastolic function of a stiff left ventricle.

Assessment of associated HFpEF symptoms

Exercise capacity is reduced in patients with diastolic dysfunction and HFpEF patients are characterized by exercise intolerance^{7, 8}, similarly *Ttn*^{*ΔIAjxn*} mice have reduced exercise capacity¹. We tested whether upregulating compliant titin has a beneficial effect on exercise performance. When given access for three weeks to a voluntary running wheel, *Ttn*^{*ΔIAjxn*} mice constitutively expressing N2BAsc titin had a slight but significantly higher average (Fig. 4 A) and maximal running speed than *Ttn*^{*ΔIAjxn*} mice (Fig. 4 B). We also submitted these mice to an exercise tolerance test (incremental speed running on a treadmill), and mice with compliant titin ran longer and for a greater distance in both the constitutive (Fig. 4 C and D) and the inducible N2BAsc expressing models (Fig. 4 E and F). Overall these findings suggest that increasing titin compliance in the heart has a beneficial effect on exercise performance in the *Ttn*^{*ΔIAjxn*} murine model.

In addition to exercise intolerance, concentric remodeling in the heart is a common clinical manifestation in HFpEF patients⁹. We therefore tested the responsiveness of mice with differing strain in titin to afterload stress. Mice were subjected to minimally invasive

transverse aortic constriction (TAC) surgery, a procedure widely used to elicit afterload-dependent hypertrophic remodeling in the left ventricle. Compared to WT mice, *Ttn*^{ΔIAjxn} mice displayed an exaggerated hypertrophic response to TAC ($p = 0.0001$), whereas the LV hypertrophy response in *Ttn*^{ΔIAjxn} mice expressing N2BAsc titin did not significantly differ from WT mice (Figure 5 A). The degree of remodeling these mice experienced in the left ventricle was determined by measuring the left ventricular end diastolic diameter (LVDD) and the relative wall thickness (WT) in diastole. These parameters were obtained using motion mode echocardiography of the left ventricle in the short axis view. By calculating WT/LVDD we can assess the degree to which the left ventricle is concentrically remodeled in response to TAC. Robust concentric remodeling after 4 weeks of pressure overload was observed in WT and *Ttn*^{ΔIAjxn} mice with the largest values in *Ttn*^{ΔIAjxn} mice, however, remodeling was lessened significantly in *Ttn*^{ΔIAjxn} mice expressing N2BAsc titin (Fig. 5B). In addition to reduced pathologic remodeling, *Ttn*^{ΔIAjxn} mice with upregulated compliant titin also exhibited superior diastolic function as revealed by Doppler imaging (Fig. 5 C-D). This data suggests that varying the length of titin isoforms alters the responsiveness to pressure overload hypertrophy in the heart and that increasing titin compliance may be advantageous for preventing diastolic dysfunction associated with afterload induced concentric remodeling of the heart.

The cardiac-specific N2B spring element in titin has long been thought to be involved in mechano-sensing and signaling in the sarcomere¹⁰ and we investigated the possible role of spring element binding partners, α B-crystallin¹¹ and four-and-a half LIM proteins 1 and 2 (FHL1 and FHL2)¹². α B-crystallin was found to be similarly expressed across genotypes and did not significantly differ in response to TAC (Fig. 6 A and D). In

contrast, FHL1 protein levels were upregulated in response to aortic constriction across genotypes, and in agreement with the previously published role of FHL1^{13, 14} in response to afterload stress. FHL2 was found to be upregulated in *Ttn^{ΔA_{ixn}}* mice (Fig. 6 C and F), however protein levels were not significantly changed in response to TAC suggesting that pressure overload signaling involves FHL1 rather than FHL2.

Chapter 1 Table 1

Hemodynamics

	WT	<i>Ttn</i> ^{ΔIAjxn}	Δ IAjxn/ Δ RRM		
<i>Echocardiography</i>					
n	8	8	8	}	
HR (bpm)	650.5 ± 10.3	650.5 ± 13.4	669.0 ± 9.3		Conscious
FS (%)	65.2 ± 1.8	57.5 ± 3.2	52.4 ± 1.7 **		
LVID;d (mm)	2.7 ± 0.1	2.8 ± 0.2	3.0 ± 0.1		
LVID;s (mm)	1.0 ± 0.1	1.2 ± 0.2	1.4 ± 0.1		
LVPW;d (mm)	1.1 ± 0.03	1.2 ± 0.1	1.1 ± 0.1		
LVPW;s (mm)	1.9 ± 0.1	1.8 ± 0.1	1.7 ± 0.1		
LVDD/WT (ratio)	2.5 ± 0.2	2.6 ± 0.3	2.7 ± 0.1		
<i>Heart rate maintained at 450 ± 25 (bpm)</i>					
LA Diameter (mm)	2.4 ± 0.2	2.7 ± 0.1	2.9 ± 0.1	}	
MV Decel Time (ms)	25.9 ± 0.7	21.9 ± 1.0 **	26.5 ± 1.5 ††		Anesthetized
MV E (mm/s)	770.5 ± 37.2	835.4 ± 22.7	780.7 ± 28.0		
MV A (mm/s)	621.6 ± 35.8	547.4 ± 14.2	650.9 ± 26.9 †		
MV E/A	1.3 ± 0.03	1.5 ± 0.04 ****	1.2 ± 0.03 ††††		
<i>Cardiac Catheterization</i>					
n	7	7	7		
HR (BPM)	431.3 ± 7.0	457.1 ± 23.2	484.0 ± 5.9		
ESP (mmHg)	98.4 ± 3.7	98.7 ± 6.9	96.2 ± 2.5		
EDP (mmHg)	2.8 ± 0.9	3.8 ± 1.0	1.2 ± 0.2		
dPmax (mmHg/sec)	7114.9 ± 368.2	8257.2 ± 667.2	9131.7 ± 259.0 *		
dPmin (mmHg/sec)	-8069.4 ± 354.2	-7073.2 ± 254.7	-9007.4 ± 231.1 †††		
ESV (uL)	36.7 ± 6.9	33.9 ± 3.2	22.5 ± 3.3		
EDV (uL)	73.0 ± 7.0	73.6 ± 4.1	59.5 ± 4.0		
SV (uL)	36.3 ± 1.4	39.7 ± 3.4	37.0 ± 1.9		
EF (%)	52.8 ± 5.0	53.9 ± 3.5	62.9 ± 3.2		
EA (mmHg/uL)	2.7 ± 0.2	2.3 ± 0.1	2.7 ± 0.2		
Tau Glantz (ms)	12.2 ± 2.9	18.2 ± 4.5	10.0 ± 0.3		
ESPVR	4.9 ± 1.0	2.9 ± 0.2	3.1 ± 0.4		
EDPVR	0.03 ± 0.004	0.08 ± 0.01 ****	0.02 ± 0.002 ††††		

Table 1: Data shown as mean ± SEM. Abbreviations: Δ IAjxn: (*Ttn* ^{Δ IAjxn}); Δ RRM (*Rbm20* ^{Δ RRM+/-}); HR: heart rate; BPM: beats per minute; FS: fractional shortening; LVIDd: left ventricular internal diastolic diameter; LVIDs; left ventricular internal systolic diameter; LVPWd: left ventricular posterior wall thickness in diastole; LVPWs: left

ventricular posterior wall thickness in systole. Eccentricity: LVDD/WT; MV DT: mitral valve deceleration time; E/A: LV pulse wave Doppler ratio; LA: left atrium PV: All measurements were obtained during a pause in ventilation. Inferior venal caval occlusions were performed to assess load - independent parameters. ESP: end - systolic pressure; EDP: end - diastolic pressure; ESV: end systolic volume; EDV: end - diastolic volume; EF: ejection fraction; Ea: effective arterial elastance; ESPVR: end - systolic PV relationship; EDPVR: end - diastolic PV relationship. Statistical significance calculated with one-way ANOVA with Bonferroni correction: * $p < 0.05$; ** $p < 0.01$; *** $p < 0.001$; **** $p < 0.0001$; (versus WT ****, versus IA^{-/††††}).

Chapter 1 Figure 1

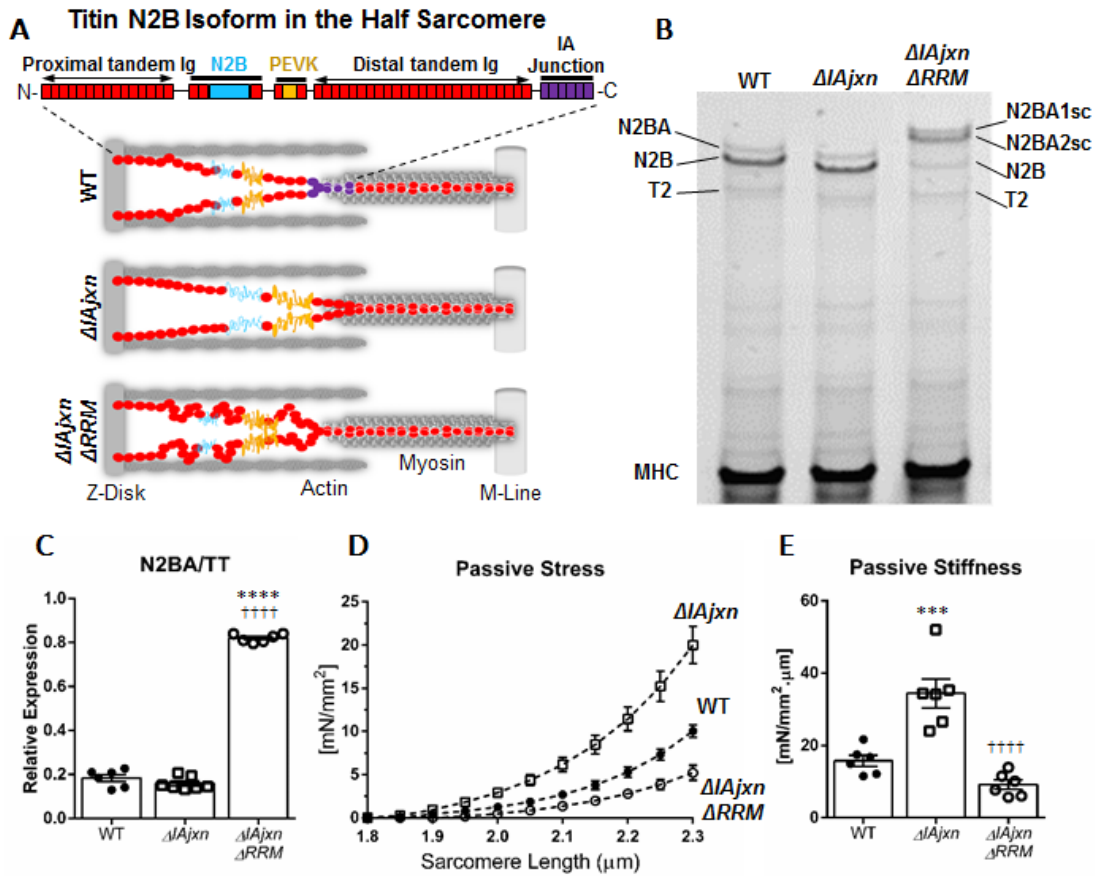


Figure 1: A) Half sarcomere models of 3 genotypes used in this work: WT, $\Delta IAjxn$ and $\Delta IAjxn/\Delta RRM$. The domain composition of titin's spring region (N2B isoform) is shown at the top. B) Representative image of 1% agarose gel for titin analysis of LV myocardium. WT myocardium expresses N2BA and N2B titin (T2 is a minor degradation product). The $\Delta IAjxn$ mouse expresses titin with a slightly higher mobility consistent with the deletion of the IA junction. Crossing the $\Delta IAjxn$ with the ΔRRM mouse results in expression of two very large N2BA isoforms that we refer to as super compliant (N2BA_{sc}). C) Ratio of N2BA isoforms over total titin. D) Representative skinned cardiomyocyte with passive stress in cardiomyocytes. E). Passive stiffness in cardiomyocytes. Abbreviations: $\Delta IAjxn$: *Ttn* ^{$\Delta IAjxn$} ; ΔRRM : *Rbm20* ^{ΔRRM} α MHC); N2BA_{sc}: super compliant N2BA titin. Data shown as mean \pm SEM. Statistical significance calculated by one-way ANOVA with Bonferroni correction: $p < 0.05$; versus WT ****, versus $\Delta IAjxn$ ††††).

Chapter 1 Figure 2

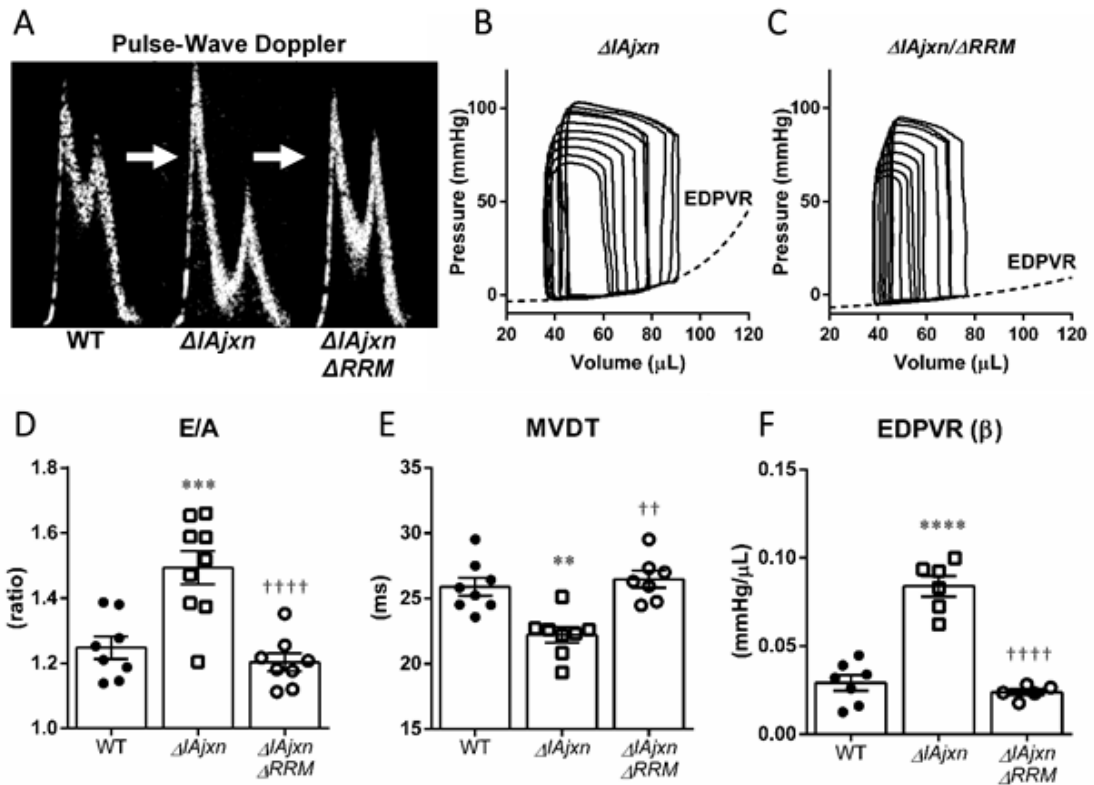


Figure 2: Diastolic function of $Ttn^{\Delta IAjxn}$ mice and $Ttn^{\Delta IAjxn}$ mice constitutively expressing N2BAsc. A) Representative pulse-wave Doppler E and A waves; B-C) cardiac catheterization PV loops; D) E/A ratio; E) MVDT: mitral valve deceleration time; F) Stiffness coefficient β of EDPVR (end-diastolic pressure volume relationship). Data shown as mean \pm SEM. Statistical significance calculated by one-way ANOVA with Bonferroni correction: $p < 0.05$; versus WT ****, versus $\Delta IAjxn$ ††††).

Chapter 1 Figure 3

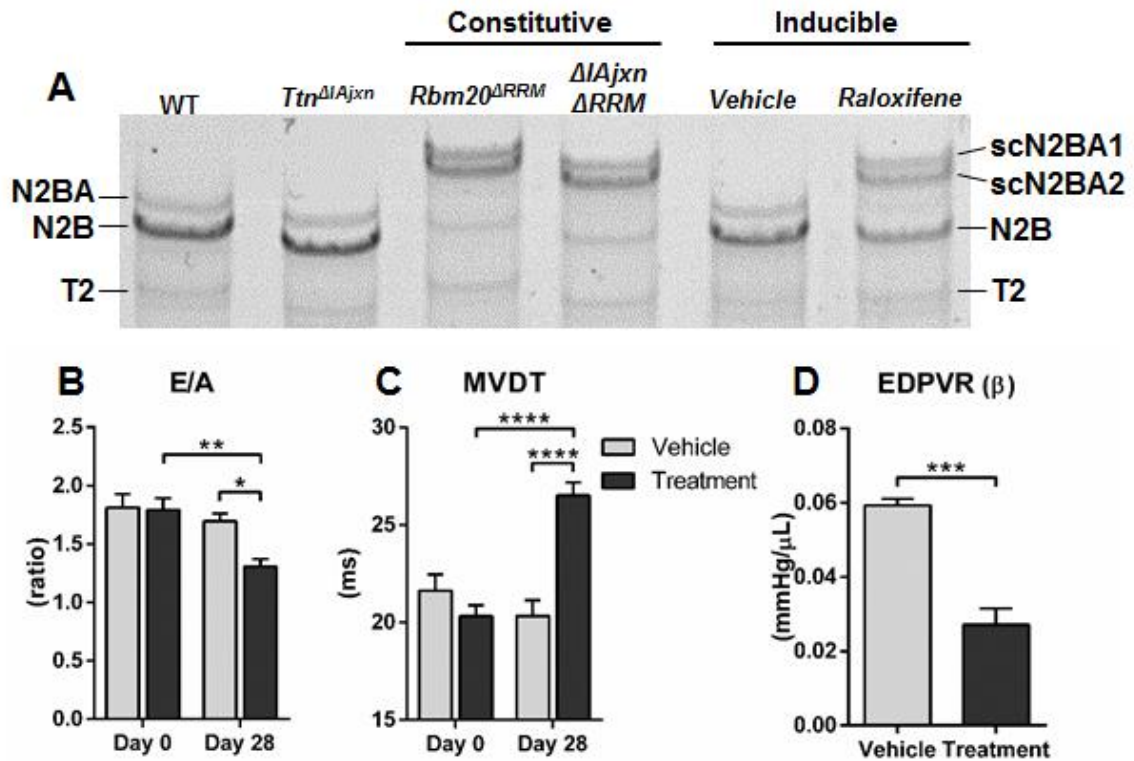


Figure 3: Diastolic function *Ttn*^{ΔIAjxn} mice and *Ttn*^{ΔIAjxn} mice with inducible expression of N2BAsc. A) Representative image of 1% agarose gel for titin analysis of LV myocardium. WT myocardium expresses N2BA and N2B titin (T2 is a minor degradation product). Crossing the *ΔIAjxn* with the *ΔRRM* mouse results in expression of two very large N2BA isoforms (scN2BA1 and 2). Right gel image: MCM-inducible *ΔIAjxn/ΔRRM*; Vehicle: DMSO and saline (50/50 mixture); Treatment: raloxifene dissolved in DMSO and saline (50/50 mixture). B) E/A ratio; C) MVDT: mitral valve deceleration time; D) EDPVR (β): end diastolic pressure volume relationship. Data shown as mean ± SEM. Statistical significance calculated with two-way ANOVA and Bonferroni correction (B and C) or t-test (D), (* p<0.05; ** p<0.01; *** p<0.001; **** p<0.0001 as indicated).

Chapter 1 Figure 4

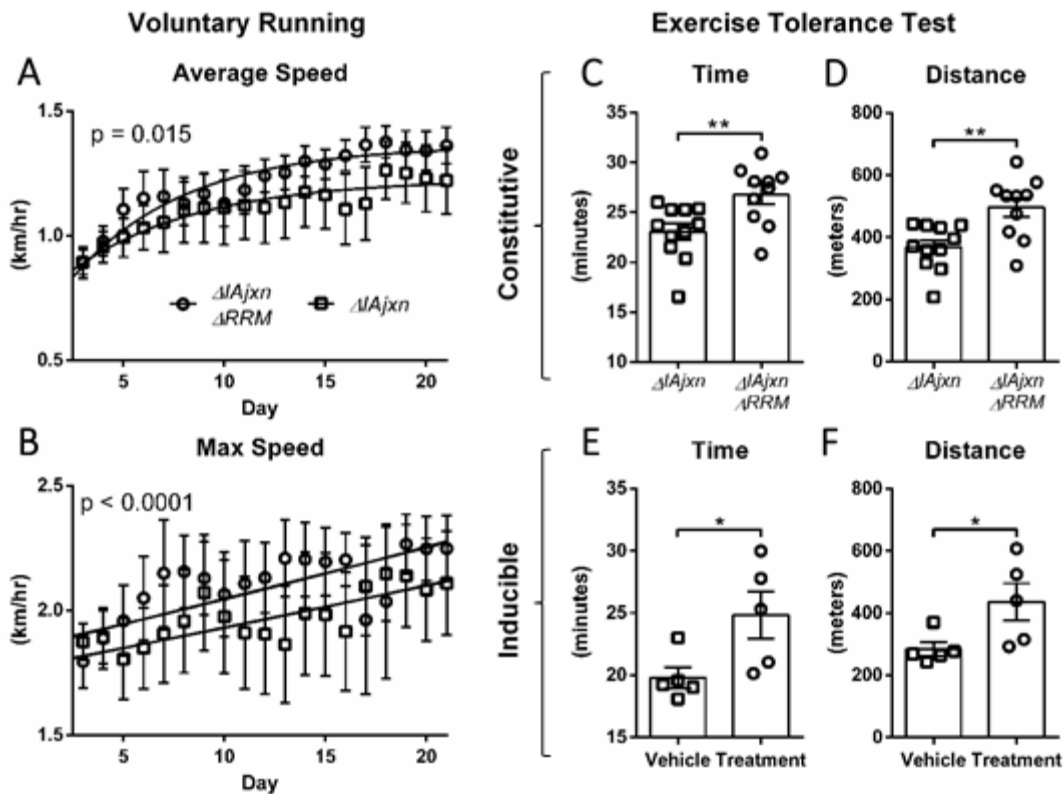


Figure 4: Mice with upregulated compliant titin display enhanced exercise performance.

A) Voluntary running wheel max speed of $Ttn^{\Delta IAjxn}$ mice and $Ttn^{\Delta IAjxn}$ mice constitutively expressing N2BAsc; B) Voluntary running wheel average speed C-D) Time and distance ran on treadmill of $Ttn^{\Delta IAjxn}$ mice and $Ttn^{\Delta IAjxn}$ mice constitutively expressing N2BAsc; E-F) Time and distance of $Ttn^{\Delta IAjxn}$ mice and $Ttn^{\Delta IAjxn}$ mice with inducible expression of N2BAsc. Data shown as mean \pm SEM. Statistical significance calculated with either t-test (C-F), linear (A) and non-linear (B) regression analysis testing whether lines are significantly different from one another : * $p < 0.05$ considered significant.

Chapter 1 Figure 5

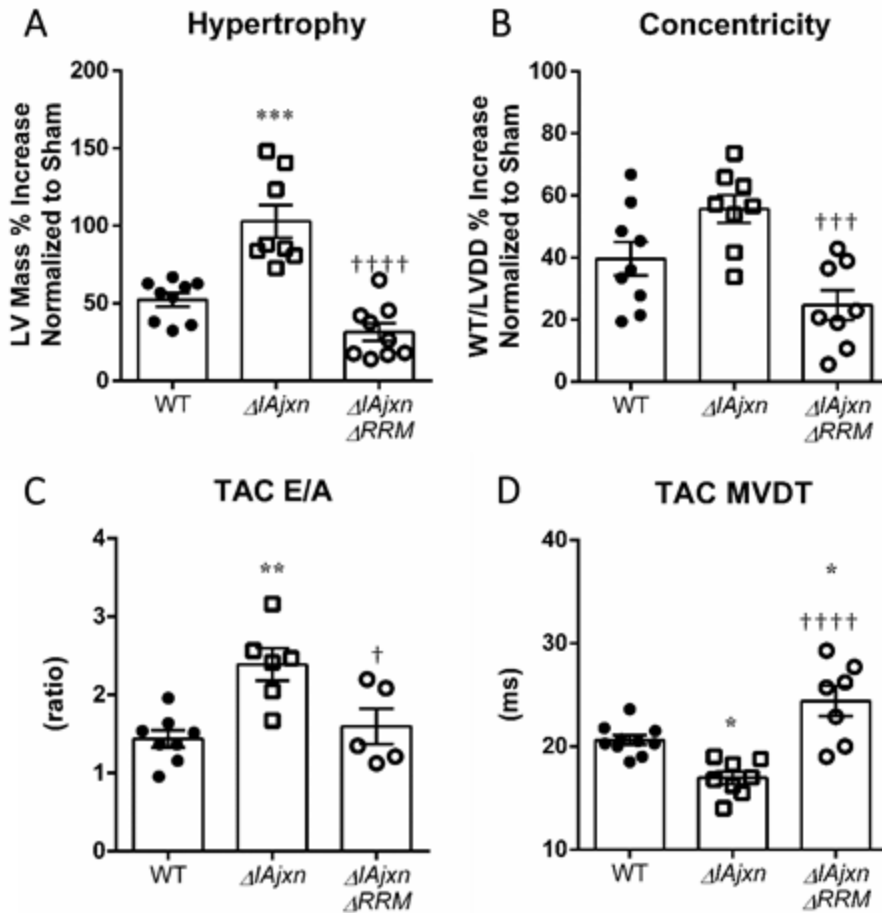


Figure 5: Increased strain on the N2B element of $Ttn^{\Delta IAjxn}$ mice results in an exaggerated response to TAC. A) Hypertrophy; B) Concentricity: WT: wall thickness in diastole; LVDD: left ventricular diameter in diastole. C) E/A ratio. D) MVDT: mitral valve deceleration time. Data shown as mean \pm SEM. Statistical significance calculated by one or two-way ANOVA with Bonferroni correction: * $p < 0.05$; ** $p < 0.01$; *** $p < 0.001$; **** $p < 0.0001$; (versus WT ****, versus $Ttn^{\Delta IAjxn}$ ††††).

Chapter 1 Figure 6

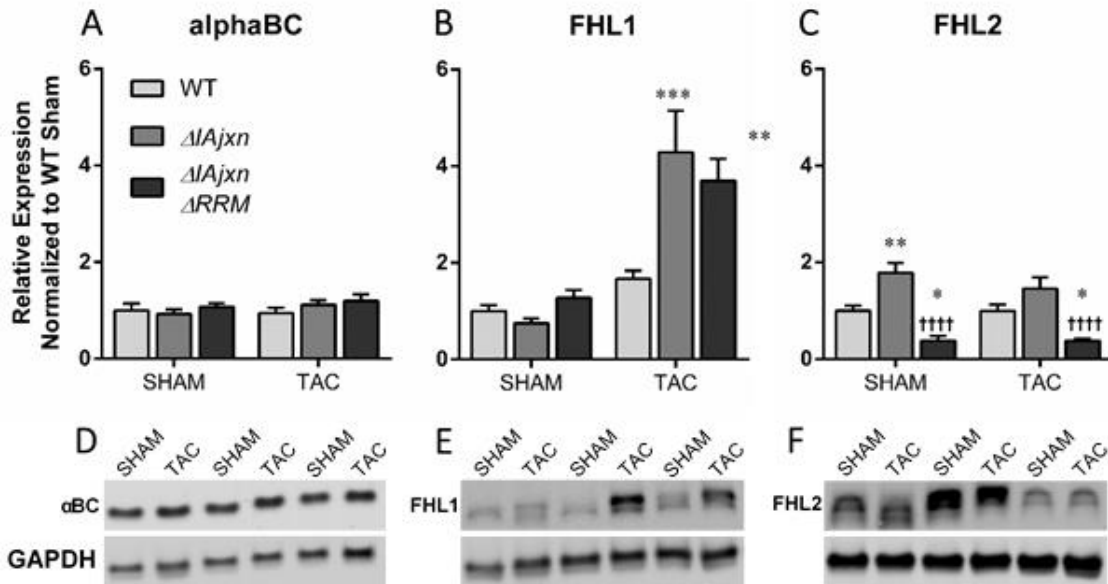


Figure 6: N2B element localized binding proteins and response to TAC. A and D) αB -crystallin; B and E) FHL1; C and F) FHL2. Data shown as mean \pm SEM. Statistical significance calculated by two-way ANOVA with Bonferroni correction: * $p < 0.05$; ** $p < 0.01$; *** $p < 0.001$; **** $p < 0.0001$; (versus WT ****, versus $\Delta IAjxn$ †††).

Discussion and Summary

We report for the first time a rescue of a HFpEF-like phenotype in the mouse through inhibition of the titin splicing factor RBM20. The *Ttn*^{ALA_{ixn}} murine model acts as a mechanical analogue of the titin-based increase in passive myocardial stiffness found in HFpEF patients¹⁵. This HFpEF-like phenotype is apparent as early as 3 months in the adult mouse and becomes exaggerated with age (Fig. S2) in the absence of pharmacological or surgical intervention. By using the *Ttn*^{ALA_{ixn}} mouse as a model of HFpEF we demonstrate that inhibiting RBM20 restores diastolic function, improves exercise tolerance and attenuates afterload induced pathologic remodeling of the left ventricle. Due to our still limited understanding of HFpEF pathophysiology, there are no specific therapies to treat this widespread disease, therefore our findings on RBM20 inhibition are clinically significant.

Cardiac titin's I-band region is a ~1.0 MDa spring composed of three distinct elements: the tandemly arranged immunoglobulin-like (Ig) element, the cardiac specific N2B element, and the proline, glutamate, valine, and lysine rich (PEVK) element¹⁶. During diastole, stretch occurs in titin's spring region and this provides elasticity to the sarcomere¹⁷. Alternative splicing of titin occurs predominantly in the spring region and is responsible for the variances found in the two main adult cardiac isoforms of titin, N2B and N2BA¹⁸. The more compliant N2BA isoform has a longer extensible spring region owing to the longer PEVK and Ig segments. The N2B isoform is the dominant isoform in both mice and men, with human LV expressing N2B and N2BA isoforms at a ratio of approximately 60:40¹⁹. Both isoforms extend the same distance for a given sarcomere length (near Z-disk to beginning of A-band), however, the force to stretch titin is greater in

the N2B isoform attributable to its shorter contour length²⁰. By reducing the level of functional RBM20 protein, additional exon incorporation into titin's spring elements minimizes passive stiffness in a manner inversely related to the size of titin¹. The *Ttn*^{ΔIAjxn} murine model has 18 exons deleted from the mouse *Ttn* gene that encode 3 Ig domains and 11 FnIII domains that constitute a 153 kDa polypeptide fragment in titin known as the I-band – A-band junction. This model is unique from previously published titin I-band truncation models (N2B²¹, PEVK²² and Ig¹⁶) in that the entire spring region of titin remains intact, including all spring element phospho-sites. Removal of titin's IA junction, results in anchoring of the C-terminal attachment of titin's distal Ig spring element further away (~ 70 nm) from the Z-disk, resulting in enhanced strain in titin's spring region and consequently an increase in force per titin molecule². This increased force mimics the pathologic conditions of oxidative stress and deranged phosphorylation evident in HFpEF patients^{15, 23}. Interestingly the *Ttn*^{ΔIAjxn} mouse recapitulates many characteristics of HFpEF, e.g., diastolic dysfunction, exercise intolerance and hypertrophy. Herein, we studied whether reducing functional RBM20 expression ameliorates these symptoms.

Evaluation of *Ttn*^{ΔIAjxn} mice with and without N2BAsc expression was performed at the cell and organ levels. The increased stiffness of cardiac myocytes from *Ttn*^{ΔIAjxn} mice (Fig. 1E) are in agreement with previous reports showing that altering the size of titin directly affects passive stiffness^{1, 2}. That this causes increased LV chamber stiffness is supported by multiple chamber-level measurements. The greater ratio of the early mitral inflow (E) to late atrial kick (A) revealed by pulse-wave Doppler imaging is indicative of increased diastolic stiffness (Fig. 2D, 3B). Moreover, LV chamber stiffening abbreviates the time of deceleration of the early mitral inflow²⁴ and the reduced deceleration time in

Ttn^{Δ*Ajxn*} mice (Fig. 2E, 3C) also support restrictive filling. In accordance with echocardiography, catheterization of the left ventricle revealed a steeper slope of the EDPVR demonstrating diastolic stiffness in the LV of *Ttn*^{Δ*Ajxn*} mice. Remarkably, inhibiting RBM20 acutely in *Ttn*^{Δ*Ajxn*} mice restored these parameters back to WT levels (Fig. 3). Assessing inducible expression of compliant titin is imperative since HFpEF patients typically develop symptoms later in adult life, therefore, an acute therapy to restore diastolic function in the elderly HFpEF patient is necessary. Upon inducing compliant titin isoform expression in *Ttn*^{Δ*Ajxn*} mice, diastolic dysfunction was corrected and these mice preformed better in exercise tolerance studies (as further discussed below). Thus, our hemodynamic studies in mice with inhibited RBM20 suggest that this intervention is beneficial for restoring compliance to the restrictive left ventricle.

The advantage of RBM20 inhibition was further evidenced by exercise testing. Exercise is considered a beneficial therapy in heart failure patients²⁵, but how titin compliance relates to exercise capacity is not well understood. Since our models are cardiac specific for RBM20 reduction, we could assess exercise performance as it directly relates to differing strain in cardiac titin. When given access to a voluntary running wheel, *Ttn*^{Δ*Ajxn*} mice expressing N2BAsc had a significantly greater average and maximal speed over the course of 21 days. Furthermore, when challenged with treadmill running, mice with upregulated compliant titin performed significantly better than *Ttn*^{Δ*Ajxn*} mice. Exercise intolerance leading to fatigue and shortness of breath has a major impact on the quality of life in HFpEF patients, therefore improved exercise performance through upregulating titin compliance is particularly encouraging.

Titin has been hypothesized to function as biomechanical sensor and our present studies support that titin mechanosensation contributes to increased afterload induced LV hypertrophy. We constricted the transverse aorta of mice to induce acute pressure overload stress to the heart. Compared to WT controls, *Ttn^{ΔA_{ixn}}* mice exhibited a 50% greater increase in LV mass characterized by robust concentric remodeling (Fig. 5). In contrast, RBM20 inhibited *Ttn^{ΔA_{ixn}}* mice (with reduced titin strain) had the least amount of LV mass increase in response to TAC (Fig. 5 A). Our results may be explained in part by regulation of signal transduction by titin binding proteins FHL1 and FHL2. Four-and-a half LIM domain (FHL) proteins are expressed in striated muscle where they facilitate diverse protein-protein interactions involved in signal transduction²⁶. Previous studies have shown localization of FHL1 and FHL2 at the N2B element in titin^{12, 14}. Furthermore, regulation of extracellular signal-regulated kinase 2 (ERK2) has been reported by both FHL1 and FHL2 in cardiomyocytes^{27, 28}. Previous studies have also shown that in response to pressure overload induced by TAC, FHL1 null mice display an attenuated hypertrophy response¹⁴ whereas the TAC response of FHL2 null mice does not significantly differ from WT²⁹. Our data are in agreement with these findings as FHL1 is significantly upregulated and FHL2 protein levels remain unaltered in response to TAC (see Figure 6). Thus, FHL1 might be involved in the exaggerated hypertrophy response in the *Ttn^{ΔA_{ixn}}* model and its normalization when N2BAsc is expressed. Interestingly, in sham mice FHL2 protein levels are significantly greater in *Ttn^{ΔA_{ixn}}* mice compared to WT controls while FHL1 remains unaltered. Upon removal of excess strain in titin, RBM20 inhibited mice displayed a significantly reduced level of FHL2 protein (Fig. 6 C and F) while FHL1 levels were not affected (Fig. 6 B and E). Collectively, these findings support that FHL1 is primarily

involved in responses to pressure overload while FHL2 may be more important in sensing strain (e.g. volume overload). Hypertrophy signaling in the myocyte is extremely complex³⁰ and mechanotransduction remains incompletely understood. Our findings suggest that the sarcomere contains a mechanosensing element (titin) that plays a critical role in hypertrophy signaling. Further studies are necessary to investigate titin as a sensor for mechanotransduction including the roles of FHL1 and FHL2.

In summary, this work reveals that manipulation of titin's spring elements has a beneficial effect on diastolic function of the heart. HFpEF patients suffer from diastolic dysfunction that leads to a myriad of symptoms including exercise intolerance and reduced quality of life³¹. Innovative therapies are urgently needed to address diastolic stiffness and our study reveals novel insights into the pathophysiology of HFpEF and the central role played by titin. Lengthening the spring region of titin through alternative splicing reduces passive myocardial stiffness and improves a HFpEF-like phenotype in the *Ttn* ^{$\Delta I A_{jxn}$} mouse. Diastolic function was recovered both chronically and acutely resulting in an enhanced exercise performance compared to littermate controls. Furthermore, afterload induced pathologic remodeling was attenuated in mice expressing N2BAsc titin. Thus, our work supports that ameliorating diastolic dysfunction and pathological chamber remodeling might be achievable through therapeutically targeting titin.

References of Chapter 1

1. Writing Committee M, Yancy CW, Jessup M, Bozkurt B, Butler J, Casey DE, Jr., Drazner MH, Fonarow GC, Geraci SA, Horwich T, Januzzi JL, Johnson MR, Kasper EK, Levy WC, Masoudi FA, McBride PE, McMurray JJ, Mitchell JE, Peterson PN, Riegel B, Sam F, Stevenson LW, Tang WH, Tsai EJ, Wilkoff BL and American College of Cardiology Foundation/American Heart Association Task Force on Practice G. 2013 ACCF/AHA guideline for the management of heart failure: a report of the American College of Cardiology Foundation/American Heart Association Task Force on practice guidelines. *Circulation*. 2013;128:e240-327.
2. Butler J, Fonarow GC, Zile MR, Lam CS, Roessig L, Schelbert EB, Shah SJ, Ahmed A, Bonow RO, Cleland JG, Cody RJ, Chioncel O, Collins SP, Dunnmon P, Filippatos G, Lefkowitz MP, Marti CN, McMurray JJ, Misselwitz F, Nodari S, O'Connor C, Pfeffer MA, Pieske B, Pitt B, Rosano G, Sabbah HN, Senni M, Solomon SD, Stockbridge N, Teerlink JR, Georgiopoulou VV and Gheorghiade M. Developing therapies for heart failure with preserved ejection fraction: current state and future directions. *JACC Heart Fail*. 2014;2:97-112.
3. Haq MA, Wong C, Mutha V, Anavekar N, Lim K, Barlis P and Hare DL. Therapeutic interventions for heart failure with preserved ejection fraction: A summary of current evidence. *World J Cardiol*. 2014;6:67-76.
4. Zile MR, Baicu CF, Ikonomidis JS, Stroud RE, Nietert PJ, Bradshaw AD, Slater R, Palmer BM, Van Buren P, Meyer M, Redfield MM, Bull DA, Granzier HL and LeWinter MM. Myocardial stiffness in patients with heart failure and a preserved ejection fraction: contributions of collagen and titin. *Circulation*. 2015;131:1247-59.
5. Bang ML, Centner T, Fornoff F, Geach AJ, Gotthardt M, McNabb M, Witt CC, Labeit D, Gregorio CC, Granzier H and Labeit S. The complete gene sequence of titin, expression of

- an unusual approximately 700-kDa titin isoform, and its interaction with obscurin identify a novel Z-line to I-band linking system. *Circ Res.* 2001;89:1065-72.
6. Labeit S and Kolmerer B. Titins: giant proteins in charge of muscle ultrastructure and elasticity. *Science.* 1995;270:293-6.
 7. Granzier HL and Irving TC. Passive tension in cardiac muscle: contribution of collagen, titin, microtubules, and intermediate filaments. *Biophys J.* 1995;68:1027-44.
 8. Trombitas K, Redkar A, Centner T, Wu Y, Labeit S and Granzier H. Extensibility of isoforms of cardiac titin: variation in contour length of molecular subsegments provides a basis for cellular passive stiffness diversity. *Biophys J.* 2000;79:3226-34.
 9. Hidalgo C and Granzier H. Tuning the molecular giant titin through phosphorylation: role in health and disease. *Trends Cardiovasc Med.* 2013;23:165-71.
 10. Guo W, Schafer S, Greaser ML, Radke MH, Liss M, Govindarajan T, Maatz H, Schulz H, Li S, Parrish AM, Dauksaite V, Vakeel P, Klaassen S, Gerull B, Thierfelder L, Regitz-Zagrosek V, Hacker TA, Saupe KW, Dec GW, Ellinor PT, MacRae CA, Spallek B, Fischer R, Perrot A, Ozcelik C, Saar K, Hubner N and Gotthardt M. RBM20, a gene for hereditary cardiomyopathy, regulates titin splicing. *Nat Med.* 2012;18:766-73.
 11. Methawasini M, Hutchinson KR, Lee EJ, Smith JE, 3rd, Saripalli C, Hidalgo CG, Ottenheijm CA and Granzier H. Experimentally increasing titin compliance in a novel mouse model attenuates the Frank-Starling mechanism but has a beneficial effect on diastole. *Circulation.* 2014;129:1924-36.
 12. van Heerebeek L, Hamdani N, Falcao-Pires I, Leite-Moreira AF, Begieneman MP, Bronzwaer JG, van der Velden J, Stienen GJ, Laarman GJ, Somsen A, Verheugt FW, Niessen HW and Paulus WJ. Low myocardial protein kinase G activity in heart failure with preserved ejection fraction. *Circulation.* 2012;126:830-9.

13. Redfield MM, Chen HH, Borlaug BA and et al. Effect of phosphodiesterase-5 inhibition on exercise capacity and clinical status in heart failure with preserved ejection fraction: A randomized clinical trial. *JAMA*. 2013;309:1268-1277.
14. Greaser ML, Krzesinski PR, Warren CM, Kirkpatrick B, Campbell KS and Moss RL. Developmental changes in rat cardiac titin/connectin: transitions in normal animals and in mutants with a delayed pattern of isoform transition. *Journal of muscle research and cell motility*. 2005;26:325-32.
15. Granzier HL, Hutchinson KR, Tonino P, Methawasin M, Li FW, Slater RE, Bull MM, Saripalli C, Pappas CT, Gregorio CC and Smith JE, 3rd. Deleting titin's I-band/A-band junction reveals critical roles for titin in biomechanical sensing and cardiac function. *Proc Natl Acad Sci U S A*. 2014;111:14589-94.
16. Chung CS, Hutchinson KR, Methawasin M, Saripalli C, Smith JE, 3rd, Hidalgo CG, Luo X, Labeit S, Guo C and Granzier HL. Shortening of the elastic tandem immunoglobulin segment of titin leads to diastolic dysfunction. *Circulation*. 2013;128:19-28.
17. King NM, Methawasin M, Nedrud J, Harrell N, Chung CS, Helmes M and Granzier H. Mouse intact cardiac myocyte mechanics: cross-bridge and titin-based stress in unactivated cells. *J Gen Physiol*. 2011;137:81-91.
18. Hu P, Zhang D, Swenson L, Chakrabarti G, Abel ED and Litwin SE. Minimally invasive aortic banding in mice: effects of altered cardiomyocyte insulin signaling during pressure overload. *American Journal of Physiology - Heart and Circulatory Physiology*. 2003;285:H1261-H1269.
19. Ohno M, Cheng CP and Little WC. Mechanism of altered patterns of left ventricular filling during the development of congestive heart failure. *Circulation*. 1994;89:2241-50.
20. Owan TE, Hodge DO, Herges RM, Jacobsen SJ, Roger VL and Redfield MM. Trends in prevalence and outcome of heart failure with preserved ejection fraction. *N Engl J Med*. 2006;355:251-9.

21. Melenovsky V, Borlaug BA, Rosen B, Hay I, Ferruci L, Morell CH, Lakatta EG, Najjar SS and Kass DA. Cardiovascular features of heart failure with preserved ejection fraction versus nonfailing hypertensive left ventricular hypertrophy in the urban Baltimore community: the role of atrial remodeling/dysfunction. *J Am Coll Cardiol.* 2007;49:198-207.
22. Zile MR, Gottdiener JS, Hetzel SJ, McMurray JJ, Komajda M, McKelvie R, Baicu CF, Massie BM and Carson PE. Prevalence and significance of alterations in cardiac structure and function in patients with heart failure and a preserved ejection fraction. *Circulation.* 2011;124:2491-501.
23. Miller MK, Granzier H, Ehler E and Gregorio CC. The sensitive giant: the role of titin-based stretch sensing complexes in the heart. *Trends Cell Biol.* 2004;14:119-26.
24. Zhu Y, Bogomolovas J, Labeit S and Granzier H. Single molecule force spectroscopy of the cardiac titin N2B element: effects of the molecular chaperone alphaB-crystallin with disease-causing mutations. *J Biol Chem.* 2009;284:13914-23.
25. Lange S, Auerbach D, McLoughlin P, Perriard E, Schafer BW, Perriard JC and Ehler E. Subcellular targeting of metabolic enzymes to titin in heart muscle may be mediated by DRAL/FHL-2. *J Cell Sci.* 2002;115:4925-36.
26. Sheikh F, Ouyang K, Campbell SG, Lyon RC, Chuang J, Fitzsimons D, Tangney J, Hidalgo CG, Chung CS, Cheng H, Dalton ND, Gu Y, Kasahara H, Ghassemian M, Omens JH, Peterson KL, Granzier HL, Moss RL, McCulloch AD and Chen J. Mouse and computational models link Mlc2v dephosphorylation to altered myosin kinetics in early cardiac disease. *J Clin Invest.* 2012;122:1209-21.
27. Sheikh F, Raskin A, Chu PH, Lange S, Domenighetti AA, Zheng M, Liang X, Zhang T, Yajima T, Gu Y, Dalton ND, Mahata SK, Dorn GW, 2nd, Brown JH, Peterson KL, Omens JH, McCulloch AD and Chen J. An FHL1-containing complex within the cardiomyocyte

- sarcomere mediates hypertrophic biomechanical stress responses in mice. *J Clin Invest.* 2008;118:3870-80.
28. Granzier H and Labeit S. Cardiac titin: an adjustable multi-functional spring. *J Physiol.* 2002;541:335-42.
 29. Granzier H, Helmes M and Trombitas K. Nonuniform elasticity of titin in cardiac myocytes: a study using immunoelectron microscopy and cellular mechanics. *Biophys J.* 1996;70:430-42.
 30. Trombitas K, Wu Y, Labeit D, Labeit S and Granzier H. Cardiac titin isoforms are coexpressed in the half-sarcomere and extend independently. *Am J Physiol Heart Circ Physiol.* 2001;281:H1793-9.
 31. Neagoe C, Kulke M, del Monte F, Gwathmey JK, de Tombe PP, Hajjar RJ and Linke WA. Titin isoform switch in ischemic human heart disease. *Circulation.* 2002;106:1333-41.
 32. Radke MH, Peng J, Wu Y, McNabb M, Nelson OL, Granzier H and Gotthardt M. Targeted deletion of titin N2B region leads to diastolic dysfunction and cardiac atrophy. *Proc Natl Acad Sci U S A.* 2007;104:3444-9.
 33. Granzier HL, Radke MH, Peng J, Westermann D, Nelson OL, Rost K, King NM, Yu Q, Tschöpe C, McNabb M, Larson DF, Labeit S and Gotthardt M. Truncation of titin's elastic PEVK region leads to cardiomyopathy with diastolic dysfunction. *Circ Res.* 2009;105:557-64.
 34. Szelenyi Z, Fazakas A, Szenasi G, Kiss M, Tegze N, Fekete BC, Nagy E, Bodo I, Nagy B, Molvarec A, Patocs A, Pepo L, Prohaszka Z and Vereckei A. Inflammation and oxidative stress caused by nitric oxide synthase uncoupling might lead to left ventricular diastolic and systolic dysfunction in patients with hypertension. *J Geriatr Cardiol.* 2015;12:1-10.
 35. Vlahovic A and Popovic AD. [Evaluation of left ventricular diastolic function using Doppler echocardiography]. *Med Pregl.* 1999;52:13-8.

36. Vromen T, Kraal JJ, Kuiper J, Spee RF, Peek N and Kemps HM. The influence of training characteristics on the effect of aerobic exercise training in patients with chronic heart failure: A meta-regression analysis. *Int J Cardiol.* 2016;208:120-7.
37. Chu P-H, Ruiz-Lozano P, Zhou Q, Cai C and Chen J. Expression patterns of FHL/SLIM family members suggest important functional roles in skeletal muscle and cardiovascular system. *Mechanisms of Development.* 2000;95:259-265.
38. Raskin A, Lange S, Banares K, Lyon RC, Zieseniss A, Lee LK, Yamazaki KG, Granzier HL, Gregorio CC, McCulloch AD, Omens JH and Sheikh F. A novel mechanism involving four-and-a-half LIM domain protein-1 and extracellular signal-regulated kinase-2 regulates titin phosphorylation and mechanics. *J Biol Chem.* 2012;287:29273-84.
39. Purcell NH, Darwis D, Bueno OF, Muller JM, Schule R and Molkentin JD. Extracellular Signal-Regulated Kinase 2 Interacts with and Is Negatively Regulated by the LIM-Only Protein FHL2 in Cardiomyocytes. *Molecular and Cellular Biology.* 2004;24:1081-1095.
40. Chu P-H, Bardwell WM, Gu Y, Ross J and Chen J. FHL2 (SLIM3) Is Not Essential for Cardiac Development and Function. *Molecular and Cellular Biology.* 2000;20:7460-7462.
41. van Berlo JH, Maillet M and Molkentin JD. Signaling effectors underlying pathologic growth and remodeling of the heart. *J Clin Invest.* 2013;123:37-45.
42. Gladden JD, Linke WA and Redfield MM. Heart failure with preserved ejection fraction. *Pflugers Arch.* 2014;466:1037-53.

Supplemental Methods of Chapter 1

Generation of Mice: $Ttn^{ΔA_{jxn}}$ and $Rbm20^{ΔRRM}$ mice previously described^{1, 2} were bred to generate homozygous $Ttn^{ΔA_{jxn}}$ mice on that were heterozygous for WT RBM20 protein on a C57BL/6J background. In our studies we used mice ~ 4 months old and male, unless indicated otherwise (see Figure S1 for breeding details). All experiments were approved by the University of Arizona Institutional Animal Care and Use Committee (IACUC) and followed the U.S. National Institutes of Health *Using Animals in Intramural Research guidelines for animal use*.

Skinned Cell Mechanics: Experiments were conducted in accordance with the Guide for the Care and Use of Laboratory Animals, and all protocols were approved by University of Arizona's Institutional Animal Care and Use Committee. Cells were isolated as described previously³². Briefly, mice were heparinized (1,000 U/kg, i.p.) and euthanized by cervical dislocation under isoflurane. The heart was removed and cannulated via the aorta with a blunted 21-gauge needle for retrograde coronary perfusion. The heart was perfused for 4 min with perfusion buffer ([in mmol/L] 90 NaCl, 34.7 KCl, 0.6 KH₂PO₄, 0.6 Na₂HPO₄, 1.2 MgSO₄, 12 NaHCO₃, 10 KHCO₃, 10 HEPES, 10 taurine, 5.5 glucose, 5 BDM, 20 Creatine, 5 Adenosine and 5 Inosine, pH 7.4), followed by digestion buffer (perfusion buffer plus 0.05 mg/ml Liberase TM research grade; Roche Applied Science, and 13 μM CaCl₂) for 20 min. When the heart was flaccid, digestion was halted and the heart was placed in myocyte stopping buffer (perfusion buffer plus bovine calf serum 0.08 [BCS]/ml and 8 μM CaCl₂) with protease inhibitors ([in mmol/L] 0.4 Leupeptin, 0.1 E64,

and 0.5 PMSF (Peptides International, Sigma-Aldrich)). The left ventricle was cut into small pieces, and the rest of the heart was discarded. The small pieces of left ventricle were triturated several times with a transfer pipette and then filtered through a 300 μ m nylon mesh filter. **Passive stress measurement in skinned cardiomyocytes.** Mouse cardiomyocytes, isolated as explained above, were skinned for 7 min in relaxing solution ([in mmol/L] 40 BES, 10 EGTA, 6.56 MgCl₂, 5.88 Na-ATP, 1.0 DTT, 46.35 K-propionate, 15 creatine phosphate, pH 7.0) with protease inhibitors ([in mmol/L] 0.4 leupeptin, 0.1 E64, and 0.5 PMSF) and 0.3% Triton X-100 (Ultrapure; Thermo Fisher Scientific). Cells were washed extensively with relaxing solution pCa 9 and stored on ice. Skinned myocytes were used for mechanic studies within 48 h after time of cell isolation. Myocyte suspension was added to a room temperature flow-through chamber mounted on the stage of an inverted microscope (Diaphot 200; Nikon). Skinned myocyte was glued at one end to a force transducer (Model 406A or 403A, Aurora Scientific). The other end was bent with a pulled glass pipette attached to micromanipulator so that the myocyte axis aligned with the microscope optical axis and cross sectional area (CSA) was measured directly. The cross sectional images of skinned cells were analyzed by ImageJ 1.41 software (National Institutes of Health) and were used to convert measured force to stress and for cell dimension study (Fig S4d). Then, the free end of the cell was glued to a servomotor (Model 308B, Aurora Scientific) that imposes controlled stretches. Sarcomere length (SL) was measured with a MyocamS and SarcLen acquisition module (IonWizard 6.2, IonOptix Co, MA) attached to a computer. To correct for ~20% lattice expansion during skinning process³³, CSA of skinned cells were divided by a correction factor of 1.44. Passive stress was measured in relaxing solution pCa 9 with protease inhibitors at room temperature.

Cells were stretched from slack length at a speed of 1 base length/sec to a SL of 2.3 μm for +/+, 2.7 μm for +/- and 3.0 μm for -/-, followed by a 20 sec hold and then a release back to the original length. Recovery time of at least 7 min in between stretches was utilized to prevent memory-effects in subsequent measurements. Data were collected using a custom LabVIEW VI (National Instruments, Austin TX) at a sample rate of 1 kHz. Measured forces were converted to stress (force/unit undeformed CSA). The stress during the 1 base length/sec stretch was plotted against the SL and fitted with a monoexponential curve to derive stress-SL relationships.

Echocardiography: A Vevo 2100 High Resolution Imaging System (Visual-Sonics, Toronto, Canada) was used with the model MS5500 scan head designed for murine cardiac imaging. Care was taken to avoid animal contact and excessive pressure which could induce bradycardia during conscious scanning. Imaging was performed at a depth setting of 11 mm. Images were collected and stored as a digital cine loop for off-line calculations. Mice were consciously echoed while scruffing the skin at the nape of the neck and a standard short axis (M-mode) cine loop was recorded at the level of the papillary muscles to assess chamber dimensions (LV systolic and diastolic dimensions (LVDs, LVDd)) posterior and anterior wall thickness (WT), and cardiac function via Fractional Shortening (%FS). Functional calculations were obtained according to American Society of Echocardiography guidelines. To investigate diastolic function we performed Doppler echo on anesthetized mice. Mice were anesthetized and ventilated with 2% isoflurane using a nose cone and body temperature was maintained at 37°C. Following anesthetic induction, the mouse was placed in dorsal recumbence on a heated platform for echocardiography.

Images were collected and stored as a digital cine loop for off-line calculations. The left atrial dimension was measured in the long-axis view directly below the aortic valve leaflets. Passive LV filling peak velocity, E (cm/sec), and atrial contraction flow peak velocity, A (cm/sec), were acquired from the images of mitral valve Doppler flow from 4-chamber apical views, according to American Society of Echocardiography guidelines. The heart rate of animals was maintained in the range of 450 ± 25 bpm for Doppler studies.

Pressure-Volume Analysis: In vivo pressure-volume analysis was performed in mice using a SciSense Advantage Admittance Derived Volume Measurement System and 1.2F catheters with 4.5 mm electrode spacing (SciSense, London, Ontario, Canada). Mice were anesthetized and ventilated with 1.5% isoflurane using a SAR-1000 Small Animal Ventilator (CWE). Body temperature under anesthesia was maintained at 37°C using a TC-1000 Temperature Controller (CWE). A lateral incision through the skin and muscle was made below the ribcage and the diaphragm was cut in order to expose the apex of the heart. A small puncture was made in the apex of the left ventricle using a 28G needle and the 1.2F catheter was inserted into the LV. Baseline functional parameters were assessed during a pause in ventilation in order to avoid respiratory influences. For load-independent indices, including the end-systolic and end-diastolic pressure-volume relationships, the IVC was temporarily occluded to vary the preload conditions. Data acquisition and analysis was performed using LabScribe 2 (iWorx, Dover, NH) and curve fitting was performed with MATLAB (MathWorks, Natick, MA). Diastolic PV data was analyzed using a mono-exponential fit with constant ($P = Ae^{\beta V} + C$) with the exponent (β) reported as the coefficient of stiffness.

Exercise Testing: We used 3-4 month old mice for voluntary exercise studies. Mice were housed individually in a cage that contained a free-running wheel. The exercise wheels were purchased from Lafayette Instrument©, model 80820 activity wheel chamber with 86060S sensor attached to the wheel support frame for continuous data collection. Data were stored in an attached CPU for further processing. **Treadmill Testing:** Mice were tested for maximal running speed using a 6-lane rodent treadmill system (Exer 3/6, Columbus Instruments, Columbus, OH). After an acclimation period during which mice were running at low speed (10 m/min), exercise testing was performed by having mice run at progressively increasing speeds (speed steps of 4 m/min). Maximal speed was determined when the mouse left the treadmill and remained on a shock pad for at least 5 sec.

Quantification of Protein Expression: Flash frozen LV tissues were cut and weighed, then pulverized into a very fine powder using a mortar and pestle in liquid nitrogen. Samples were then placed into a -20°C freezer for 20minutes. 8M urea buffer ([in mol/L] 8 Urea, 2 Thiourea, 0.05 Tris-HCl, 0.075 Dithiothreitol with 3% SDS and 0.03% Bromophenol blue pH 6.8) and 50% glycerol with protease inhibitors ([in mmol/L] 0.04 E64, 0.16 Leupeptin and 0.2 PMSF) were added to the samples (in a 40:40:1 ratio) and solubilized for 10minutes at 60°C. The solubilized samples were centrifuged, aliquoted into smaller volumes, and stored at -80°C.

Titin isoform expression analysis: titin isoform expression analysis was performed via electrophoresis of the solubilized samples on a 1% agarose gel (Hoefer gel system). The gels are loaded with six different volumes of the sample and run at 15mA per gel for 3hours and 20minutes. The protein was then fixed on the gel using a fixing solution, stained with coomassie brilliant blue (Acros organics), then scanned (Epson commercial scanner) in order to capture an image for the analysis of the various Titin isoform bands. The images were analyzed using OneD scan software by determining the integrated optical density of Titin and myosin heavy chain as a function of the various volumes loaded on the gel. The isoform expression ratios of the samples are determined by using the slope of the optical density of the different loading volumes.

Western Blotting: The solubilized samples were run on SDS PAGE gels (different percentages depending on target protein). Gels were run for approximately 2 hours then samples were transferred to PDVF membranes (Immobilon, Millipore) using a semi-dry transfer unit (Trans-Blot Cell, Bio-Rad). Transfer amperage was based on area of membrane(s) multiplied by 1.3 and was run for 2.5hours. The membranes were stained with Ponceau S (Sigma) to visually ensure protein transfer. The Ponceau S stain was later removed by .1M NaOH, and blots were placed in a blocking solution (Odyssey Block) for 1hour to prevent non-specific binding of the antibody. Blocking solution was removed and blots were then soaked in the primary antibody solution overnight. Primary antibody was removed and blots were washed with PBS-tween solution before secondary fluorescent antibody was added. The blots soaked in secondary antibody for 1hour before they were scanned using an Odyssey Infrared Imaging System (Li-COR Biosciences). Images obtained were analyzed using Li-COR Odyssey software.

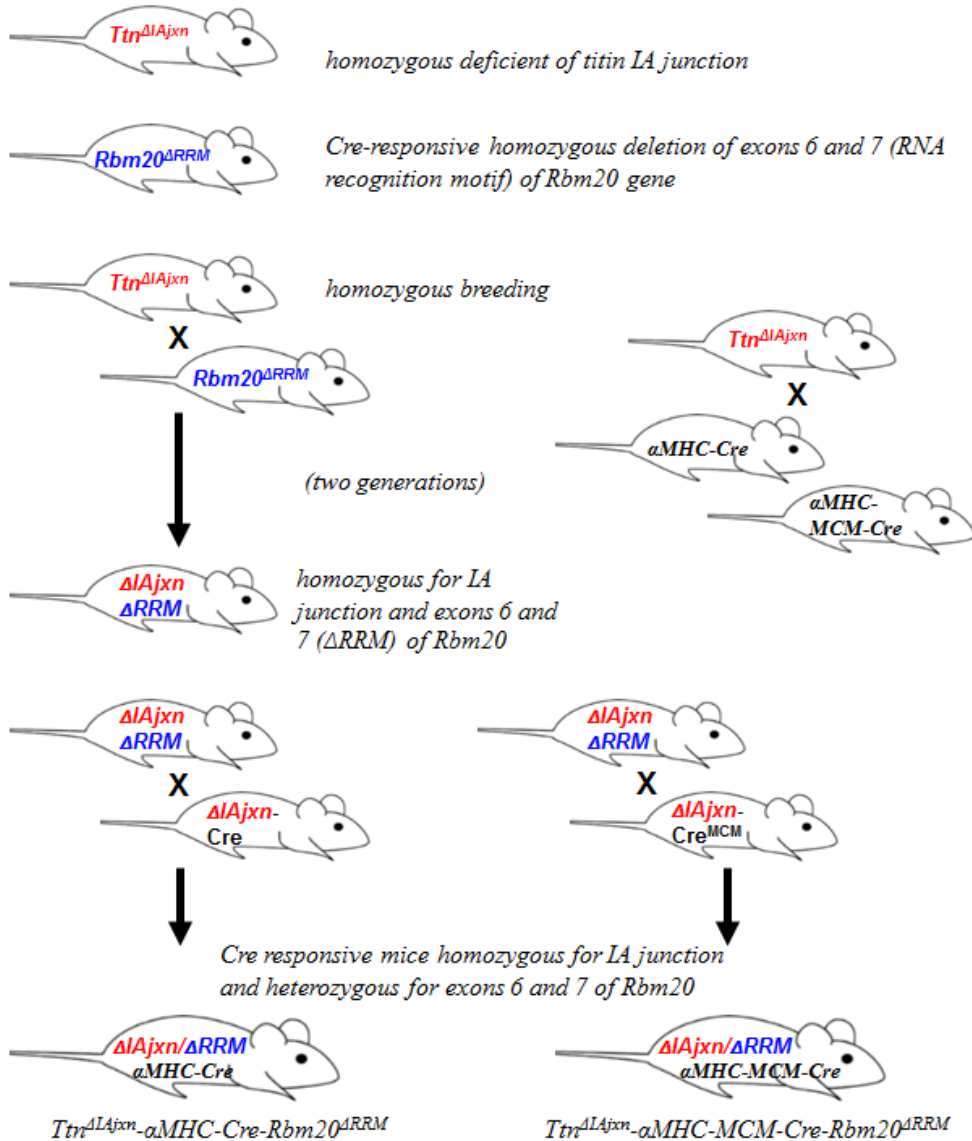
Antibody	Source	Host	Dilution
FHL2	MBL	Rabbit	1:5000
FHL1	Millipore	Rabbit	1:5000
α BCrystallin	Cell Signaling Technology	Rabbit	1:1500
GAPDH	Thermo Pierce	Mouse	1:5000

Transverse Aortic Constriction: For minimally invasive Transverse Aortic Constriction (TAC) surgeries, anesthesia was induced by intraperitoneal (i.p.) injection of ketamine hydrochloride (120 mg/kg) plus xylazine (12 mg/kg) for a depth of anesthesia ~45 min, long enough to finish the surgery. The aortic banding procedure was performed similar to that previously described in ³⁴ with minor adaptations. Briefly, a small incision in the chest cavity was created between the first and second intercostal ribs and the transverse portion of the aorta was bluntly dissected from the surrounding tissue. A curved forceps was then placed under the transverse aorta, 7-0 silk was grasped by the forceps and moved underneath the aorta between the right innominate and left carotid arteries, and a loose double knot was made. A 27-gauge needle with OD 0.42 mm was delivered through the loose double knot and placed directly above and parallel to the aorta. The loop was then tied around the aorta and needle and secured with the second knot (this was done very quickly, to minimize ischemia). The needle was immediately removed to provide a lumen with a stenotic aorta. Following the surgery, all layers of muscle and skin were closed with 6-0 continuous absorbable and nylon sutures, respectively, and the wound was treated with Betadine. Immediately after the operation, 0.5 ml of 37°C saline was given intraperitoneally, and a dose of analgesic (SR-buprenorphine, 0.1 mg/kg) was also given subcutaneously. For the sham operation (control) the mice underwent the identical

procedure, except placing of the ligature. The surgical survival rate following TAC was >90% and mortality rate within the first month following TAC was low (<5%). Successful surgical ligation of the transverse aorta, determined by a Doppler flow velocity measurement indicated by a large pressure gradient following constriction. Animals were sacrificed, weighed and cardiac tissue was flash frozen in liquid nitrogen (-80°C) for further analysis.

Supplemental Figure 1 of Chapter 1

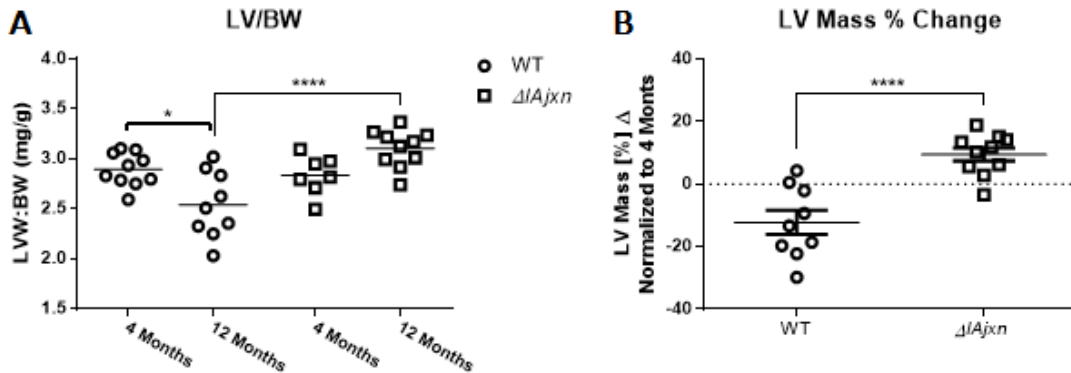
Breeding Scheme for Mice



Supplemental Figure 1: Schematic explaining breeding of $Ttn^{\Delta IAjxn}$ to $Rbm20^{\Delta RRM}$ mice¹.

². Generation of constitutive and inducible homozygous $Ttn^{\Delta IAjxn}$ mice with heterozygous reduction of functional $Rbm20$.

Supplemental Figure 2 of Chapter 1



Supplemental Figure 2: LVW:BW increases with age in $Ttn^{\Delta IAjxn}$ compared with WT mice. A) Left ventricular weight (LVW) normalized to body weight (BW). B) Percent left ventricle (LV) mass increase in WT and $Ttn^{\Delta IAjxn}$ mice. Data shown as mean \pm SEM. Statistical significance calculated with two-way ANOVA and Bonferroni correction (A) and t-test (B), (* $p < 0.05$; ** $p < 0.01$; *** $p < 0.001$; **** $p < 0.0001$ as indicated).

Supplemental Table 1 of Chapter 1

	WT	$\Delta I Ajxn$	$\Delta I Ajxn/\Delta RRM$
n	6	7	7
N2BA/N2B	0.27 ± 0.02	0.23 ± 0.02	7.8 ± 1.1 ****,††††
N2BA/TT	0.18 ± 0.02	0.16 ± 0.01	0.82 ± 0.008 ****,††††
N2B/TT	0.67 ± 0.02	0.70 ± 0.02	0.11 ± 0.01 ****,††††
TT/MHC	0.19 ± 0.02	0.27 ± 0.03 *	0.28 ± 0.03 *
N2BA/MHC	0.03 ± 0.003	0.04 ± 0.002	0.22 ± 0.02 ****,††††
N2B/MHC	0.12 ± 0.01	0.19 ± 0.01 ***	0.03 ± 0.005 ****,††††
T2/T1	0.16 ± 0.05	0.15 ± 0.03	0.09 ± 0.01
MHC (OD/mg)	123.6 ± 12.0	109.6 ± 3.8	136.1 ± 13.0
TT (OD/mg)	24.0 ± 4.9	29.4 ± 1.7	39.1 ± 7.3

Supplemental Table 1: Data shown as mean ± SEM.; Abbreviations: $\Delta I Ajxn$: ($Ttn^{\Delta I Ajxn}$); ΔRRM ($Rbm20^{\Delta RRM+/-}$); TT: total titin; MHC: myosin heavy chain; T1: sum of titin isoforms N2BA and N2B; T2: titin degradation product. Statistical significance calculated with one-way ANOVA with Bonferroni correction: * p<0.05; ** p<0.01; *** p<0.001; **** p<0.0001; (versus WT ****, versus $Ttn^{\Delta I Ajxn}$ ††††).

Supplemental Table 2 of Chapter 1

	WT	$\Delta IAjxn$	$\frac{\Delta IAjxn}{\Delta RRM}$
n	15.0	15.0	16.0
BW (g)	26.7 ± 0.6	28.3 ± 0.7	28.1 ± 0.6
HW (mg)	124.3 ± 2.2	131.2 ± 3.0	130.1 ± 2.5
LV (mg)	84.9 ± 1.3	89.5 ± 2.1	86.5 ± 1.6
RV (mg)	25.2 ± 0.7	27.8 ± 0.8	28.7 ± 0.9**
ATR (mg)	7.1 ± 0.3	7.0 ± 0.3	7.4 ± 0.3
HW/BW (mg/g)	4.7 ± 0.1	4.6 ± 0.1	4.6 ± 0.1
LV/BW (mg/g)	3.2 ± 0.1	3.2 ± 0.1	3.1 ± 0.05
RV/BW (mg/g)	0.9 ± 0.02	1.0 ± 0.02	1.0 ± 0.03
ATR/BW (mg/g)	0.3 ± 0.01	0.3 ± 0.01	0.3 ± 0.01

Supplemental Table 2: Dissection of male mice age ~4 months old. Abbreviations: $\Delta IAjxn$: ($Tn^{\Delta IAjxn}$); ΔRRM ($Rbm20^{\Delta RRM+/-}$); BW: body weight; HW: heart weight; LV: left ventricle; RV: right ventricle; ATR: atrium. Data shown as mean ± SEM; statistical significance calculated with one-way ANOVA with Bonferroni correction: * p<0.05; ** p<0.01; *** p<0.001; **** p<0.0001; (versus WT ****, versus $Tn^{\Delta IAjxn}$ †††).

Supplemental Table 3 of Chapter 1

Conscious Echocardiography of *Ttr^{ΔLA;kn}* mice

	Vehicle	Treatment
n	8	9
Age (days)	133.6 ± 9.0	136.2 ± 8.9
HR (bpm)	675.4 ± 26.3	678.4 ± 33.7
FS (%)	52.7 ± 25.7	50.6 ± 1.9
LVID;d (mm)	2.7 ± 2.7	2.6 ± 0.1
LVID;s (mm)	1.4 ± 0.1	1.3 ± 0.04
LVPW;d (mm)	1.1 ± 0.04	1.1 ± 0.04
LVPW;s (mm)	1.4 ± 0.1	1.4 ± 0.1
LVDD/WT(ratio)	2.6 ± 0.1	2.4 ± 0.1

Supplemental Table 3: Vehicle: DMSO and saline. Treatment: (40 mg/kg) raloxifene injections (x8 days). Abbreviations: HR: heart rate; BPM: beats per minute; FS: fractional shortening; LVIDd: left ventricular internal diastolic diameter; LVIDs: left ventricular internal systolic diameter; LVPWd: left ventricular posterior wall thickness in diastole; LVPWs: left ventricular posterior wall thickness in systole. Eccentricity: LVDD/WT. Data shown as mean ± SEM; statistical significance calculated with Student's t-test: * p<0.05 considered significant.

References of Chapter 1 Supplemental Methods

1. Granzier HL, Hutchinson KR, Tonino P, Methawasin M, Li FW, Slater RE, Bull MM, Saripalli C, Pappas CT, Gregorio CC and Smith JE, 3rd. Deleting titin's I-band/A-band junction reveals critical roles for titin in biomechanical sensing and cardiac function. *Proc Natl Acad Sci U S A*. 2014;111:14589-94.
2. Methawasin M, Hutchinson KR, Lee EJ, Smith JE, 3rd, Saripalli C, Hidalgo CG, Ottenheijm CA and Granzier H. Experimentally increasing titin compliance in a novel mouse model attenuates the Frank-Starling mechanism but has a beneficial effect on diastole. *Circulation*. 2014;129:1924-36.
3. O'Connell TD, Rodrigo MC and Simpson PC. Isolation and culture of adult mouse cardiac myocytes. *Methods Mol Biol*. 2007;357:271-96.
4. Irving TC, Konhilas J, Perry D, Fischetti R and de Tombe PP. Myofilament lattice spacing as a function of sarcomere length in isolated rat myocardium. *American journal of physiology Heart and circulatory physiology*. 2000;279:H2568-73.
5. Hudson B, Hidalgo C, Saripalli C and Granzier H. Hyperphosphorylation of mouse cardiac titin contributes to transverse aortic constriction-induced diastolic dysfunction. *Circ Res*. 2011;109:858-66.

CHAPTER 2

The Cardiac Specific N2B Element in Titin is Necessary for Volume Overload Induced Hypertrophy

Abstract

Rationale – Cardiac hypertrophy is a common maladaptive feature of heart failure patients and the mechanical triggers that determine pathologic growth are not well understood. The elastic N2B element found in cardiac titin’s I-band region has been proposed as a mechanical sensor and signaling “hot spot” in the cell that is important in cardiac hypertrophy.

Objective –To investigate the role of the cardiac specific N2B spring element in titin as a mechanical sensor for cardiac hypertrophy.

Methods and Results – A N2B element knock-out (KO) mouse was subjected to a variety of stressors including exercise, continuous pressure and volume overload and *beta*-adrenergic stimulation. We found that pressure induced hypertrophy mechanisms were unaltered in N2B deficient mice compared with wild-type (WT) controls, however, volume induced hypertrophy was significantly attenuated. Additionally, KO mice displayed a blunted response to isoproterenol injections. Significant mortality and attenuated hypertrophy was exhibited in N2B deficient mice in response to chronic volume overload. Protein levels of scaffolding protein four and a half LIM domains 2 (FHL2) are drastically reduced and stretch activated signaling through Akt is altered.

Conclusions – We report that cardiac specific N2B element titin is a necessary mechanosensor for volume induced hypertrophy. Early Akt signaling in volume overload was disrupted leading to high mortality and attenuated cardiac hypertrophy in KO mice. Furthermore, beta-adrenergic hypertrophy response was significantly attenuated in KO

mice suggesting a common link between stretch and neurohormonal regulation of cardiac hypertrophy.

Introduction

An adult heart contracts and relaxes more than 85,000 times per day assuming 60 bpm on average. The work load that the heart experiences compared to other organs is unparalleled and its ability to adapt to various physiologic and pathologic stressors without failing over a life time is a marvelous feat. Since little if any hyperplasia exists in adult cardiac muscle, hypertrophy/atrophy mechanisms are the principal methods by which the heart can adapt to stress¹. Apart from genetic and environmental stressors, the heart experiences two principle types of hemodynamic stress. In systole the heart must propel blood against peripheral vascular resistance known as afterload, while, in diastole the heart experiences wall stress as the ventricle passively fills with blood known as preload. If pressure or volume in the heart is perturbed, then the heart must adjust wall thickness accordingly to normalize wall stress as described by the Law of Laplace². Thus, in order to reduce wall stress in response to increased work load, the heart must increase cellular size. Neurohormonal signaling through adrenergic stimulation is one way in which gene expression is turned on to direct growth of the cell³. Simultaneously, innate mechanical triggers can initiate signal transduction to augment gene expression⁴.

The basic unit of muscle is the sarcomere, a fluid crystalline structure composed of myofilaments and their associated binding proteins. Growth of striated muscle occurs either through serial or parallel addition of sarcomeres. The heart responds to pressure by growing sarcomeres in parallel known as concentric growth⁵. Increased volume load to the heart provokes growth of sarcomeres in series, or eccentric growth⁶. What distinguishes this phenomena as physiologic or pathologic, is the balance between concentric and eccentric growth and the ensuing outcome on cardiac function⁷. It is still

unclear, however, how the heart mechanically senses pressure or volume changes and transmits these signals into downstream events that orchestrate the addition of sarcomeres.

Titin, the largest known protein, extends the half-sarcomere from Z-disk to M-band and has been proposed as a mechanical sensor in the heart⁸. Unique to cardiac titin is the N2B spring element located within the elastic I-band region. Flanked by immunoglobulin-like (Ig) domains, the N2B element contains a large 572 amino acid sequence of unknown structure. It is predicted to contain coiled-coil α -helical conformations⁹ that unfold with considerably less force than Ig domains comprised of beta-pleated sheets¹⁰. Molecular dissection of cardiac titin's extensibility revealed that the N2B element extends at the upper end of the physiologic sarcomere length range when Ig spring elements are taut^{11, 12}. Due to its ideal position within the sarcomere and elastic properties, the N2B element has been proposed to modulate mechanotransduction in response to strain changes in titin⁸. Various signaling enzymes are localized to the N2B element by scaffolding protein four-and-a-half LIM domains 2 (FHL2)¹³. Furthermore, the N2B itself is a substrate for nodal kinases relevant in heart disease (e.g. PKA¹⁴, PKG¹⁵, CAMKII δ ^{16, 17} and ERK2¹⁸).

In this study we investigated the role of titin's cardiac specific N2B element as a sensor for stress induced remodeling in the heart. Using the previously published N2B knock-out (KO) murine model¹⁹, we hemodynamically stressed mice intermittently through two types of exercise and chronically through pressure (TAC) and volume (ACF) overload. We found that the N2B element is necessary for the hypertrophy response to volume rather than pressure as determined by changes in cardiac remodeling. Furthermore, N2B KO mice displayed an attenuated hypertrophy response to beta-adrenergic stimulation

suggesting a link between N2B element mechano-sensation and adrenergic signal transduction in the heart.

Materials and Methods

Protein Expression Analysis

Protein expression analysis was performed by using standard gel electrophoresis methods³. (See Supplemental Methods for additional details).

Microarray

GeneChip: LV tissue was dissected from male mice (~4 months old) of each WT and KO ISO and saline controls stored in RNAlater (Invitrogen). Total RNA was isolated using the RNeasy Fibrous Tissue Mini Kit (Qiagen). RNA quality was assessed by NanoDrop 1000 Spectrophotometer and 2100 Bioanalyzer (Agilent); all samples had RIN ≥ 8.0 . Samples were hybridized with the Mouse Gene 1.0ST Array (Affymetrix); processing (labeling through scanning) was performed by the Genomics Core, University of Arizona, using Affymetrix protocols, supplies and equipment; Affymetrix software (Expression Console and Transcriptome Analysis Console) was used, incorporating RMA processing and Analysis of Variance with Benjamini–Hochberg False Discovery Rate (FDR) correction for multiple testing (see Supplemental Methods for additional details).

Hemodynamics

Anesthetized and conscious echocardiography was performed on mice and pressure volume relations were evaluated using admittance-based cardiac catheterization. Cardiac function in diastole was assessed in mice using continuous flow two percent isoflurane inhaled anesthetic with a target heart rate of 450 ± 25 bpm. (See Supplemental Methods for details.)

Voluntary Wheel Running

Mice given access to a voluntary running wheel for 3 weeks to evoke physiologic exercise stress to the heart as previously described³⁵ (see Supplemental Methods for details).

Chronic Swimming

We developed a swimming chamber for mice that produced a consistent undercurrent across the surface of the water to force mice to swim at a desired exertion and time. After an initial ramp up phase, mice were swam for 2 hours a day for three weeks (see Supplemental Methods for additional details).

TAC Surgery

Male mice 3-4 months old were subjected to minimally invasive transverse aortic constriction (TAC)⁵ performed under Ketamine/Xylazine (120/12 mg/kg) anesthesia; details are explained in the Supplemental methods. Briefly, 27-gauge needle was used for banding and mice were studied by echocardiography at 28 days and then euthanized. Hearts were immediately dissected, weighed and frozen for further analysis. Experiments were approved by the University of Arizona Institutional Animal Care and Use Committee and followed the U.S. National Institutes of Health *Using Animals in Intramural Research guidelines for animal use*.

ACF Surgery

Aortocaval fistula (ACF) surgeries were performed in mice to evaluate cardiac response to volume overload as previously described³⁶. Briefly, a midline abdominal

incision was made and blunt dissection exposed the abdominal aorta and inferior vena cava (IVC). Vascular clips were placed above the iliac bifurcation and below the iliolumbar vessels. A 23-g needle was inserted into the aorta and through the common midwall of the IVC, creating an ACF. The needle was removed, and cyanoacrylate glue (Vetbond) was used to seal the aortic puncture. Shunt patency was visually confirmed by mixture of bright red arterial blood in the IVC (see Supplemental Methods for additional details). Mice were sacrificed 1 or 4 weeks following surgery. All Experiments were approved by the University of Arizona Institutional Animal Care and Use Committee and followed the U.S. National Institutes of Health *Using Animals in Intramural Research guidelines for animal use*.

Isoproterenol Injections

We injected mice subcutaneously with a minimal dose of isoproterenol for 5 days to evoke ventricular hypertrophy following a protocol previously described³⁷. (See Supplemental Methods for additional details).

Statistics

Statistical analysis was performed in Graphpad Prism (GraphPad Software, Inc). Group significance was defined using one or two-way ANOVA followed by multiple testing correction. Student t-test was when comparing two groups and Log-Rank Mantel-Cox test was used in Figure 3 (F). Results are shown as mean \pm standard error of the mean, $p < 0.05$ was considered significant.

Results

Characterization under baseline conditions

It is known from previous work that removal of the N2B element in titin reduces the contour length of the spring and generates enhanced passive stiffness in cardiomyocytes²¹. Herein, we first evaluated the hemodynamic characteristics of the mouse under baseline conditions. Catheterization and of the left ventricle revealed enhanced slope (Ees) of the end-systolic pressure volume relationship (ESPVR) accompanied by reduced chamber compliance in diastole (Fig.1 A-B and Table 1). The coefficient of stiffness (β) of the end-diastolic pressure volume relationship (EDPVR) was found to be significantly elevated in KO mice (Fig. 1 C-D). Furthermore, KO mice exhibit left atrial hypertrophy signifying elevated filling pressures (Fig. 1 F). Echocardiography revealed enhanced fractional shortening (FS) (Table 1) in KO mice and pulse-wave Doppler imaging in the 4-chamber apical view demonstrated a greater E/A ratio and sharper E-wave deceleration time (Figure S1), indicating diastolic dysfunction. Motion-mode (M-Mode) imaging in the short axis view of the left ventricle (LV) of adult mice showed reduced chamber dimensions while eccentricity (LVDD/WT) was similar to WT mice (Fig. 1 G and Table 1 Sedentary).

Characterization of titin binding proteins in sedentary mice demonstrates that four-and-a half LIM domains protein 2 (FHL2) is the dominant titin binding protein affected in mice with deletion of the N2B spring element. Greater than 90% reduction in FHL2 protein levels were found in KO LV tissue (Fig. 1 H). In contrast, Ankyrin repeat-domain containing protein 1 (Ankrd1, also known as CARP – cardiac Ankyrin repeat protein) was found to be significantly elevated in KO myocardium (Fig. 1 H). Additional titin I-band

binding proteins, Muscle-LIM protein (MLP), *alpha*-B-crystallin (α BC) and FHL1 were all unaltered between WT and KO LV tissue samples (Fig. 1 H).

Intermittent versus continuous exercise

In order to investigate the role of the N2B element in cardiac remodeling, we subjected both WT and KO mice to exercise stress. Mice were given access to a voluntary running wheel for three weeks to assess physiologic cardiac remodeling. Average speed (km/hr), duration (hr/day) and distance (km/day) were similar between WT and KO mice (see Fig. S2). After 3 weeks, mice were evaluated by echocardiography and then dissected to obtain cardiac tissue weights (Table 1). Normalized LV mass was found to be similarly increased in both groups of mice (Fig. 2 A-B) and eccentricity (LVDD/WT) was the same (5.5) (Table 1). FS was also comparable as evaluated by M-Mode echocardiography ($26.4 \pm 1.5\%$ in WT vs $28.6 \pm 0.8\%$ in KO mice). Thus, the data indicate that physiologic cardiac hypertrophy in response to voluntary running was similar in N2B deficient mice compared to WT controls.

Although WT and KO mice ran comparably, we were unable to control the type of running (i.e., short bursts versus longer individual run times), therefore, we also swam mice to investigate cardiac remodeling in response to controlled exercise pace and duration. In settings where excessive volume is introduced to the heart, extension of the N2B element is thought to translate additional strain in the sarcomere into downstream signal transduction³⁸. To test this hypothesis mice were swam for 2 hours a day for 3 weeks after an initial ramp up phase (see Supplemental Methods for additional details) to induce a

continuous preload challenge to the heart. A swimming chamber with undercurrent was developed in order to generate a consistent swimming pace between WT and KO mice (Fig. S2). Cardiac function was assessed by echocardiography after completion of the study and cardiac tissue weights obtained. Systolic function was significantly enhanced in both genotypes (Table 1 Swimming). WT mice displayed an increase in normalized LV mass of ~15% while hypertrophy in KO mice was significantly attenuated (normalized LV mass increase of ~ 9% (Fig. 2C-D)). Furthermore, eccentricity was reduced in KO mice compared to WT controls suggesting cardiac remodeling was affected (Table 1 Swimming). Thus, continuous exercise induced by swimming revealed significant alterations in cardiac hypertrophy between WT and KO mice.

Normal pressure response abnormal volume response

To further examine the role of the N2B element in cardiac hypertrophy we subjected mice to chronic pressure and volume overload stress. Using the minimally invasive transverse aortic binding method previously described³⁹, WT and KO mice were imposed to chronic pressure overload for 4 weeks. After 1 week mice were assessed by echocardiography to determine the trans-stenotic gradient and evaluate LV remodeling. Calculated LV mass was similar between WT and KO mice at 1 week as determined by M-Mode imaging (Table 1, 1 Week TAC) and this finding was consistent with normalized LV tissue weights at 4 weeks (Fig. 3 A and Table 1, 4 Week TAC). Hearts were concentrically remodeled in both genotypes (Table 1 TAC studies) though KO mice had a slight but significantly greater LV mass increase after 4 weeks of chronic pressure overload (Fig. 3 B). Therefore, consistent with physiologic hypertrophy induced by voluntary wheel

running, KO mice responded similarly to WT controls subjected to chronic pressure overload. Collectively, our data suggests that the N2B element is not critical for mechanisms involving afterload evoked cardiac hypertrophy.

Chronic volume overload was produced by creating a shunt between the common wall of the abdominal aorta and inferior vena cava (IVC) as previously described³⁶. By creating a fistula between the abdominal aorta and IVC, additional blood volume is diverted to the heart. Fistula patency was confirmed by Doppler imaging of the IVC 1 week after surgery followed by dissection to obtain cardiac tissue weights. Continuous preload stress resulted in robust hypertrophic remodeling in the WT left ventricle after 1 week (Fig. 3 C). Relative to sham controls, WT mice experienced a ~26% (Fig. 3 C and D lower left bar) increase in LV mass while KO mice did not respond (~ -2%) (Fig. 3 C and E lower right bar). We repeated the ACF study for a longer duration of 4 weeks and then re-evaluated the mice. 4 weeks of continuous volume overload induced a substantial increase in LV mass of ~63% in WT mice (Fig. 3 D and E upper left bar). KO mice did display hypertrophy (~46% increase) but the LV mass increase was attenuated compared to WT controls ($p < .05$). Additionally, there was significant mortality ($p = 0.0068$) within the first week in both the 1 week and 4 week ACF study for N2B deficient mice (Fig. 3 F). Delayed hypertrophy and high mortality in KO mice suggests that volume induced hypertrophy signaling requires the N2B element particularly in the early phase of ventricular remodeling in response to preload stress.

N2B deficient mice display attenuated hypertrophy response due to β -adrenergic stimulation

Previous studies report that FHL2 KO mice display exaggerated hypertrophy to *beta*-adrenergic stimulation⁴⁰. Protein levels of FHL2 are severely reduced in N2B KO mice²¹, therefore we tested the responsiveness of N2B KO mice to isoproterenol (ISO). Mice were injected subcutaneously with a single bolus (2 mg/kg ISO) for 5 days and on the 6th day were evaluated by echocardiography followed by cardiac dissection. Compared to saline controls, the LV mass of WT mice increased by ~20% (Fig. 4 A-B and Table 1 Isoproterenol). In contrast, KO mice did not respond with significant changes in LV mass. We repeated this protocol using a higher dose (20 mg/kg ISO) and found that mice devoid of the N2B element display an attenuated hypertrophy response compared to WT controls (~12% vs. ~31% in WT) (Fig. 4 A and C). We injected FHL2 KO mice following the same protocol and found that LV mass increase was similar to WT mice (Fig. S3 A-B). To ensure similar beta-adrenergic responsiveness between genotypes, we tested WT and N2B KO mice with acute stimulation with β 1 adrenergic receptor agonist dobutamine. Neurohormonal signaling was similar in WT and N2B KO mice (Fig. 4 D-F). The dP/dt_{max} and the slope of the end-systolic pressure volume relationship (Ees) increased significantly in WT and KO mice with infusion of dobutamine (2.5 μ g/kg/min) into the jugular vein (Fig. 4 D-E). Furthermore, the lusitropic effect of dobutamine dominated in KO mice as ventricular stiffness was normalized to WT levels evident by a reduction in the EDPVR (β) (Fig. 4 F).

Altered signal transduction in KO mice

Gene expression analysis was performed on the low dose (2 mg/kg) isoproterenol study. This revealed that several transcription factors related to cardiac hypertrophy are

differentially regulated between WT and KO mice (Fig. 5 A-B). Furthermore, pathway analysis revealed angiogenesis was downregulated in KO vs WT ISO groups (see Supplemental Data) and HIF1a signaling was pronounced (Fig. 5 A and Online Supplement). Additionally, pathway analysis revealed syndecan-4 (*synd4*) mediated signaling was downregulated in KO mice. Candidate studies revealed that activated Akt is significantly reduced in KO mice (Fig. 6 A). Furthermore, total PKC α levels were reduced in sedentary KO LV tissue (Fig 6 B) and activated glycogen synthase kinase 3 *beta* (GSK3 β) was upregulated (Fig 6 C). After one week of chronic volume overload, activated Akt levels were elevated in WT LV tissue, however, KO pAkt signaling was attenuated (Fig. 6 D). At 4 weeks there was a striking reversal between WT and KO Akt signaling that reflected significant differences in activated MTOR (Fig 6 E-G). Perturbed Akt signaling at 1 week of volume overload in KO mice suggests that early responsiveness to volume overload stress is interrupted. We investigated FHL2 signaling in response to volume and pressure overload (Fig. 6 H) and found that FHL2 was elevated at 1 week in response to volume overload and significantly downregulated in TAC induced pressure overload. (More work is needed in this section).

Chapter 2 Table 1

	WT	KO	p-value
Sedentary			
HR (bpm)	446.2 ± 9.3	446.3 ± 6.3	0.9892
FS (%)	22.2 ± 1.2	27.5 ± 1.2	0.0057
LVDD/WT (ratio)	6.1 ± 0.2	5.9 ± 0.2	0.6528
LV/BW (mg/g)	2.9 ± 0.1	2.4 ± 0.04	0.0000
Voluntary Running			
HR (bpm)	449.9 ± 7.6	462.2 ± 8.5	0.2940
FS (%)	26.4 ± 1.5	28.6 ± 0.8	0.2185
LVDD/WT (ratio)	5.5 ± 0.3	5.5 ± 0.4	0.8422
LV/BW (mg/g)	3.6 ± 0.1	3.0 ± 0.1	0.0001
1 Week TAC			
HR (bpm)	505.8 ± 24.1	494.5 ± 23.5	0.8004
FS (%)	33.2 ± 2.2	32.6 ± 2.1	0.8771
LVDD/WT (ratio)	4.4 ± 0.1	4.0 ± 0.1	0.1277
Calc. LV Mass*	88.0 ± 5.2	88.3 ± 5.2	0.9368
4 Week TAC			
HR (bpm)	497.3 ± 28.7	505.5 ± 18.4	0.8195
FS (%)	29.2 ± 1.5	30.7 ± 2.1	0.5767
LVDD/WT (ratio)	3.7 ± 0.3	4.2 ± 0.2	0.1379
LV/BW (mg/g)	4.0 ± 0.1	3.8 ± 0.1	0.2598
Swimming			
HR (bpm)	451.1 ± 14.8	447.4 ± 10.3	0.8346
FS (%)	30.2 ± 1.9	31.03 ± 1.1	0.6841
LVDD/WT (ratio)	5.7 ± 0.3	5.04 ± 0.2	0.0974
LV/BW (mg/g)	3.4 ± 0.04	2.8 ± 0.02	0.0000
1 Week ACF			
HR (bpm)	533.1 ± 19.3	528.3 ± 11.8	0.8342
FS (%)	30.6 ± 1.6	42.7 ± 1.7	0.0001
LVDD/WT (ratio)	5.8 ± 0.2	5.7 ± 0.3	0.7504
LV/BW (mg/g)	4.0 ± 0.1	2.8 ± 0.1	0.0000
4 Week ACF			
HR (bpm)	502.6 ± 20.1	500.0 ± 6.8	0.8524
FS (%)	23.1 ± 1.8	27.6 ± 2.3	0.1427
LVDD/WT (ratio)	6.1 ± 0.3	6.1 ± 0.2	0.9036
LV/BW (mg/g)	4.5 ± 0.2	3.7 ± 0.2	0.0008
Isoproterenol			
HR (bpm)	462.9 ± 9.0	478.5 ± 8.3	0.2262
FS (%)	26.9 ± 1.4	24.7 ± 1.8	0.3562
LVDD/WT (ratio)	5.1 ± 0.2	5.6 ± 0.2	0.1095
LV/BW (mg/g)	3.4 ± 0.1	2.8 ± 0.1	0.0000

Table 1: Extensive studies were performed to determine the cardiac specific N2B element's role in hypertrophy and remodeling responses to stress in the heart. Abbreviations: HR: heart rate; BPM: beats per minute; FS: fractional shortening; Eccentricity: LVDD/WT; LV/BW: left ventricular weight normalized to body weight; Calculated LV mass for 1 week TAC was obtained by M-Mode echocardiography in the short axis view because tissue weights were not available. Data shown as mean \pm SEM; statistical significance calculated with A. Student's T-test: * $p < 0.05$ considered significant.

Chapter 2 Figure 1

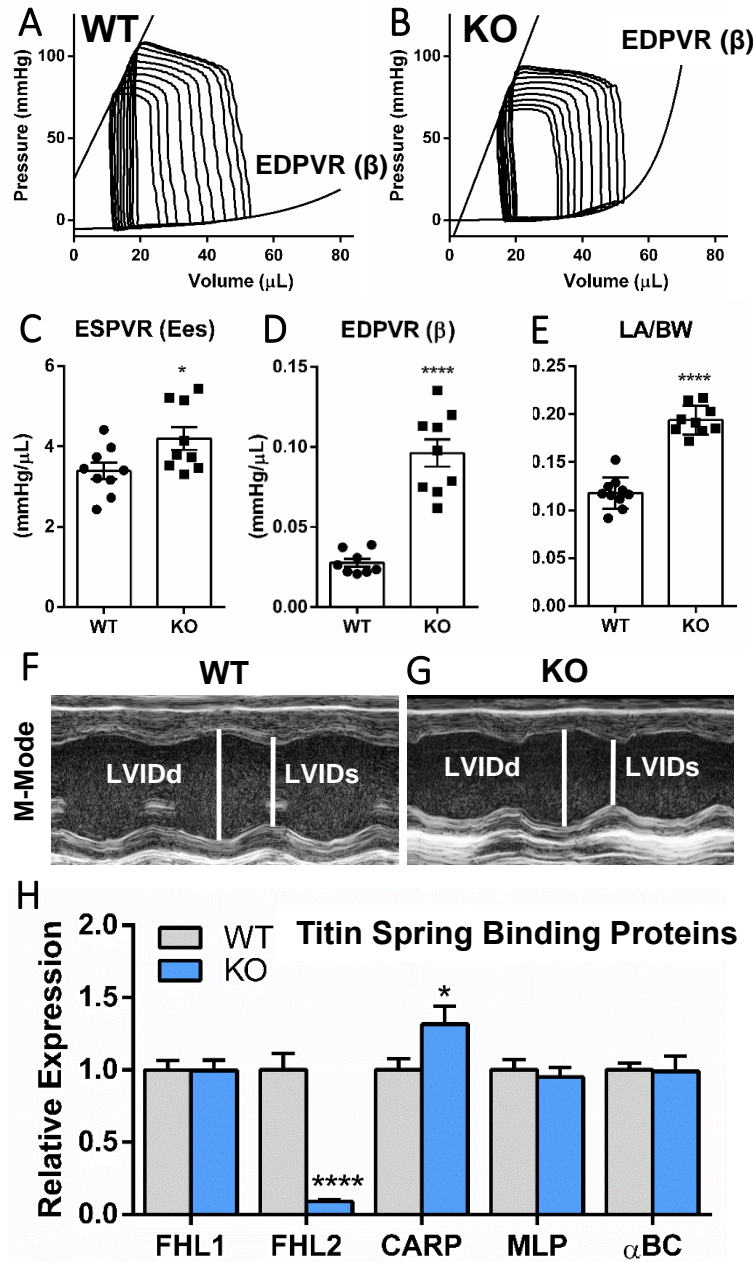


Figure 1: Basic Characterization of N2B KO mice. A-B) Representative cardiac catheterization PV loops; C) Slope (Ees) of ESPVR (end-systolic pressure volume relationship); D) Stiffness coefficient β of EDPVR (end-diastolic pressure volume relationship); E) Left atrial weight (LA) normalized to body weight (BW); F-G) representative M-Mode, (LVIDd): left ventricular internal diastolic diameter; (LVIDs): left ventricular internal systolic diameter; H) cardiac titin I-band binding proteins. Data shown as mean \pm SEM; statistical significance calculated with t-test (C-E) or one-way ANOVA and Bonferroni correction (H), (* $p < 0.05$; ** $p < 0.01$; *** $p < 0.001$; **** $p < 0.0001$ as indicated).

Chapter 2 Figure 2

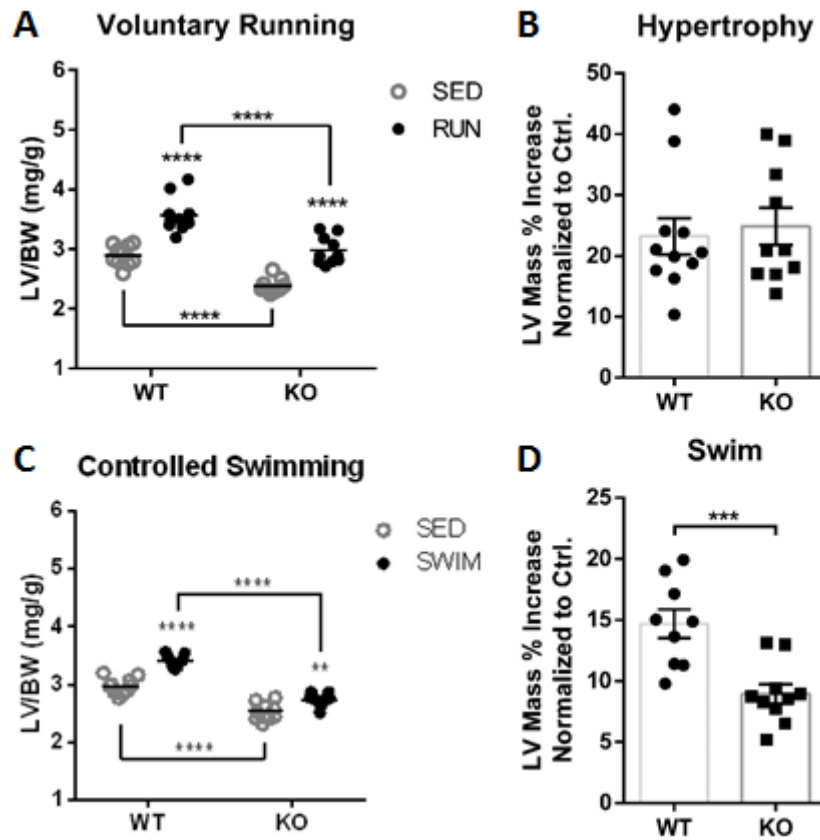


Figure 2: Voluntary and controlled exercise. A) Voluntary running left ventricular weight (LV) normalized to body weight (BW); B) Percent left ventricle (LV) mass increase in running study; C) Chronic swimming left ventricular weight (LV) normalized to body weight (BW); B) Percent left ventricle (LV) mass increase in swimming study; data shown as mean \pm SEM. Statistical significance calculated with two-way ANOVA and Bonferroni correction (A and C) and t-test (B and D), (* $p < 0.05$; ** $p < 0.01$; *** $p < 0.001$; **** $p < 0.0001$ as indicated).

Chapter 2 Figure 3

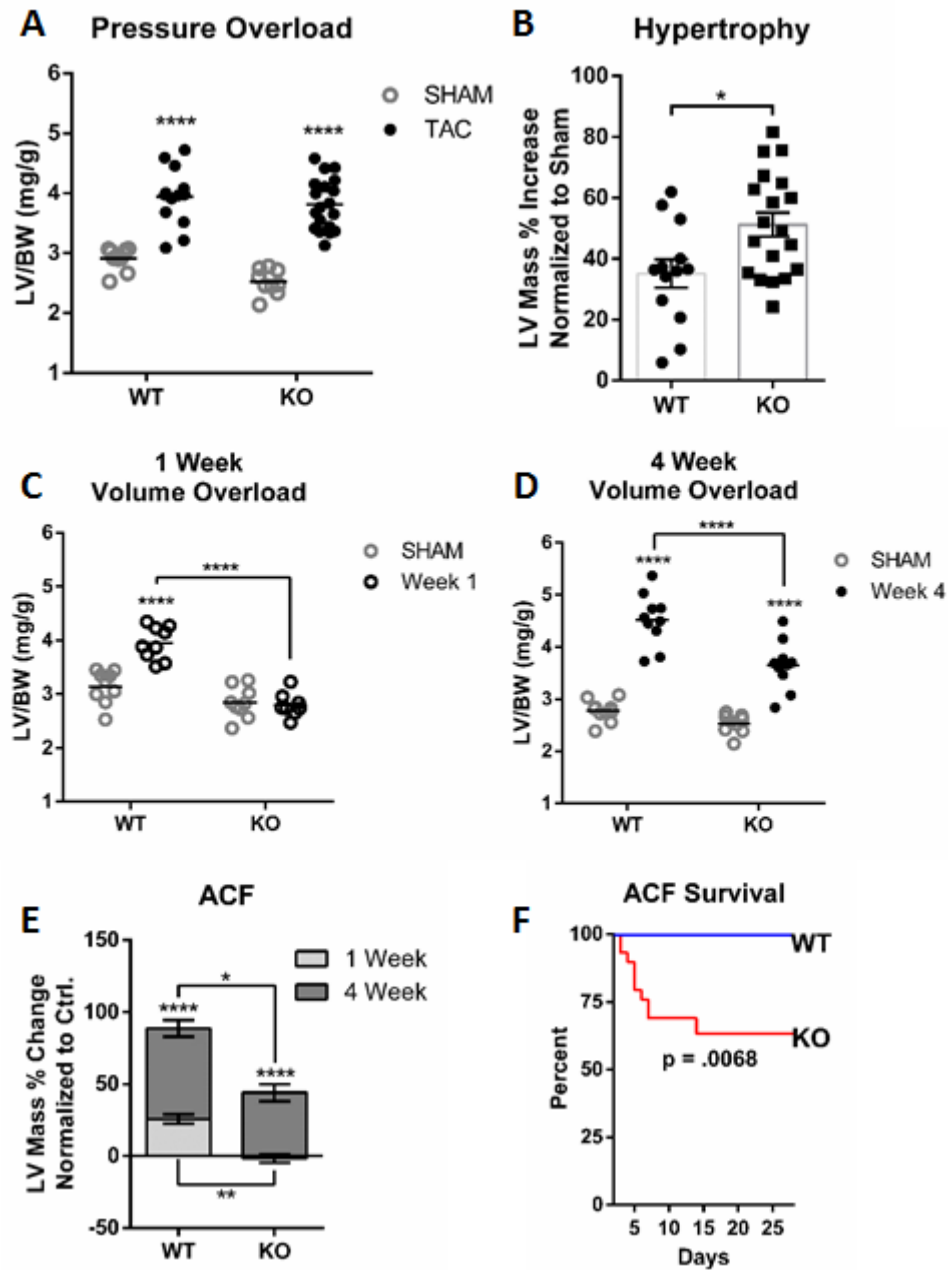


Figure 3: Chronic pressure and volume overload. A) TAC left ventricular weight (LV) normalized to body weight (BW); B) Percent left ventricle (LV) mass increase in afterload study; C) 1 week ACF left ventricular weight (LV) normalized to body weight (BW); D) 4 week ACF left ventricular weight (LV) normalized to body weight (BW); E) Percent left ventricle (LV) mass increase in ACF studies; F) ACF survival curve. Data shown as mean \pm SEM. Statistical significance calculated with two-way ANOVA and Bonferroni correction (A and C-E), t-test (B) and Log-Rank Mantel-Cox test (F); (* $p < 0.05$; ** $p < 0.01$; *** $p < 0.001$; **** $p < 0.0001$ as indicated).

Chapter 2 Figure 4

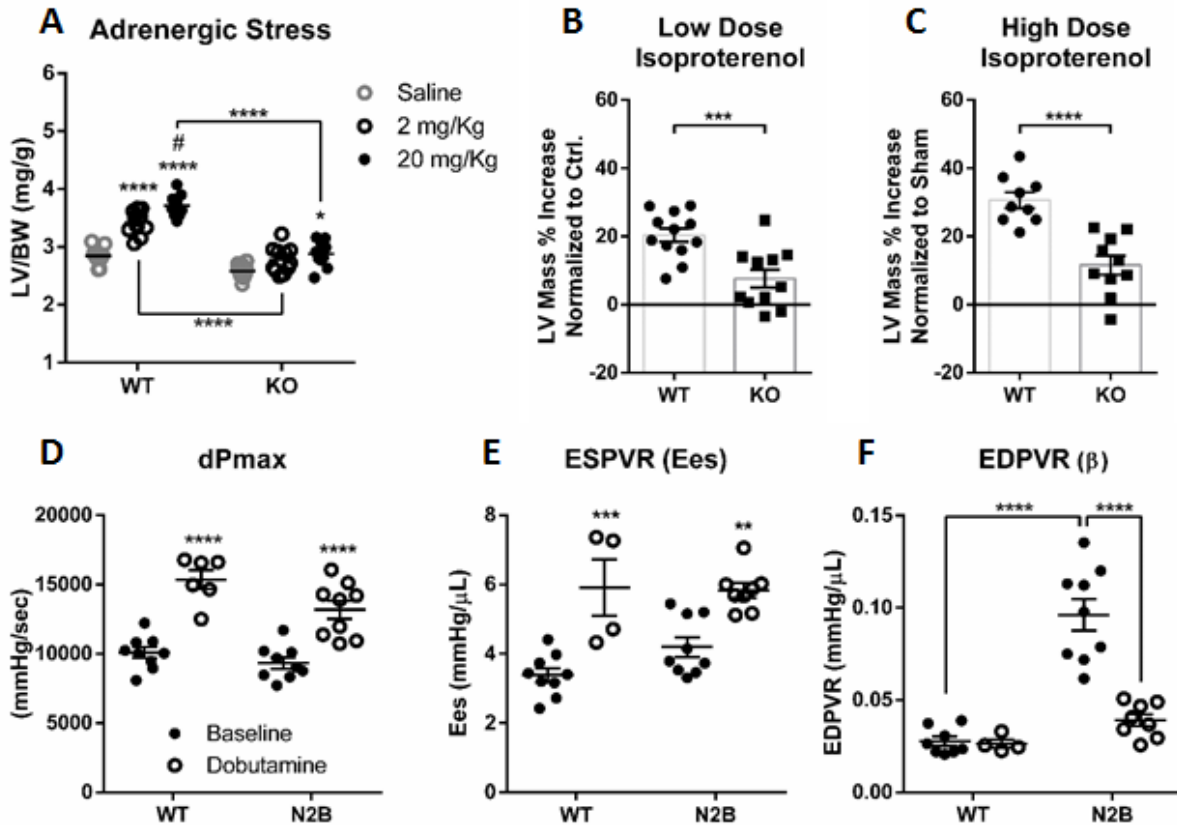


Figure 4: Isoproterenol injection study. A) 2 and 20 mg/kg dose injection studies, (LV) normalized to body weight (BW); B-C) Percent left ventricle (LV) mass increase in low dose (B) and high dose (C); D) dPmax; E) Slope (Ees) of ESPVR (end-systolic pressure volume relationship); F) Stiffness coefficient β of EDPVR (end-diastolic pressure volume relationship). Data shown as mean \pm SEM. Statistical significance calculated with two-way ANOVA and Bonferroni correction (A and D-F) and t-test (B-C), (* $p < 0.05$; ** $p < 0.01$; *** $p < 0.001$; **** $p < 0.0001$ as indicated).

Chapter 2 Figure 5

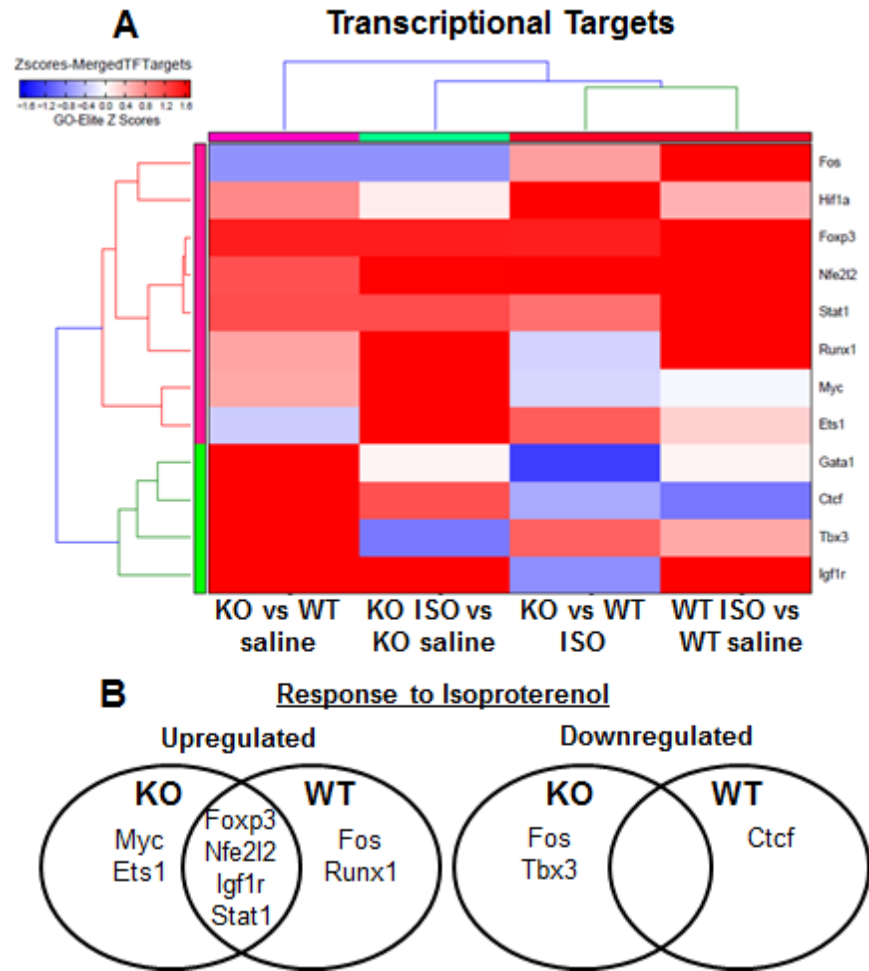


Figure 5: Transcriptional targets differentially regulated in isoproterenol study. A) Heat-plot; B) Venn diagram.

Figure 6: Western blot analysis of signal transduction. A) pAkt/Akt; B) PKC α / β -tubulin; C) pGSK3 β /GSK3 β ; D) pAkt/Akt in 1 week ACF study; E) pAkt/Akt in 4 week ACF study; F) pMTOR/MTOR in 1 week ACF study; G) pMTOR/MTOR in 4 week ACF study; H-I) FHL2 western blot images and corresponding images to (D-G). Data shown as mean \pm SEM. Statistical significance calculated with t-test (A-C) and two-way ANOVA and Bonferroni correction (D-G), (* $p < 0.05$; ** $p < 0.01$; *** $p < 0.001$; **** $p < 0.0001$ as indicated).

Figure 7

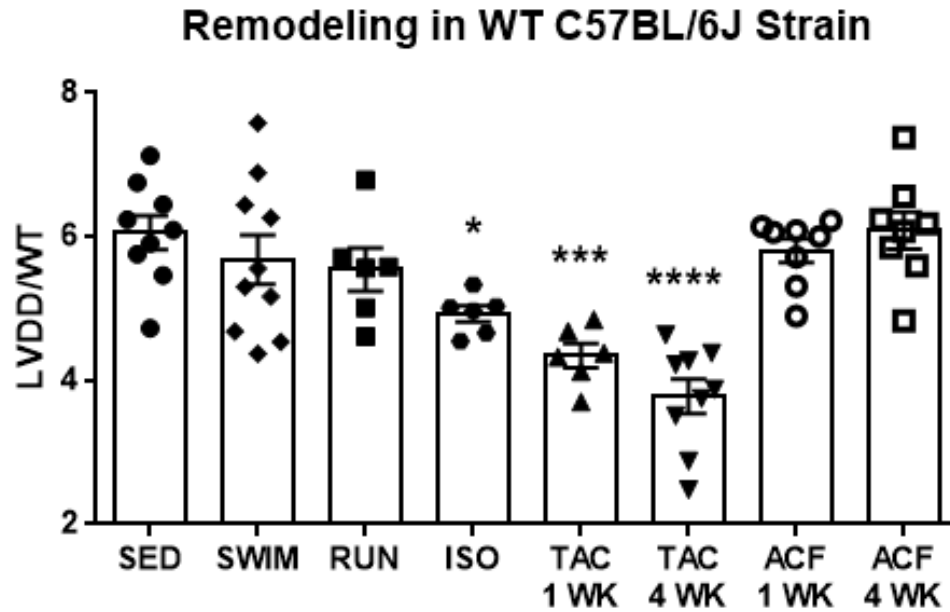


Figure 7: Eccentricity of WT mice in response to cardiac stress. Abbreviations: SED: sedentary analysis; SWIM: controlled swim training; RUN: voluntary wheel running; ISO: daily isoproterenol injections (2 mg/kg); TAC 1WK: 1 week chronic pressure overload induced by transverse aortic constriction; TAC 4WK: 4 week chronic pressure overload induced by transverse aortic constriction; ACF 1WK: 1 week chronic volume overload induced by aortocaval fistula; ACF 4WK: 4 week chronic volume overload induced by aortocaval fistula. Data shown as mean \pm SEM. Statistical significance calculated with one-way ANOVA and Bonferroni correction (D-G), (* $p < 0.05$; ** $p < 0.01$; *** $p < 0.001$; **** $p < 0.0001$ compared to SED).

Discussion and Summary

Hemodynamic stress through volume or pressure overload is characterized by distinct phenotypic differences. Chronic pressure or afterload is characterized by fibrotic hypertrophy and inflammation, and concentric remodeling of the heart. Comparatively, chronic preload results in better function and lower mortality²⁸. In pressure overload, calcium/calmodulin-dependent protein kinase II δ (CAMKII δ) signaling is activated while increased phosphorylation of Akt results from chronic volume overload stress^{28, 29}. Furthermore, gene expression analysis revealed unique transcriptional signatures associated with preload versus afterload stress²⁸. While signal transduction in cardiac hypertrophy has been studied at length, mechanotransduction is still poorly understood. The present study investigates the role of titin's N2B spring element as a mechanosensor in cardiac hypertrophy. We found that the N2B element is necessary for the early response to chronic volume overload stress and adrenergic stimulation through isoproterenol injections. Furthermore, swim training induced significantly less hypertrophy in KO versus WT mice. Conversely, voluntary wheel running and chronic afterload stress resulted in a similar cardiac hypertrophy response between genotypes. Our study highlights the diversity of cardiac adaptations to stress (see Fig. 7 for reference in WT mice) and reveals that the N2B element in titin is a necessary mechanosensor for stretch-activated Akt signaling in the heart.

Titin, is an ideal candidate for stretch-mediated signal transduction in striated muscle due to its ~ 1.0 MDa elastic spring region that spans the entire I-band of the sarcomere. This spring generates passive tension in diastole and regulates the passive filling properties of the heart³⁰. Skeletal muscle contains two primary elements, the tandem

Ig and the proline, glutamate, valine and lysine-rich (PEVK) elements that extend at different sarcomere lengths^{31, 32}. In cardiac muscle, there is an additional spring element: the N2B unique sequence that contains a central binding site for FHL2^{11-13, 33}. Extension of the N2B element occurs only when the sarcomere is maximally stretched (i.e., increased volume load), at what time mechanotransduction thought to occur. *Alpha*-B crystallin (α BC), FHL1 and FHL2 have been shown to localize to the N2B element in titin where they co-localize signaling enzymes^{13, 34, 35}. FHL2, however, has a dramatic reduction in protein levels in the heart upon removal of the N2B element while α BC and FHL1 protein content are unaffected¹⁹ (see also Fig. 1 H). This is a striking finding due to the vast protein interactome involving FHL2³⁶ (greater than 80 interacting proteins validated by either co-immunoprecipitation or direct interaction assays). These interactions take place at the cell membrane, cytoplasm and nucleus indicating FHL2's important role in signal transduction. We hypothesized that the N2B element can trigger gene expression in response to stress through its anchoring of FHL2. We have recently shown that not only is the N2B elements presence necessary to maintain WT FHL2 protein levels, but also its accessibility (INSERT IAxRBM20 REF). Inhibition of RBM20, a splicing factor of titin, creates super compliant (N2BAsc) titin isoforms that prevent extension of the N2B element within the physiologic sarcomere length range³⁷. In these mice FHL2 levels drop to ~20% of WT levels (data unpublished). Due to the complexity of protein-protein interactions that are mediated by FHL2 it is difficult to determine the sum of consequences created by removing its primary anchor within the cell.

Our studies with acute dobutamine infusion suggests that *beta*-1 adrenergic responsiveness is similar in N2B KO and WT mice, thus, pointing to *beta*-2 receptor

signaling differences. In order to avoid fibrosis and modifications in blood pressure, we chose to use a minimal dose of isoproterenol required to elicit cardiac hypertrophy²⁴. A single bolus injection of isoproterenol daily is also more similar to bouts of exercise since the stress is intermittent in contrast to chronic pump infusion methods. We initially considered that N2B KO mice may display exaggerated hypertrophy in response to beta-adrenergic stress since FHL2 null mice were reported to exhibit substantially greater hypertrophy than WT controls^{27, 38}. In our studies with isoproterenol, FHL2 mice responded similarly to WT mice while N2B KO mice did not respond at 2 mg/kg dosing (Fig. 4 and S3). Higher dosing, however, evoked an attenuated hypertrophy response in KO mice. We hypothesize is that FHL2 is stored within the N2B element in its folded state and then released upon extension. By removing the anchor of FHL2 within the cytoplasm, once it is translated it would be free to influence signal transduction and then be processed for degradation. This would explain why FHL2 null mice experience significant hypertrophy to isoproterenol but N2B KO mice with very minimal FHL2 protein exhibit a suppressed adrenergic hypertrophy response. Further molecular investigation is necessary to illuminate the disparate responses to isoproterenol in N2B and FHL2 KO mice.

When given access to a voluntary running wheel, WT and N2B KO mice ran approximately 8 kilometers per day (Fig. S2 C) after an initial ramp up phase and this stimulus resulted in robust cardiac remodeling. In contrast, controlled swimming for 2 hours a day, resulted in hypertrophic cardiac remodeling in WT mice that was significantly attenuated in KO mice. Exercise by swim or run training both cause beneficial cardiac adaptations in the heart, however, there are key differences in hemodynamic stress. In our study, mice were forced to swim continuously for 1 hour at a time to mimic endurance

training. Due to the buoyancy of water, swimming offers less resistance to venous return and allows for greater preload stress to the heart. Additionally, heart rate is higher during run vs swim training, while resting heart rate is similar in trained animals³⁹. Furthermore, norepinephrine levels are elevated in swim versus run trained rat myocardium suggesting that cardiac adaptations to swimming may require greater neurohormonal involvement³⁹. This might explain why KO mice had an attenuated response to both adrenergic stress and swim training. It is tempting to speculate that the common hypertrophic intermediary between beta-adrenergic receptor signaling and swim induced remodeling of the heart is the N2B element. Adrenergic stress may contribute to hypertrophic remodeling during swim training, however, isoproterenol alone induces concentric remodeling in WT mice while chamber dimensions are preserved after swim training (Fig. 7). Considering that swimming evokes a greater preload challenge in comparison to voluntary running which is a more balanced hemodynamic stressor to the heart, our exercise studies were in agreement with chronic hemodynamic stress suggesting that titin is necessary in stretch signaling.

Our ACF study revealed that the N2B element is critical for early hypertrophy signal transduction in chronic volume overload stimulation. The pro-survival Akt/mTOR signaling pathway has been shown to regulate eccentric cardiac hypertrophy in response to swimming⁴⁰ and volume overload^{28, 41, 42}. High mortality and blunted Akt signaling in KO mice at 1 week of volume overload suggests that mechanotransduction occurs through the N2B element to activate Akt initially. Previous studies have shown that activated Akt is significantly upregulated after 1 week of chronic volume overload and then diminishes by 4 weeks^{28, 29}. These findings were replicated in WT mice (Fig. 6 D) but the opposite occurred in KO mice (Fig. 6 E). This implies that Akt signaling in KO tissue at 4 weeks is

activated through a different pathway than what occurs in WT mice. Our gene expression studies revealed that Synd4 signaling was depressed in KO mice. Synd4 is plasma membrane proteoglycan that activates protein kinase C (PKC)⁴³ which is necessary for Akt mediated hypertrophy⁴⁴. Total PKC α levels were significantly reduced in sedentary KO mice (Fig. 6 B) and this could explain in part why Akt mediated signaling was affected. Titin is a known substrate of PKC phosphorylation⁴⁵⁻⁴⁷, therefore, it is conceivable that PKC activation of Akt also occurs within the spring region of titin. Immunolocalization studies of activated Akt would be necessary to determine if there is a distinct interaction with titin in early volume overload hypertrophy signaling. While our studies shed light on a prevailing hypothesis regarding titin as a stretch activator of hypertrophy signaling, a deeper molecular dissection is necessary to investigate the exact interactions responsible for mechanotransduction through the N2B element and FHL2.

Regrettably heart disease remains the number one cause of death world-wide and current therapies to treat morbidity and prevent mortality are inadequate. Pathological remodeling is responsible for the functional deficits characteristic of heart failure patients and while understanding of mechanotransduction is limited, it holds potential to provide novel therapeutic targets to treat heart failure. The N2B element in titin is a mechanosensor worth studying in greater detail as it dramatically affects cardiac remodeling as revealed by our work.

References of Chapter 2

1. Bernardo BC, Weeks KL, Pretorius L and McMullen JR. Molecular distinction between physiological and pathological cardiac hypertrophy: experimental findings and therapeutic strategies. *Pharmacol Ther.* 2010;128:191-227.
2. Basford JR. The Law of Laplace and its relevance to contemporary medicine and rehabilitation. *Archives of Physical Medicine and Rehabilitation.* 2002;83:1165-1170.
3. Vidal M, Wieland T, Lohse MJ and Lorenz K. beta-Adrenergic receptor stimulation causes cardiac hypertrophy via a Gbetagamma/Erk-dependent pathway. *Cardiovascular research.* 2012;96:255-64.
4. Lyon RC, Zanella F, Omens JH and Sheikh F. Mechanotransduction in cardiac hypertrophy and failure. *Circulation research.* 2015;116:1462-76.
5. van Berlo JH, Maillet M and Molkentin JD. Signaling effectors underlying pathologic growth and remodeling of the heart. *The Journal of clinical investigation.* 2013;123:37-45.
6. Frey N, Katus HA, Olson EN and Hill JA. Hypertrophy of the Heart: A New Therapeutic Target? *Circulation.* 2004;109:1580-1589.
7. Dorn GW, Robbins J and Sugden PH. Phenotyping Hypertrophy: Eschew Obfuscation. *Circulation Research.* 2003;92:1171-1175.

8. Miller MK, Granzier H, Ehler E and Gregorio CC. The sensitive giant: the role of titin-based stretch sensing complexes in the heart. *Trends Cell Biol.* 2004;14:119-26.
9. Gautel M, Lehtonen E and Pietruschka F. Assembly of the cardiac I-band region of titin/connectin: expression of the cardiac-specific regions and their structural relation to the elastic segments. *Journal of muscle research and cell motility.* 1996;17:449-61.
10. Rief M, Pascual J, Saraste M and Gaub HE. Single molecule force spectroscopy of spectrin repeats: low unfolding forces in helix bundles. *Journal of molecular biology.* 1999;286:553-61.
11. Trombitas K, Freiburg A, Centner T, Labeit S and Granzier H. Molecular dissection of N2B cardiac titin's extensibility. *Biophysical journal.* 1999;77:3189-96.
12. Helmes M, Trombitas K, Centner T, Kellermayer M, Labeit S, Linke WA and Granzier H. Mechanically driven contour-length adjustment in rat cardiac titin's unique N2B sequence: titin is an adjustable spring. *Circulation research.* 1999;84:1339-52.
13. Lange S, Auerbach D, McLoughlin P, Perriard E, Schafer BW, Perriard JC and Ehler E. Subcellular targeting of metabolic enzymes to titin in heart muscle may be mediated by DRAL/FHL-2. *J Cell Sci.* 2002;115:4925-36.
14. Yamasaki R, Wu Y, McNabb M, Greaser M, Labeit S and Granzier H. Protein kinase A phosphorylates titin's cardiac-specific N2B domain and reduces passive tension in rat cardiac myocytes. *Circulation research.* 2002;90:1181-8.

15. Kruger M, Kotter S, Grutzner A, Lang P, Andresen C, Redfield MM, Butt E, dos Remedios CG and Linke WA. Protein kinase G modulates human myocardial passive stiffness by phosphorylation of the titin springs. *Circulation research*. 2009;104:87-94.
16. Hidalgo CG, Chung CS, Saripalli C, Methawasin M, Hutchinson KR, Tsapralis G, Labeit S, Mattiazzi A and Granzier HL. The multifunctional Ca(2+)/calmodulin-dependent protein kinase II delta (CaMKIIdelta) phosphorylates cardiac titin's spring elements. *J Mol Cell Cardiol*. 2013;54:90-7.
17. Hamdani N, Krysiak J, Kreusser MM, Neef S, Dos Remedios CG, Maier LS, Kruger M, Backs J and Linke WA. Crucial role for Ca2(+)/calmodulin-dependent protein kinase-II in regulating diastolic stress of normal and failing hearts via titin phosphorylation. *Circulation research*. 2013;112:664-74.
18. Perkin J, Slater R, Del Favero G, Lanzicher T, Hidalgo C, Anderson B, Smith JE, 3rd, Sbaizero O, Labeit S and Granzier H. Phosphorylating Titin's Cardiac N2B Element by ERK2 or CaMKIIdelta Lowers the Single Molecule and Cardiac Muscle Force. *Biophysical journal*. 2015;109:2592-601.
19. Radke MH, Peng J, Wu Y, McNabb M, Nelson OL, Granzier H and Gotthardt M. Targeted deletion of titin N2B region leads to diastolic dysfunction and cardiac atrophy. *Proc Natl Acad Sci U S A*. 2007;104:3444-9.
20. Chung CS, Hutchinson KR, Methawasin M, Saripalli C, Smith JE, 3rd, Hidalgo CG, Luo X, Labeit S, Guo C and Granzier HL. Shortening of the elastic tandem

- immunoglobulin segment of titin leads to diastolic dysfunction. *Circulation*. 2013;128:19-28.
21. Li F, Buck D, De Winter J, Kolb J, Meng H, Birch C, Slater R, Escobar YN, Smith JE, 3rd, Yang L, Konhilas J, Lawlor MW, Ottenheijm C and Granzier HL. Nebulin deficiency in adult muscle causes sarcomere defects and muscle-type-dependent changes in trophicity: novel insights in nemaline myopathy. *Hum Mol Genet*. 2015.
 22. Hu P, Zhang D, Swenson L, Chakrabarti G, Abel ED and Litwin SE. Minimally invasive aortic banding in mice: effects of altered cardiomyocyte insulin signaling during pressure overload. *American Journal of Physiology - Heart and Circulatory Physiology*. 2003;285:H1261-H1269.
 23. Hutchinson KR, Saripalli C, Chung CS and Granzier H. Increased myocardial stiffness due to cardiac titin isoform switching in a mouse model of volume overload limits eccentric remodeling. *J Mol Cell Cardiol*. 2015;79:104-14.
 24. Hohimer AR, Davis LE and Hatton DC. Repeated daily injections and osmotic pump infusion of isoproterenol cause similar increases in cardiac mass but have different effects on blood pressure. *Can J Physiol Pharmacol*. 2005;83:191-7.
 25. LeWinter MM and Granzier H. Cardiac titin: a multifunctional giant. *Circulation*. 2010;121:2137-45.
 26. Hu P, Zhang D, Swenson L, Chakrabarti G, Abel ED and Litwin SE. Minimally invasive aortic banding in mice: effects of altered cardiomyocyte insulin signaling during pressure overload. *Am J Physiol Heart Circ Physiol*. 2003;285:H1261-9.

27. Kong Y, Shelton JM, Rothermel B, Li X, Richardson JA, Bassel-Duby R and Williams RS. Cardiac-Specific LIM Protein FHL2 Modifies the Hypertrophic Response to α -Adrenergic Stimulation. *Circulation*. 2001;103:2731-2738.
28. Toischer K, Rokita AG, Unsold B, Zhu W, Kararigas G, Sossalla S, Reuter SP, Becker A, Teucher N, Seidler T, Grebe C, Preuss L, Gupta SN, Schmidt K, Lehnart SE, Kruger M, Linke WA, Backs J, Regitz-Zagrosek V, Schafer K, Field LJ, Maier LS and Hasenfuss G. Differential cardiac remodeling in preload versus afterload. *Circulation*. 2010;122:993-1003.
29. Miyamoto T, Takeishi Y, Takahashi H, Shishido T, Arimoto T, Tomoike H and Kubota I. Activation of distinct signal transduction pathways in hypertrophied hearts by pressure and volume overload. *Basic research in cardiology*. 2004;99:328-37.
30. Trombitas K, Jin JP and Granzier H. The mechanically active domain of titin in cardiac muscle. *Circulation research*. 1995;77:856-61.
31. Trombitas K, Greaser M, Labeit S, Jin JP, Kellermayer M, Helmes M and Granzier H. Titin extensibility in situ: entropic elasticity of permanently folded and permanently unfolded molecular segments. *The Journal of cell biology*. 1998;140:853-9.
32. Linke WA and Granzier H. A spring tale: new facts on titin elasticity. *Biophysical journal*. 1998;75:2613-4.

33. Linke WA, Rudy DE, Centner T, Gautel M, Witt C, Labeit S and Gregorio CC. I-band titin in cardiac muscle is a three-element molecular spring and is critical for maintaining thin filament structure. *The Journal of cell biology*. 1999;146:631-44.
34. Sheikh F, Raskin A, Chu PH, Lange S, Domenighetti AA, Zheng M, Liang X, Zhang T, Yajima T, Gu Y, Dalton ND, Mahata SK, Dorn GW, 2nd, Brown JH, Peterson KL, Omens JH, McCulloch AD and Chen J. An FHL1-containing complex within the cardiomyocyte sarcomere mediates hypertrophic biomechanical stress responses in mice. *The Journal of clinical investigation*. 2008;118:3870-80.
35. Zhu Y, Bogomolovas J, Labeit S and Granzier H. Single molecule force spectroscopy of the cardiac titin N2B element: effects of the molecular chaperone alphaB-crystallin with disease-causing mutations. *The Journal of biological chemistry*. 2009;284:13914-23.
36. Tran MK, Kurakula K, Koenis DS and de Vries CJM. Protein–protein interactions of the LIM-only protein FHL2 and functional implication of the interactions relevant in cardiovascular disease. *Biochimica et Biophysica Acta (BBA) - Molecular Cell Research*. 2016;1863:219-228.
37. Methawasin M, Hutchinson KR, Lee EJ, Smith JE, 3rd, Saripalli C, Hidalgo CG, Ottenheijm CA and Granzier H. Experimentally increasing titin compliance in a novel mouse model attenuates the frank-starling mechanism but has a beneficial effect on diastole. *Circulation*. 2014;129:1924-36.

38. Hojayeve B, Rothermel BA, Gillette TG and Hill JA. FHL2 binds calcineurin and represses pathological cardiac growth. *Molecular and cellular biology*. 2012;32:4025-34.
39. Geenen D, Buttrick P and Scheuer J. Cardiovascular and hormonal responses to swimming and running in the rat. *Journal of applied physiology (Bethesda, Md : 1985)*. 1988;65:116-23.
40. Ma Z, Qi J, Meng S, Wen B and Zhang J. Swimming exercise training-induced left ventricular hypertrophy involves microRNAs and synergistic regulation of the PI3K/AKT/mTOR signaling pathway. *European journal of applied physiology*. 2013;113:2473-86.
41. Drolet MC, Desbiens-Brassard V, Roussel E, Tu V, Couet J and Arsenault M. Blockade of the acute activation of mTOR complex 1 decreases hypertrophy development in rats with severe aortic valve regurgitation. *SpringerPlus*. 2015;4:435.
42. Ikeda M, Ide T, Fujino T, Matsuo Y, Arai S, Saku K, Kakino T, Oga Y, Nishizaki A and Sunagawa K. The Akt-mTOR axis is a pivotal regulator of eccentric hypertrophy during volume overload. *Scientific reports*. 2015;5:15881.
43. Oh ES, Woods A and Couchman JR. Multimerization of the cytoplasmic domain of syndecan-4 is required for its ability to activate protein kinase C. *The Journal of biological chemistry*. 1997;272:11805-11.

44. Xie J, He G, Chen Q, Sun J, Dai Q, Lu J, Li G, Wu H, Li R, Chen J, Xu W and Xu B. Syndecan 4 signaling is required for exercise-induced cardiac hypertrophy. *Molecular medicine (Cambridge, Mass)*. 2016.
45. Hidalgo C, Hudson B, Bogomolovas J, Zhu Y, Anderson B, Greaser M, Labeit S and Granzier H. PKC phosphorylation of titin's PEVK element: a novel and conserved pathway for modulating myocardial stiffness. *Circulation research*. 2009;105:631-8, 17 p following 638.
46. Anderson BR, Bogomolovas J, Labeit S and Granzier H. The effects of PKC α phosphorylation on the extensibility of titin's PEVK element. *J Struct Biol*. 2010;170:270-7.
47. Hudson BD, Hidalgo CG, Gotthardt M and Granzier HL. Excision of titin's cardiac PEVK spring element abolishes PKC α -induced increases in myocardial stiffness. *J Mol Cell Cardiol*. 2010;48:972-8.

Supplemental Methods of Chapter 2

Generation of Mice: The N2B genetic murine model previously described¹ were bred to generate homozygous N2B deficient mice on a C57BL/6J background. In our studies we used mice ~ 4 months old and male, unless indicated otherwise. All experiments were approved by the University of Arizona Institutional Animal Care and Use Committee (IACUC) and followed the U.S. National Institutes of Health Using Animals in Intramural Research guidelines for animal use.

Echocardiography: A Vevo 2100 High Resolution Imaging System (Visual-Sonics, Toronto, Canada) was used with the model MS5500 scan head designed for murine cardiac imaging. Care was taken to avoid animal contact and excessive pressure which could induce bradycardia during conscious scanning. Imaging was performed at a depth setting of 11 mm. Images were collected and stored as a digital cine loop for off-line calculations. Mice were consciously echoed while scruffing the skin at the nape of the neck and a standard short axis (M-mode) cine loop was recorded at the level of the papillary muscles to assess chamber dimensions (LV systolic and diastolic dimensions (LVDs, LVDd)) posterior and anterior wall thickness (WT), and cardiac function via Fractional Shortening (%FS). Functional calculations were obtained according to American Society of Echocardiography guidelines. To investigate diastolic function we performed Doppler echo on anesthetized mice. Mice were anesthetized and ventilated with 2% isoflurane using a nose cone and body temperature was maintained at 37°C. Following anesthetic induction, the mouse was placed in dorsal recumbence on a heated platform for echocardiography.

Images were collected and stored as a digital cine loop for off-line calculations. The left atrial dimension was measured in the long-axis view directly below the aortic valve leaflets. Passive LV filling peak velocity, E (cm/sec), and atrial contraction flow peak velocity, A (cm/sec), were acquired from the images of mitral valve Doppler flow from 4-chamber apical views, according to American Society of Echocardiography guidelines. The heart rate of animals was maintained in the range of 450 ± 25 bpm for Doppler studies.

Pressure-Volume Analysis: In vivo pressure-volume analysis was performed in mice using a SciSense Advantage Admittance Derived Volume Measurement System and 1.2F catheters with 4.5 mm electrode spacing (SciSense, London, Ontario, Canada). Mice were anesthetized and ventilated with 1.5% isoflurane using a SAR-1000 Small Animal Ventilator (CWE). Body temperature under anesthesia was maintained at 37°C using a TC-1000 Temperature Controller (CWE). A lateral incision through the skin and muscle was made below the ribcage and the diaphragm was cut in order to expose the apex of the heart. A small puncture was made in the apex of the left ventricle using a 28G needle and the 1.2F catheter was inserted into the LV. Baseline functional parameters were assessed during a pause in ventilation in order to avoid respiratory influences. For load-independent indices, including the end-systolic and end-diastolic pressure-volume relationships, the IVC was temporarily occluded to vary the preload conditions. Data acquisition and analysis was performed using LabScribe 2 (iWorx, Dover, NH) and curve fitting was performed with MATLAB (MathWorks, Natick, MA). Diastolic PV data was analyzed using a mono-exponential fit with constant ($P = Ae^{\beta V} + C$) with the exponent (β) reported as the coefficient of stiffness.

Voluntary Wheel Running: We used 3-4 month old mice for voluntary exercise studies. Mice were housed individually in a cage that contained a free-running wheel. The exercise wheels were purchased from Lafayette Instrument®, model 80820 activity wheel chamber with 86060S sensor attached to the wheel support frame for continuous data collection. Data were stored in an attached CPU for further processing. **Controlled Swimming:** A swimming chamber for mice was developed to control duration and pace of swimming. Mice were swam for 1 hour twice a day for three weeks after an initial ramp up phase. The swimming chamber temperature was held constant at 84° F or (+/- 1 °). A magnetically driven water circulator was attached at the bottom of the tank to produce an even under current across the tank.

Quantification of Protein Expression: Flash frozen LV tissues were cut and weighed, then pulverized into a very fine powder using a mortar and pestle in liquid nitrogen. Samples were then placed into a -20°C freezer for 20minutes. 8M urea buffer ([in mol/L] 8 Urea, 2 Thiourea, 0.05 Tris-HCl, 0.075 Dithiothreitol with 3% SDS and 0.03% Bromophenol blue pH 6.8) and 50% glycerol with protease inhibitors ([in mmol/L] 0.04 E64, 0.16 Leupeptin and 0.2 PMSF) were added to the samples (in a 40:40:1 ratio) and solubilized for 10minutes at 60°C. The solubilized samples were centrifuged, aliquoted into smaller volumes, and stored at -80°C. **Titin isoform expression analysis:** titin isoform expression analysis was performed via electrophoresis of the solubilized samples on a 1% agarose gel (Hoefer gel system). The gels are loaded with six different volumes of the sample and run at 15mA per gel for 3hours and 20minutes. The protein was then fixed on the gel using a fixing solution, stained with coomassie brilliant blue (Acros

organics), then scanned (Epson commercial scanner) in order to capture an image for the analysis of the various Titin isoform bands. The images were analyzed using OneD scan software by determining the integrated optical density of Titin and myosin heavy chain as a function of the various volumes loaded on the gel. The isoform expression ratios of the samples are determined by using the slope of the optical density of the different loading volumes. **Western Blotting:** western blotting is a technique used to quantify protein expression. The solubilized samples were run on SDS PAGE gels (different percentages depending on target protein). Gels were run for approximately 2 hours then samples were transferred to PDVF membranes (Immobilon, Millipore) using a semi-dry transfer unit (Trans-Blot Cell, Bio-Rad). Transfer amperage was based on area of membrane(s) multiplied by 1.3 and was run for 2.5hours. The membranes were stained with Ponceau S (Sigma) to visually ensure protein transfer. The Ponceau S stain was later removed by .1M NaOH, and blots were placed in a blocking solution (Odyssey Block) for 1hour to prevent non-specific binding of the antibody. Blocking solution was removed and blots were then soaked in the primary antibody solution overnight. Primary antibody was removed and blots were washed with PBS-tween solution before secondary fluorescent antibody was added. The blots soaked in secondary antibody for 1hour before they were scanned using an Odyssey Infrared Imaging System (Li-COR Biosciences). Images obtained were analyzed using Li-COR Odyssey software.

Antibody	Source	Host	Dilution
PKC alpha	R&D Systems	Goat	1:1000
pGSK3beta	Cell Signaling Technology	Rabbit	1:1000
GSK3beta	Cell Signaling Technology	Mouse	1:1000
pAkt	Cell Signaling Technology	Rabbit	1:1000
Akt	Cell Signaling Technology	Mouse	1:1000
pMTOR	Cell Signaling Technology	Rabbit	1:1000
MTOR	Cell Signaling Technology	Mouse	1:1000
MLP	Biogenes	Rabbit	1:1000
CARP	Santa Cruz Biotech	Rabbit	1:1000
FHL1	MBL	Rabbit	1:5000
FHL2	MBL	Rabbit	1:5000
alphaBCrystallin	Millipore	Rabbit	1:1500
Beta Tubulin	Cell Signaling Technology	Mouse	1:5000
GAPDH	Thermo Pierce	Mouse	1:5000

Transverse Aortic Constriction: For minimally invasive Transverse Aortic Constriction (TAC) surgeries, anesthesia was induced by intraperitoneal (i.p.) injection of ketamine hydrochloride (120 mg/kg) plus xylazine (12 mg/kg) for a depth of anesthesia ~45 min, long enough to finish the surgery. The aortic banding procedure was performed similar to that previously described² with minor adaptations. Briefly, a small incision in the chest cavity was created between the first and second intercostal ribs and the transverse portion of the aorta was bluntly dissected from the surrounding tissue. A curved forceps was then placed under the transverse aorta, 7-0 silk was grasped by the forceps and moved underneath the aorta between the right innominate and left carotid arteries, and a loose double knot was made. A 27-gauge needle with OD 0.42 mm was delivered through the loose double knot and placed directly above and parallel to the aorta. The loop was then tied around the aorta and needle and secured with the second knot (this was done very quickly, to minimize ischemia). The needle was immediately removed to provide a lumen

with a stenotic aorta. Following the surgery, all layers of muscle and skin were closed with 6-0 continuous absorbable and nylon sutures, respectively, and the wound was treated with Betadine. Immediately after the operation, 0.5 ml of 37°C saline was given intraperitoneally, and a dose of analgesic (SR-buprenorphine, 0.1 mg/kg) was also given subcutaneously. For the sham operation (control) the mice underwent the identical procedure, except placing of the ligature. The surgical survival rate following TAC was >90% and mortality rate within the first month following TAC was low (<5%). Successful surgical ligation of the transverse aorta, determined by a Doppler flow velocity measurement indicated by a large pressure gradient following constriction. Animals were sacrificed, weighed and cardiac tissue was flash frozen in liquid nitrogen (-80° C) for further analysis.

Aortocaval Fistula:

Mice were anesthetized with 2% isoflurane, and cardiac volume overload was induced³ in 3 month old male C57BL/6J mice. Briefly, a midline abdominal incision was made and the abdominal aorta and inferior vena cava were exposed. Vascular clips were placed above the iliac bifurcation and below the iliolumbar vessels. A 23-g needle was inserted into the aorta and through the common midwall, creating an ACF. The needle was removed, and cyanoacrylate glue (Vetbond) was used to seal the aortic puncture. Shunt patency was visually confirmed by mixture of bright red arterial blood in the vena cava. The abdominal muscle and skin were closed using 6-0 vicryl absorbable suture and 7-mm surgical staples, respectively. Sham animals were treated identically except no aortic puncture was made. Mice were sacrificed 1 or 4 wks following surgery. All experiments were performed in

accordance with the Principles of Laboratory Animal Care from the National Institutes of Health (8th Revision, 2011) and were approved by the Institutional Animal Care and Use Committee (IACUC) at the University of Arizona.

Isoproterenol Injections: Mice received 2.0 or 20 $\mu\text{g}/(\text{g}\cdot\text{d})$ of isoproterenol as previously described⁴. The dose was given as a single subcutaneous injection daily. After 5 days of exposure, the animals were sacrificed and cardiac tissue weights were determined.

GeneChip: LV tissue was dissected from male mice (4 month-old) of each genotype for isoproterenol studies, and stored in RNAlater. Total RNA was isolated using the RNeasy Fibrous Tissue Mini Kit (Qiagen) after preparation with RNAlater-ICE (Invitrogen). RNA quality was assessed by NanoDrop 1000 Spectrophotometer and 2100 Bioanalyzer (Agilent); all samples had RIN 9.0-9.3. Samples were hybridized with the GeneChip Mouse Gene 1.0 ST Array (Affymetrix); processing (labeling through scanning) was performed by the Genomics Core, University of Arizona, following Affymetrix protocols and using Affymetrix supplies and equipment. Data analysis was conducted using three different packages: Expression Console (Affymetrix) with RMA, BRB-ArrayTools (BRB-NCI) with RMA, and Gene Array Analyzer (<http://gaa.mpi-bn.mpg.de/>) with either PLIER or RMA.

Supplemental Figure 1

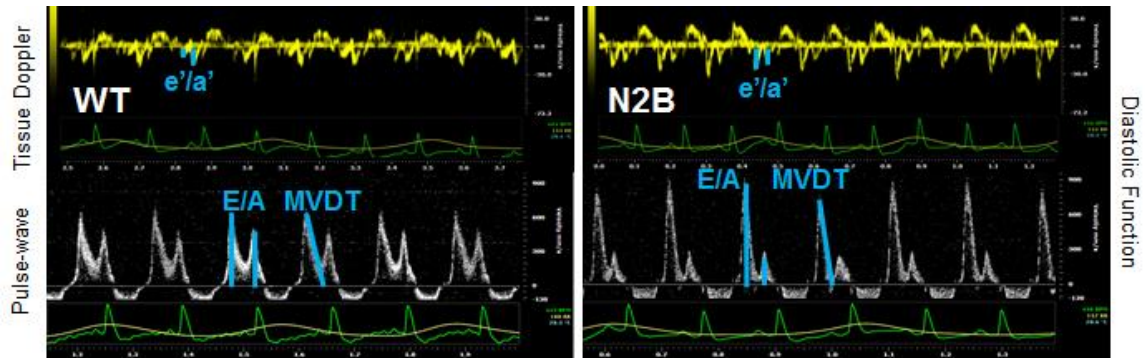


Figure S1: Representative Doppler characterization of WT and N2B KO mice. Upper left: WT tissue Doppler; Lower left: WT pulse-wave Doppler; Upper right: N2B tissue Doppler; Lower right N2B pulse-wave Doppler.

Supplemental Figure 2

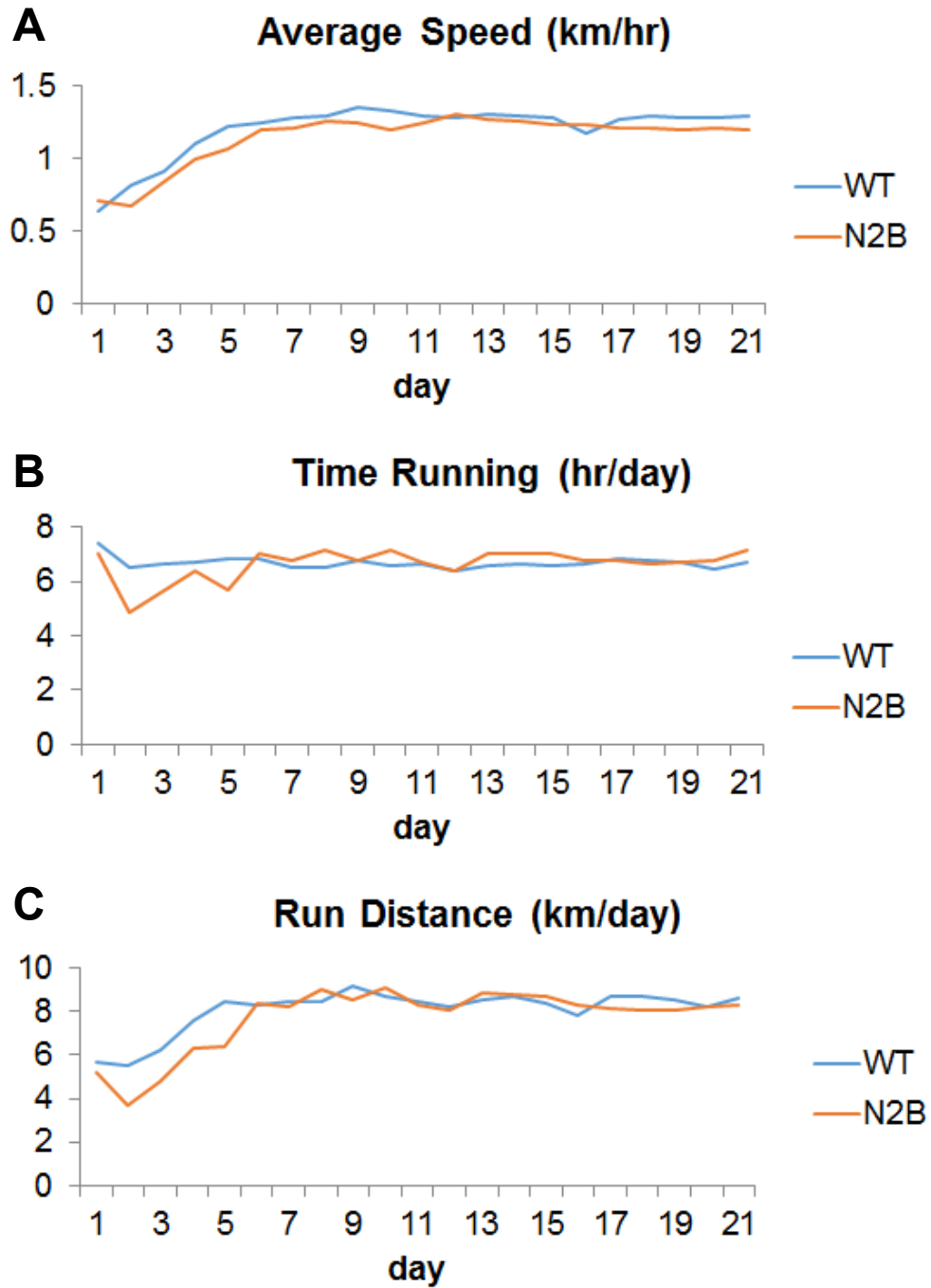


Figure S2: Voluntary wheel running in WT and KO mice. A) Average speed; B) time; C) distance.

Supplemental Figure 3

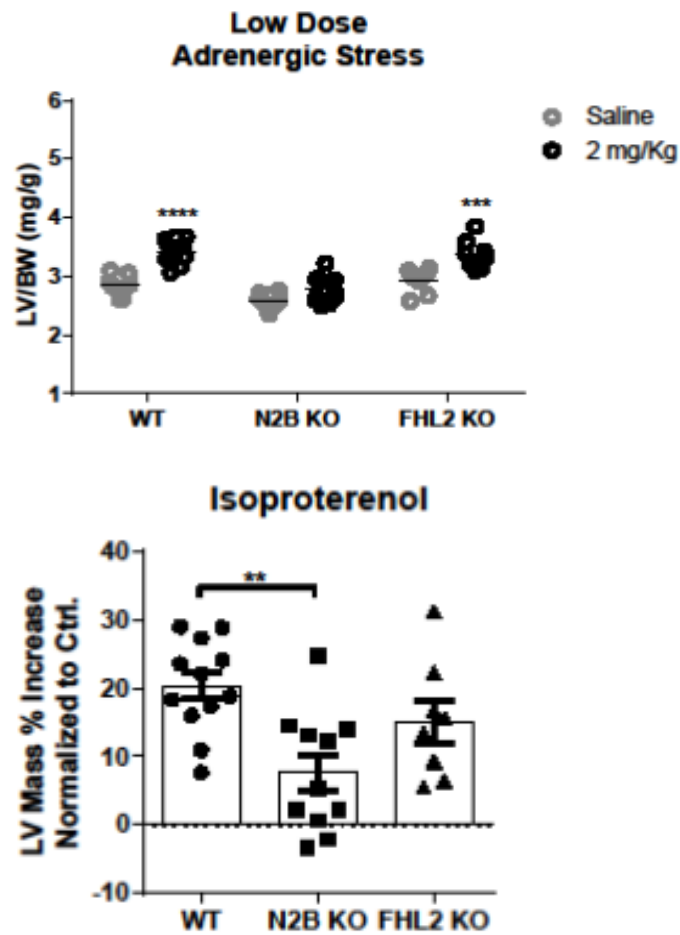


Figure S3: Low dose (2 mg/kg) isoproterenol injection study in WT, N2B KO and FHL2 KO mice. A) Normalized left ventricular weight to body weight; B) percent LV mass increase. Data shown as mean \pm SEM. Statistical significance calculated with one or two-way ANOVA and Bonferroni correction (* $p < 0.05$; ** $p < 0.01$; *** $p < 0.001$; **** $p < 0.0001$).

References of Chapter 1 Supplemental Methods

1. Radke MH, Peng J, Wu Y, McNabb M, Nelson OL, Granzier H and Gotthardt M. Targeted deletion of titin N2B region leads to diastolic dysfunction and cardiac atrophy. *Proc Natl Acad Sci U S A*. 2007;104:3444-9.
2. Hudson B, Hidalgo C, Saripalli C and Granzier H. Hyperphosphorylation of mouse cardiac titin contributes to transverse aortic constriction-induced diastolic dysfunction. *Circulation research*. 2011;109:858-66.
3. Scheuermann-Freestone M, Freestone NS, Langenickel T, Hohnel K, Dietz R and Willenbrock R. A new model of congestive heart failure in the mouse due to chronic volume overload. *European journal of heart failure*. 2001;3:535-43.
4. Hohimer AR, Davis LE and Hatton DC. Repeated daily injections and osmotic pump infusion of isoproterenol cause similar increases in cardiac mass but have different effects on blood pressure. *Canadian journal of physiology and pharmacology*. 2005;83:191-7.

DISCUSSION AND SUMMARY

In **chapter 1**, I focused on post-transcriptional modification of titin as an alternative strategy for treating patients with diastolic dysfunction. Our studies on Rbm20 inhibition are exciting and relevant to heart disease, as we report for the first time a therapy to treat HFpEF-like symptoms in the mouse. HFpEF is a complex disease with several etiologies, and the pathophysiology is not well understood. Hypo-phosphorylation of titin PKA/PKG sites in addition to oxidative stress contribute to increased myocardial stiffness in HFpEF patients. Titin's cardiac specific N2B element contains 6 cysteine residues that have the potential to form disulfide bonds in response to oxidative stress. Single molecule studies revealed that disulfide linkage within the N2B unique sequence reduces the contour length of this spring element and enhances passive tension (Grutzner et al., 2011). Further analysis of WT and N2B KO myocardium revealed that the N2B element is responsible for reducing the energy needed per beat by ~2% (Nedrud J et al., 2011). Therefore, in conditions of oxidative stress, disulfide linkage not only increases passive myocardial stiffness but also increases the energy demand on the heart. Logically, deranged phosphorylation would be expected to enhance energy loss in a similar manner. PKG phosphorylation of the N2B spring element has the effect of increasing titin and therefore sarcomere compliance, therefore, interest in treatment of HFpEF patients with phosphodiesterase inhibitors to prevent cGMP degradation has led to the recent RELAX trial. Earlier work in canine models of HF suggested that sildenafil, a PDE5 inhibitor, would be a promising therapy in the treatment of HFpEF (Bishu et al., 2011). Furthermore, expression of PDE9A has recently been shown to be heightened in HFpEF patients and

inhibition of PDE9A in mice was found to be cardio-protective (Kotter et al., 2013). An alternative approach is to by-pass post-translational modifications through upregulating super compliant titin isoforms. My work in chapter 1 has shown that manipulating titin spring compliance through alternative splicing is beneficial in titin-centric HFpEF model and further work is needed to confirm alternative splicing of titin as a means of treating disorders of the pathologically stiff heart.

In **chapter 2**, I studied the cardiac specific N2B spring element in titin and provide convincing evidence that it is necessary for stretch-activated hypertrophy signaling in the heart in response to excess preload. There has been a long standing hypothesis in the field that titin's spring region is a strain/stress sensing and signaling "hot-spot" in the sarcomere. Signaling has been proposed to localize to the N2B, PEVK and N2A spring elements within titin's I-band region. Not only are these elements thought to localize signaling enzymes within the sarcomere, but our lab and others have shown that they are themselves substrates for phosphorylation by major kinases relevant to heart disease (ERK2, PKA, PKG and CAMKII δ). Previous spring element deletion models (IA, Ig, and PEVK) share a similar hypertrophic phenotype along with amplified protein expression of four-and-a-half LIM domain (FHL) proteins. In contrast, deletion of the N2B element causes a significantly reduced ventricular size. To further examine titin's role in signal transduction I did extensive western blot analysis of major nodal kinases involved in hypertrophy signaling. Of note, activated GSK3 β is significantly elevated in sedentary N2B KO LV tissue. GSK3 β is widely considered an anti-hypertrophic master regulator in the cell. The direct connection between titin and GSK3 β is yet to be determined, but previous studies have

linked FHL2 as a co-activator of the WNT pathway. It is tempting to speculate that the drastic decrease in FHL2 protein expression may deregulated WNT signaling in N2B KO mice leading in part to the atrophied phenotype. Whichever the case, the N2B KO phenotype has led to the hypothesis that the N2B unique sequence is the central spring element required for mechanotransduction in titin. My work in chapter 2 confirms this hypothesis, however, it would be interesting to evaluate volume overload in other stress-sensitive elements in titin.

Future Directions

Chapter 2 of this dissertation addresses the long-standing hypothesis that the N2B element is a mechanosensor for cardiac hypertrophy. We have shown that eccentric growth of the heart is attenuated in the N2B KO mouse and this may be explained by reduced activation of Akt in response to preload stress. Furthermore, eccentric growth may involve neurohormonal activation of Akt, which was also suppressed in the N2B KO mouse. A greater depth of understanding of the Akt pathway that is activated during preload stress (ACF) and beta-adrenergic stimulation is necessary to narrow in on the exact mechanisms that trigger signaling through the N2B element. Probing for specific isoforms of Akt may also reveal that the activated Akt at 4 weeks of ACF in the KO mouse may in fact be related to an alternative signaling pathway. Furthermore, since Akt is involved in numerous cellular processes in the myocyte, an analysis of downstream signaling events (e.g., FOXOs, TSC2, S6K, 4E-BP1, NFAT, GATA) would illuminated how stretch activated hypertrophy is regulated at the nuclear level. However, since Akt is likely activated at the membrane and/or cytosol, where the N2B element resides, then a focused study on

upstream targets (e.g., PI3K, MTOR, PDK1, Synd4) may reveal where the early activation of Akt is inhibited in the N2B KO mouse. It will be important to look at early time points (i.e. 1 week ACF and 10-30 mins post ISO injection) to determine the difference in signaling that occurs in N2B deficient mice. It is likely that a later time point (4 Week ACF) is missing the direct link between N2B and Akt signaling in response to cardiac stress.

One set of experiments (not discussed in this dissertation) that could be expanded upon are acute isoproterenol injections (10 min) that may reveal changes in signaling between WT and N2B KO mice. Upon injection of mice subcutaneously with 2 mg/kg dosing of isoproterenol, mice are euthanized 10 minutes later and hearts are immediately explanted into liquid nitrogen. Preliminary western blot data showed that ERK1/2 and calcineurin (CN) were significantly upregulated in hearts of mice in these experiments, however, we did not examine Akt signaling at this time. There was no difference between WT or KO mice in activated ERK1/2 or total CN in these experiments but they did confirm the protocol is effective at catching early in vivo signaling events as they occur. Further analysis of 1 week ACF samples may also illuminate early Akt signaling, however, it is possible that alternative signaling mechanisms have already started to occur in the KO mouse at 1 week, therefore, results may be less apparent in the 1 week ACF study than in the ISO study.

Our gene-chip data in the isoproterenol study also revealed that Syndecan 4 (Synd4), signaling is downregulated in the N2B KO mouse. Synd4 is a transmembrane proteoglycan necessary to activate cardiac remodeling in response to stress. A recent study by Xie et al., 2016, revealed that Synd4 was necessary to mediate swimming induced

hypertrophy through the Akt pathway. Additionally, it was found that inhibition of protein kinase C (PKC) prevented the Synd4 induced hypertrophic phenotype and Akt phosphorylation (Xie et al., 2016). In sedentary KO mice, total PKC α is downregulated (Chapter 2 Figure 6B) and this may explain differences in activated Akt between WT and KO mice in our studies. A further analysis of Synd4 mediated Akt signaling may be beneficial in determining a molecular phenotype in the N2B KO mouse. If Synd4 signaling is indeed altered in N2B KO mice, it would directly link signal transduction at the plasma membrane to titin.

An alternative set of experiments that may be useful in determining signal transduction through the N2B element would be to compare stress responses in the *Ttn*^{ΔIAjxn} and *Rbm20*^{ARRM} murine models and the N2B deficient model. These models in combination are powerful tools to study the N2B element. The *Ttn*^{ΔIAjxn} mouse has further strain placed on the N2B element causing upregulation of FHL2 protein levels while the *Rbm20*^{ARRM} mouse completely reduces strain on the N2B element and shows a significant drop (< 20%) in FHL2 protein expression. Evaluating activated Akt signaling in these 3 models might provide novel insights.

While both of these chapters focus on major topics in the field of titin research, there are other relevant issues surrounding titin that are worth discussion and the following will address some of these issues.

Titin is a major human disease gene

TTN is a 364 exon gene that encodes the largest known protein and third most abundant filament in muscle, titin. Composed of four distinct regions, (N-terminal Z-line, I-band, A-band, and C-terminal M-line), titin acts as a molecular spring that is responsible for the assembly and maintenance of ultrastructure in the sarcomere. Additionally, titin is the chief contributor of passive stiffness in the heart, and functions as a molecular mechano-sensor for stress and strain in the myocyte¹⁻².

Until recently it has been difficult to link TTN mutations to disease phenotypes due to the complexity and gigantic size of the gene's coding sequence (~ 100 kb). Prior to the breakthrough study by Herman et al., 2012, there were limited studies identifying mutations in titin with skeletal and cardiac myopathies³⁻⁵. With the advent of Next Generation Sequencing (NGS), however, it became apparent that TTN truncating mutations are the most common genetic cause of dilated cardiomyopathy (DCM). Interestingly, TTN DCM mutations are non-randomly segregated to the A-Band region where titin associates with the thick filament. To date, there are more than 130 reported TTN disease causing mutations in patients with 10 different clinical manifestation⁶. This number, however, is expected to increase significantly as more patients with myopathies receive a full TTN screen. These mutations present as isolated cardiac and isolated skeletal disease phenotypes, as well as combined skeletal/cardiac congenital disease. As more evidence sheds light on TTN as a major human disease gene, there are some perplexing questions that remain to be answered.

Why do some mutations cause skeletal pathology and others cardiac pathology?

Interest in the protein titin is at an all-time high as NGS has sky-rocketed the TTN gene to the forefront of clinicians' minds. Titin has long been known to be a key protein involved in diastolic function and passive stiffness of the heart⁷. Since greater than half of all heart failure patients suffer from diastolic dysfunction, titin has been intensely studied over the past 30 years. Moreover, TTN mutations are now recognized as being responsible for greater than 30% of patients diagnosed with idiopathic DCM. Unfortunately, there are no available therapeutic options specifically aimed to treat patients with diastolic heart failure otherwise known as heart failure with preserved ejection fractions (HFpEF) at this time. With all of the focus surrounding titin and cardiomyopathies, it is surprising that there are not more reported mutations in skeletal muscle.

Of the greater than 130 known TTN mutations, only 35 mutations are reported to cause skeletal muscle myopathies (CNM: centronuclear myopathy, LGMD2J: limb-girdle muscular dystrophy type 2J, TMD: tibial muscular dystrophy, MFM: myofibrillar myopathy, HMERF: hereditary myopathy with early respiratory failure and MCA: myopathy with cytoplasmic aggregates)⁸⁻⁹. 96 TTN mutations cause a purely cardiac phenotype (DCM: dilated cardiomyopathy, HCM: hypertrophic cardiomyopathy, MmD-HD: multi-minicore disease with heart disease and RCM: restrictive cardiomyopathy) and the remaining mutations affect both skeletal and cardiac muscle. 73% of TTN mutations are found within the A-band and M-Line regions. Experts in the field have suggested that because the A-band and M-line regions of titin are important for biomechanical sensing and signaling, mutations in this region may have profound effects on gene expression and myocyte remodeling⁸. Though mutations localize similarly⁸ in the A-band and M-line in

both cardiac and skeletal muscle, it is puzzling that some patients display only cardiac pathology and others skeletal pathology.

One detail worth considering, is that many of the patients involved in the reported TTN mutations have not undergone a full TTN screen. Besides, a past-medical and family history is not available for the majority of these patients. It is possible that in most cases of titin myopathies, both skeletal and cardiac muscles are effected but not clinically noted. Additionally, TTN mutations that display a disease phenotype are often compound heterozygous suggesting that environmental or genetic modifiers may be required¹⁰⁻¹². Finally, one must consider the variability of titin isoforms in cardiac versus skeletal muscle. Cardiac muscle is composed primarily of N2B (2960 kDa), N2BA (3780 kDa) and Novex I (2980 kDa) isoforms. Whereas the N2A (3680 kDa) isoform is the primary titin in skeletal muscle along with Novex II (2980 kDa). Novex III (616 kDa), the smallest titin isoform is expressed in both cardiac and skeletal muscle. Unique to cardiac muscle is the N2B-U_s found only in N2B and N2BA isoforms. This sequence is only responsible for 3 of the reported mutations. Skeletal muscle isoforms tend to be longer than cardiac isoforms and may underscore why cardiac mutation phenotypes are more prevalent. As a molecular spring, smaller stiffer isoforms like the N2B isoform would be effected by a truncation mutation to a greater degree. Also, improper folding and unfolding in a stiffer isoform would hypothetically cause a higher degree of stress on the spring. We must also consider the mileage that both muscles experience in a life time.

For the average person with a normal heart rate of 60 BPM, the heart will contract and relax 86,400 times in a single day, or 31.5 M times per year, and 1.26 billion times by the age of 40. Titin in cardiac muscle never rests and is stretching/shortening from the very first heart beat to the very last. In contrast, skeletal muscle titin is only working under voluntary movements. Infants that display both striated muscle phenotypes typically have a known family history of recessive heterozygous mutation alleles. Furthermore, the skeletal phenotypes that are most severe are the muscles used most often (tibial, limb-girdle, and diaphragm). As TTN screens become more common and available, a population based study in TTN mutations may illuminate why cardiac muscles develop spontaneous mutations at a faster rate than skeletal muscles.

Why do mutations that occur towards titin's C-terminus have the most severe cardiac phenotype?

Approximately 15% of the reported mutations in titin are found in the M-line. One explanation is that this region of titin is a “hotspot” for mutations, but more likely, the relatively high number of mutations might be due to preferential sequencing in that region. Whichever the reason for this uneven distribution of mutations towards the C-terminus of titin, it does not explain why these mutations have a more severe phenotype. Until 2012, much of the animal models designed to study titin were aimed at the I-band region with some exceptions (Gotthardt et al. 2003, Peng et al. 2005, and Granzier et al. 2014). Truncation mutations in the I-band region of titin ultimately will not be incorporated in the sarcomere since attachment to myosin in the A-band, and M-line proteins myomesin and M-protein as well as MyBP-C contribute to structural linkage of titin toward the C-

terminus. A truncation mutation towards the C-terminus of titin is thought to be incorporated in the sarcomere. This could lead to higher rates of turnover and disruption of sense-signaling properties of titin in this region. If this mechanism in the A-band is correct, it still does not explain why mutations are more severe towards the C-terminus. It is also plausible that TTN truncation mutations in the A-band are phenotypically silent until an accumulation of stressors later in life exacerbate the mutant titin¹³.

One interaction worthy of investigation, is the association of nbr1 and p62 proteins that complex with titin in the M-line region. Both proteins have ubiquitin-associated domains (UBA) and associate with MURF proteins at titin's C-terminus¹⁴. Hypothetically, mutations that alter titin's structure and function closer to this ubiquitin-ligase complex could activate ubiquitination and protein degradation through enhanced MURF activity. It was found that MURF-1 null mice show resistance to muscle denervation atrophy by Bodine et al., 2001. One could design a series of experiments in which activity of MURF proteins were followed in animal models with and without truncating mutations in titin's A-band – M-line regions. Also, mutations at various positions in relation to titin's C-terminus could be evaluated to look for increased degradation through nbr1-p62-MURF interactions. If titin mutations closer to the C-terminus have a higher rate of degradation, cellular senescence and apoptosis is likely to occur. Atrophy of muscles with higher rates of activity could lead to more severe phenotypes and explain why C-terminal titin mutations are more detrimental.

In summary the current body of work is highly significant because it examines titin's role in cardiac remodeling and provides novel insight in heart disease that affect millions of people world-wide. Alternative splicing of titin holds great therapeutic promise as a means to alleviate restrictive filling in the heart. In addition, the limited understanding surrounding pathologic remodeling in heart failure patients establishes our work on titin's N2B element as clinically relevant and important.

References of Discussion and Summary

1. Granzier HL & Irving TC (1995) Passive tension in cardiac muscle: contribution of collagen, titin, microtubules, and intermediate filaments. *Biophysical journal* 68(3):1027-1044.
2. Centner T, *et al.* (2001) Identification of muscle specific ring finger proteins as potential regulators of the titin kinase domain. *Journal of molecular biology* 306(4):717-726.
3. Siu BL, *et al.* (1999) Familial dilated cardiomyopathy locus maps to chromosome 2q31. *Circulation* 99(8):1022-1026.
4. Gerull B, *et al.* (2002) Mutations of TTN, encoding the giant muscle filament titin, cause familial dilated cardiomyopathy. *Nature genetics* 30(2):201-204.
5. Herman DS, *et al.* (2012) Truncations of Titin Causing Dilated Cardiomyopathy. *New England Journal of Medicine* 366(7):619-628.
6. Chauveau C, Rowell J, & Ferreiro A (2014) A Rising Titan: TTN Review and Mutation Update. *Human mutation*.
7. Helmes M, Trombitas K, & Granzier H (1996) Titin develops restoring force in rat cardiac myocytes. *Circulation research* 79(3):619-626.
8. Linke WA & Hamdani N (2014) Gigantic business: titin properties and function through thick and thin. *Circulation research* 114(6):1052-1068.

9. LeWinter MM & Granzier HL (2014) Cardiac titin and heart disease. *Journal of cardiovascular pharmacology* 63(3):207-212.
10. Ceyhan-Birsoy O, *et al.* (2013) Recessive truncating titin gene, TTN, mutations presenting as centronuclear myopathy. *Neurology* 81(14):1205-1214.
11. Chauveau C, *et al.* (2014) Recessive TTN truncating mutations define novel forms of core myopathy with heart disease. *Human molecular genetics* 23(4):980-991.
12. Evila A, *et al.* (2014) Atypical phenotypes in titinopathies explained by second titin mutations. *Annals of neurology* 75(2):230-240.
13. Gramlich M, *et al.* (2009) Stress-induced dilated cardiomyopathy in a knock-in mouse model mimicking human titin-based disease. *Journal of molecular and cellular cardiology* 47(3):352-358.
14. Hoshijima M (2006) Mechanical stress-strain sensors embedded in cardiac cytoskeleton: Z disk, titin, and associated structures. *American journal of physiology. Heart and circulatory physiology* 290(4):H1313-1325.